

**SPECTRAL REFLECTANCE OF NEAR-EARTH ASTEROIDS:
IMPLICATIONS FOR COMPOSITION, ORIGIN AND EVOLUTION**

A DISSERTATION SUBMITTED TO THE GRADUATE DIVISION OF
THE UNIVERSITY OF HAWAII IN PARTIAL FULFILLMENT
OF THE REQUIREMENTS FOR THE DEGREE OF

DOCTOR OF PHILOSOPHY

IN GEOLOGY AND GEOPHYSICS

MAY 1983

by

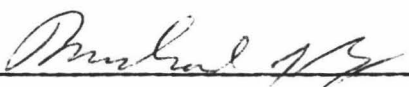
Lucy-Ann Adams McFadden

Dissertation Committee:

Michael J. Gaffey, Chairman
Thomas B. McCord
Shiv K. Sharma
John M. Sinton
David Morrison, Outside Member

We certify that we have read this dissertation and that in our opinion it is satisfactory in scope and quality as a dissertation for the degree of Doctor of Philosophy in Geology and Geophysics.

DISSERTATION COMMITTEE



Chairman



SK Sharma

Th B. [unclear]

D. [unclear]

Acknowledgements

It is a pleasure to pay tribute to those who have helped me advance to this stage in my career. Tom McCord has encouraged and supported my efforts from the beginning. His background and vision to the future has been invaluable to my scientific training. Mike Gaffey has followed and nurtured my progress in detail and I am honored to have been one of his students. His patience, understanding and insights have contributed to the success of this dissertation.

I couldn't have completed this work without the help and moral support of all those around me. The people of the Planetary Geosciences Division create a unique chemistry which successfully contributes to scientific investigations of the Solar System. Thank you all for your efforts.

Mark Rognstad was responsible for the instrumentation with which I acquired my data. The computing facilities were provided by Karl Hinck, Roger Clark, Jeff Hoover and Rodney Kam. Kevin Reed helped prepare the figures and Debbie Kikuchi helped with the layout. Thank you all for providing your technical expertise which I do not have.

Bob Singer, Roger Clark, Ray Hawke and Fraser Fanale comprise a valuable resource of experience and expertise in reflection spectroscopy and planetary science for which I am grateful. This work has benefitted from my discussions with them.

This work was completed with the financial assistance of a Space Industrialization Fellowship provided by The Space Foundation of Houston, Texas. I hope to continue my research on near-Earth asteroids with the encouragement provided by this fellowship.

ABSTRACT

The visible (0.33-1.0 μ m) reflectance spectrum of nine near-Earth asteroids have been measured with a two-beam photoelectric photometer and the 2.2m telescope at Mauna Kea Observatory. Reflectance spectra of eight additional near-Earth asteroids are compiled and presented with the new measurements. Infrared data exist for eight of these 17 objects and are used to augment interpretation of the visible spectra. Mineralogical-petrological interpretation assuming cosmically abundant material is made based on the principles of crystal field theory. No rare or unusual minerals are seen on the surface of these objects. The surface composition of near-Earth asteroids (with one exception) contain common rock-forming minerals such as olivine, pyroxene and phyllosilicates. Opaque components are present but cannot be mineralogically identified. The spectra of near-Earth asteroids have stronger mafic silicate absorption bands than normally present in spectra of main belt asteroids. The spectrum of 2201 1947XC cannot be interpreted in terms of common asteroidal components. This spectrum is examined for evidence of cometary features but no active comet features are seen. Further consideration of low level cometary activity is warranted based on its orbital elements and unusual spectrum.

There are presumably observational biases in the observed near-Earth asteroid population. A technique to test whether the observed brightness bias is a function of observational circumstances is proposed. The excess of high albedo near-Earth asteroids may be a function of the composition of their source region.

The mineralogical-petrological interpretation of near-Earth asteroids is made to address the following questions: (1) What are the source regions of near-Earth asteroids? (2) What is the relation of

near-Earth asteroids to meteorites? and (3) Are near-Earth asteroids potential extra-terrestrial resources?

A number of asteroid analogues exist in proposed source regions, near the Kirkwood gaps, the $(1/6)$ resonance, and the Flora family. There is one analogue of a large main belt asteroid. The Mars-crossers have not been adequately sampled to determine whether or not near-Earth asteroids are supplied from this population. There are no near-Earth analogues among the seven Mars-crossers that have measured reflectance spectra. Additional spectral coverage or albedo determinations are needed to confirm the similarity of surface composition that is suggested by some asteroids with similar reflectance spectra to some near-Earth asteroids. Some interesting analogues include 1580 Betulia and 2 Pallas, 1685 Toro and 349 Dembowska, and 1915 Quetzàlcoatl and 4 Vesta because these main belt compositions were unique among the asteroids until the near-Earth asteroid analogues were discovered. Perhaps these compositions are common in small asteroids which have not previously been measured because of their size. The existing data suggest there are representatives of near-Earth asteroid sources in all of the regions proposed on dynamical grounds (except for Mars-crossers which have not been adequately tested). There is no satisfactory test for the relation of near-earth asteroids to extinct cometary nuclei. Two asteroids have compositions suggestive of cometary compositions: 2201 1947XC and 1580 Betulia (a phyllosilicate-rich assemblage of which comets are expected to be composed). The compositions of the other measured asteroids do not agree with the most often assumed notion that comets are dirty (hydrated silicate) snowballs.

Seven near-Earth asteroids are meteoritic analogues. The following types are represented in the presently known population: LL4 ordinary chondrite, shocked-black L chondrite, carbonaceous chondrite type 3, and

diogenite. There are no irons, stony-irons, low metamorphic grade carbonaceous chondrites (types 1 or 2) and many achondrite types are not represented. The low frequency of ordinary chondrite compositions compared to that in the meteorite collection is consistent with the hypothesis that a few parent bodies are located in dynamically favorable regions to supply 90% of the observed meteorite falls. The number of non-meteoritic analogues is consistent with the recently discovered diversity of the meteorite population. There are some near-Earth asteroids which are not favorably positioned to collide with the Earth as frequently as others. Rare meteorite types may come from these near-Earth asteroids that do not have measured reflectance spectra to date. The absence of assemblages dominated by nickel-iron supports the observed old cosmic ray exposure age and dynamical models using sources from regions with mean lifetimes consistent with the cosmic ray ages, outside of the near-Earth population.

The presently known near-Earth asteroid population consists of material potentially useful for extra-terrestrial activities. There are abundant silicates. The presence of phyllosilicates and opaques can provide water and other volatiles (2100 Ra-Shalom, 1580 Betulia). At least two objects are inferred to have fine-grained metal (1980AA, 1862 Apollo).

TABLE OF CONTENTS

ACKNOWLEDGEMENTS.....	iii
ABSTRACT.....	iv
LIST OF TABLES.....	viii
LIST OF FIGURES.....	ix
PREFACE.....	xiii
CHAPTER 1 MINERALOGICAL-PETROLOGICAL CHARACTERIZATION OF NEAR-EARTH ASTEROIDS.....	1
CHAPTER 2 REVIEW OF ESTIMATES OF POPULATION SIZE, ORIGINS OF NEAR-EARTH ASTEROIDS AND METEORITES.....	105
CHAPTER 3 RELATION OF NEAR-EARTH ASTEROIDS TO POTENTIAL SOURCE REGIONS BASED ON MINERALOGY AND PETROLOGY.....	135
CHAPTER 4 SUMMARY AND FUTURE DIRECTIONS.....	188
APPENDIX A.....	191

LIST OF TABLES

Table		Page
I	Observing Condition and Geometry of Measured Asteroids.....	62
II	Photometric Measurements of 17 Near-Earth Asteroids.....	63
III	Physical Measurements of 17 Near-Earth Asteroids.....	64
IV	Mineralogical characterization of near-Earth asteroids.....	65
V	Possible Resonances and Encounters in the Inner Solar System.....	133
VI	Meteorites Associated with Large Impact Craters.....	134
VII	Analogues of Near-Earth Asteroids in the Solar System.....	158
VIII	Asteroid Compositional Types.....	160
IX	Large Asteroids with Semimajor Axis within 0.1 AU of 2:1 Kirkwood Gap.....	161
X	Large Asteroids with Semimajor Axis within 0.1 AU of 5:2 Kirkwood Gap.....	162

LIST OF FIGURES

Figure		Page
1	Some near-Earth asteroid orbits.....	73
2	2100 Ra-Shalom/Sun via two calibration techniques.....	74
3	Visible reflectance spectra of 17 near-Earth asteroids.....	75
4	High resolution IR reflectance of near-Earth asteroids and JHK reflectance.....	76
5	Spectral groups A-D of near-Earth asteroids.....	77
6a	Representation of a condition creating color centers	78
6b	Some color center absorptions.....	78
6c	Schematic representation of a semi-conductor.....	78
6d	Reflectance spectrum of sulphur, a semiconductor..	78
7a	Reflectance spectrum of nickel, a metal conductor.	79
7b	Absorption edges of metals with plasma frequencies in the UV-Vis spectral region.....	79
8	The effect of an opaque on the reflectance and albedo of a transparent mineral.....	80
9	A charge transfer absorption band and variations with temperature and pressure.....	81
10	Schematic of transition metal ion in a crystal field and reflectance spectrum of pyroxene due to intra-electronic transitions of Fe ²⁺ in octahedral coordination.....	82

11a	Spectrum of two olivines with different chemistry.....	83
11b	Decrease in albedo of olivine as a function of increasing iron.....	83
12a-d	Reflectance spectra of asteroidal material at different phase angles.....	84
13	Reflectance spectra of powders with different packing densities.....	86
14	Reflectance spectrum of enstatite of different particle sizes.....	87
15a-d	Variation in reflectance as a function of body shape for different materials.....	88
16a	Variation in reflectance as a function of temperature for enstatite.....	90
16b	Variation in reflectance as a function of mixing ratio of olivine and pyroxene.....	90
17	Reflectance as a function of shock pressure.....	91
18	Reflectance spectra of ordinary chondrite shock facies of Dodd and Jarosewich.....	92
19a-b	VUV spectra of unshocked and shocked plagioclase..	93
20	Olivine-orthopyroxene mixtures convolved to JHK bandpasses.....	94
21	Olivine-clinopyroxene mixtures convolved to JHK bandpasses.....	95
22	Clinopyroxene-orthopyroxene mixtures convolved to JHK bandpasses.....	96
23a	Reflectance spectra of ordinary chondrite and opaque mixtures.....	97
23b	Spectra of meteorite types.....	97

24	Average spectra of C3V and C30 meteorite types....	98
25	Spectrum of diopside, high-calcium pyroxene.....	99
26	Compilation of spectra of 1566 Icarus.....	100
27	Spectra of 1685 Toro at two apparitions and L-type ordinary chondrites.....	101
28	Laboratory spectra of two eucrite meteorites.....	102
29	Spectra of 1915 Quetzàlcoat1 and ferric iron-bearing silicates.....	103
30	Spectrum of comets.....	104
31a-c	Spectra of Mercury, Mars and the Moon.....	166
32a-e	Spectra of the satellites of the outer solar system.....	169
33	Spectrum of 1915 Quetzàlcoat1 and 4 Vesta. 173	
34	Asteroid histogram.....	174
35a-b	Spectra of near-earth asteroids and analogues near the 5:2 Kirkwood gap.....	175
36	Spectrum of 1862 Apollo and asteroids with similar visible spectral features.....	176
37a-b	Visible and IR spectrum of 1862 Apollo, 39 Laetitia and 349 Dembowska.....	177
38	Spectrum of 1685 Toro and 349 Dembowska.....	178
39	spectrum of 1036 Ganymed compared to five aster- oids near the 5:2 Kirkwood gap.....	179
40	Location of secular resonances in a-i space.....	180
41	Spectrum of 1981QA and analogue, 18 Melpomene near the $(1/6)$ resonance..... 181	
42	Spectrum of 433 Eros and 40 Harmonia.....	182
43	Spectrum of 887 Alinda and two analogues in the Flora family.....	183

44	Spectrum of 1036 Ganymed and two analogues in the Flora family.....	184
45a-b	Flora family analogues to 1620 Geographos and 1627 Ivar.....	185
46	Flora family analogues to 1981QA.....	186
47	Flora family analogues to 1862 Apollo.....	187

PREFACE

In the past 25 years the solar system has been aggressively explored with both spacecraft and ground-based telescopes. The solar system beyond Saturn and the asteroids remain to be explored with spacecraft. Ground-based telescopic investigations are a precursor to spacecraft exploration of solar system bodies. A group of small asteroids which temporarily (10^6 - 10^7 years) occupy orbits in the near-Earth environment had not been studied extensively with ground-based techniques until recently when an effort was made to locate these objects and instrumentation became sensitive enough to measure their physical properties. The results of these efforts have expanded our knowledge of the solar system and the Earth within it by comparison. Ground-based data are used in planning future spacecraft missions which provide direct and higher resolution measurements of physical properties.

This dissertation is a study of the mineralogical and petrological properties of 17 near-Earth asteroids which are members of the Apollo, Amor or Aten groups. These asteroids by definition, occupy orbits that cross that of the Earth and sometimes Mars (Apollos), cross that of Mars and sometimes the Earth (Amors), and cross that of the Earth and never Mars (Atens). Spectral reflectance measurements between 0.33 and 1.0 μm were measured and mineralogical-petrological interpretations made to characterize the population. This information addresses four basic scientific questions: (1) What is their surface mineralogical composition? (2) What are the source regions of near-Earth asteroids? (3) What is the relation of near-Earth asteroids to meteorites? (4) How useful are near-Earth asteroids as extra-terrestrial resources? Each question will be addressed in the following chapters.

The first problem is to determine the nature of these bodies of which there are many aspects. One of importance is their mineralogy and the combination of minerals that constitute the asteroid's petrology. In the absence of an in situ geological survey, the average mineralogy and petrology of their surface can be constrained from ground-based measurements of the reflectance spectrum and knowledge of their albedo, polarization and radar properties, and phase coefficients. To this end, the visible reflectance spectrum (0.33-1.00 μm) of 17 near-Earth asteroids were measured using a 2-beam photoelectric photometer and the 2.2m telescope operated by the University of Hawaii at Mauna Kea Observatory. The mineralogical and petrological components of the asteroid are interpreted from the spectra according to the principles of crystal field theory and laboratory experiments of the behavior of minerals and their mixtures in reflected light. The assumption is made that these objects are made of cosmically abundant minerals until interpretation on this basis is not possible or independent evidence indicates otherwise. The assumption is relaxed if necessary. This technique is limited by the signal/noise and wavelength resolution of the data, the availability of additional measurements and calculations such as albedo, near-infrared reflectance, and the strength and breadth of our theoretical and experimental data base. In Chapter 1 the data and interpretive technique are described and mineralogical interpretation of each observed asteroid is made. The results are compiled into a characterization of the population based on the existing data and evaluated in terms of its representativeness of the whole population. With this information additional questions can be addressed.

From statistical analyses of their orbital evolution it has been shown that the fate of near-Earth asteroids is collision with the Earth, another terrestrial planet or ejection from the solar system. Their

mean lifetime is $10^7 - 10^8$ years. The numbers and mass of these asteroids, had they diminished from a primordial population, would be staggering. It is therefore concluded that there are one or more replenishing sources. The existing knowledge of the mineralogy and petrology of source regions proposed on dynamical grounds is compared to near-Earth asteroids to provide observational constraints to theory in Chapter 3. A literature review of the population size estimates and origin are presented in Chapter 2.

By comparing the mineralogical-petrological composition of near-Earth asteroids with solar system objects proposed (or not favored) as sources for dynamical reasons, their origin can be constrained by observational information. Unfortunately it is not possible to prove a genetic relation between two objects without direct sampling of both regions. Even then the task would be formidable. Negative results are definitive and positive correlations support a given hypothesis.

The most diverse source of extra-terrestrial material available to study on Earth is meteorites. Lacking in our knowledge of meteorites is the region of the solar system in which they formed. They were in Earth-crossing orbits before becoming meteorites. What is their relation to near-Earth asteroids? Are meteorites fragments of near-Earth asteroids or fragments from elsewhere in the solar system, or both? The mineralogical character of the near-Earth asteroids is related to the meteorites in Chapter 3 as well.

The fourth question which these data address is the usefulness of these materials for space industrialization. This question is also briefly addressed in Chapter 3.

Chapter 1

**MINERALOGICAL-PETROLOGICAL CHARACTERIZATION OF NEAR-EARTH
ASTEROIDS**

INTRODUCTION

The near-Earth asteroids are a dynamically-defined group of small asteroids. They are divided into three subgroups: Amors, Apollos, and Atens. The orbits of the Amors have a semi-major axis >1.0 and perihelion $1.02 < q < 1.30$ AU, the orbits of the Apollos have a semi-major axis >1.0 , and perihelion < 1.02 AU (Figure 1), and the orbits of the Atens have a semi-major axis <1.0 and aphelion >0.98 AU. Shoemaker et al. (1979) have estimated that this population of asteroids consists of 500 Amors, 800 ± 300 Apollos, and 100 Atens; however, there are currently known only 36 Amors, 34 Apollos, and 3 Atens, a count which is subject to change with new discoveries. The mean lifetime of the near-Earth asteroids against collision with a planet or ejection from the solar system has been calculated to be on the order of $10^7 - 10^8$ years (Arnold, 1964) as opposed to the main-belt asteroids between Mars and Jupiter with orbits stable over the lifetime of the solar system.

An observational study in which the visible reflectance of near-Earth asteroids was measured from $0.33-1.0 \mu\text{m}$ was carried out to determine their mineralogy. This information addresses a number of scientific questions and engineering applications while contributing to the exploration of the solar system. The scientific questions will be addressed in subsequent chapters. In this chapter, the near-Earth asteroid population is mineralogically and petrologically characterized with presently available data to expand our knowledge of the objects in the solar system.

DATA

Instrumentation and New Data

An observational program to measure visible (0.33-1.0 μ m) reflectance spectra of near-Earth asteroids began in December, 1979 using the 2.2m telescope of the Mauna Kea Observatory and a 2-beam photoelectric spectrophotometer (McCord, 1968). By August, 1981, data had been collected on ten near-Earth objects, eight of them previously unobserved. The Amor object 433 Eros and the Apollo-type 1685 Toro were remeasured.

Due to the small size and high apparent magnitude of these objects, only the reflected sunlight between 0.33-1.0 μ m can be measured with existing ground-based telescopes and instrumentation. Twenty-two interference filters with a half-height bandwidth of 0.025 μ m rotate through the optical path transmitting light to the InGaAs photomultiplier (RCA type 31034C) [Measurements of 2201 1947XC were made with a GaAs tube RCA type 31034B]. A chopper mirror measures sky and asteroid flux alternately at 10Hz. The flux is amplified, counted and recorded on magnetic tape. The data are calibrated using standard stars to correct for instrumental signatures and atmospheric extinction (Chapman and Gaffey, 1979). The data reduction calculations were made using an interactive spectrum processing routine (Clark, 1980). The calibration procedure results in a reflectance relative to Sun, scaled to unity at 0.56 μ m by convention (Chapman and Gaffey, 1979) (Figure 2). Not all objects have an albedo determination, therefore the relative scale is warranted. Table I lists the observing conditions and geometry of near-Earth asteroids measured in this observing program.

Two standard star calibrations were made with measurements of 2100 Ra-Shalom. A standard star (α Equ) from the Planetary Geosciences standard star catalogue (unpublished) and a solar spectral analogue (HR 7504, 16 Cyg B) (Hardorp, 1981) were measured. The data reduced using both stars (Figure 2) produce the same results except at the ultraviolet (UV) edge of the spectrum. This is an endorsement for the continued use

of both sets of standards. One of the disadvantages of using 16 Cyg B is that it is not in the ecliptic ($+50^{\circ} 17^m$). This presents two problems: It is not always observable, and the atmospheric conditions may not be the same at great angular distances from the object under observation. Extinction corrections may therefore not always be adequate with this star, as evidenced by the lack of agreement in the UV.

Existing Data

Previously measured spectra of seven near-Earth asteroids using the same instrumentation (Chapman and Gaffey, 1979 and references therein) are also included in the data set to characterize this population. Four of these spectra have not been previously interpreted (1566 Icarus, 1620 Geographos, 1580 Betulia and 1036 Ganymed, Figure 3). The spectra of 1685 Toro (Chapman et al., 1973), 433 Eros (Pieters et al., 1976) and 887 Alinda (Gaffey and McCord, 1978) will be reinterpreted.

8-Color Photometry

Dave Tholen of the University of Arizona and Dr. Ed Tedesco of the Jet Propulsion Laboratory have provided 8-color photometry of near-Earth asteroids prior to publication in some cases (Figure 3). These data are used primarily for verification of new and previously existing measurements unless there are no higher resolution data available. The 8-color spectra of 1943 Anteros (Veeder et al., 1981) and 1979VA (Tedesco and Tholen, unpublished) will be interpreted without higher resolution 24-filter spectra as they are not available.

Additional physical measurements

In order to strengthen, constrain or expand upon mineralogical interpretations, additional physical measurements are necessary and/or

useful. These data were used as available and are compiled in Tables II and III.

Albedo measurements - Albedo measurements are necessary to constrain interpretations with widely different implications. The data used in this analysis from both radiometric (e.g., Morrison, 1977) and polarization (e.g., Zellner and Gradie, 1976) measurements are presented in Table III. The standard model for determining albedo from radiometric data has been shown to fail for some near-Earth asteroids (Lebofsky et al., 1979). When adequate models are produced additional knowledge of surface properties will be known.

Visible and Infrared Photometry - The existing UVV photometry converted to flux relative to V magnitude is presented in Table II. These data are used to confirm higher resolution measurements in overlapping spectral regions. Broad-band JHK photometry can also constrain interpretations in a manner to be discussed in the interpretation section. JHK photometry exists for 433 Eros (Chapman and Morrison, 1976), 1862 Apollo (Hartmann et al., 1982), 1943 Anteros (Veeder et al., 1981) 2100 Ra-Shalom (Lebofsky et al., 1979) 2201 1947XC (Soiffer et al., personal communication), and 1979VA (Hartmann et al., 1982) (Figure 4). These data are compiled in Table II having been converted to flux relative to 1.6 μm using the JHK values for the sun of Degewij et al. (1980). Only the data of Hartmann et al. (1982) were measured with simultaneous broad band visible (V) photometry. The JHK reflectance is arbitrarily scaled to 1.0 at H and the vertical scale should be thought of as floating relative to the visible reflectance except in the case of 1862 Apollo and 1979VA. 433 Eros (Larson and Veeder, 1979) has been measured with sufficient wavelength resolution to permit a more secure and detailed mineralogical analysis (Figure 4). 433 Eros has also been measured in the 3.0- μm region (Eaton et al., 1982).

DESCRIPTION OF SPECTRA

A compilation of available visible reflectance spectra are presented in Figure 3. In Figure 5, spectra with similar spectral characteristics are shown together. For descriptive purposes the observed spectra form four groups each with different spectral characteristics (albedo is ignored). The spectrum of 2201 1947XC does not fit into any of these groups.

Group A - The spectra in Figure 5a have a non-linear ultra-violet (UV) absorption edge with a minimum relative reflectance of 0.40 or less, a maximum reflectance approximately 0.70 μm of between 1.1 and 1.2, and a near-infrared (NIR) absorption band with a minimum reflectance between 0.90 and 0.75.

Group B - These spectra (Figure 5b) have a linear UV absorption edge between 0.40 and 0.76 μm . There is a break in slope near 0.40 μm with minimum reflectance varying between 0.2 and 0.5. The maximum reflectance of 1.10-1.25 is at 0.76 μm . The minimum reflectance in the NIR absorption band is >1.0 .

Group C - The UV absorption edge slope is lower in the group C types (Figure 5c) than group B. The minimum reflectance is 0.50 or greater. The UV break in slope near 0.40 μm is in the same position as group B spectra. The NIR break in slope occurs near 0.73 μm . The NIR absorption is weak and poorly defined. The minimum reflectance in the absorption band is > 1.0 .

Group D - Group D spectra (Figure 5d) are flat in the visible. Minimum UV reflectance is 0.80 with a break in slope near 0.43 μm . The NIR break in slope occurs at approximately 0.80 μm with a minimum reflectance of 0.90.

MINERALOGICAL-PETROLOGICAL INTERPRETIVE TECHNIQUES

Introduction

Mineralogical and petrological interpretation of visible reflectance spectra is made from consideration of the possible photon interactions with mineral phases. Mineralogy and absorption features are correlated in laboratory studies of controlled samples (e.g., Adams, 1974) and/or a theoretical understanding of the phenomena (e.g., Burns, 1970). Interpretation techniques of reflectance spectra of planetary objects is discussed in various places in the literature and to various degrees of completeness. Most notable for their thoroughness in terms of interpreting asteroid reflectance spectra is the work by Gaffey and McCord (1978).

A procedure for mineralogical and petrological interpretation of reflectance spectra is based on the possible causes of spectral features. Certain mineral structures have electronic configurations of ions with energy levels separated by the energy equivalent to visible and near-infrared photons. With incident light of the allowed energy, the photons are absorbed creating absorption bands diagnostic of the crystal structure. The mean photon path length is a function of physical properties such as composition, particle size and texture. The reflectance (including the scattered and absorbed components of the incident light) is affected by physical parameters but the true position of the absorption bands is controlled by the mineralogy alone. In a mineralogical interpretation one wishes to first define the nature of the absorption, what chemical species are involved and in what crystallographic structure the cations and anions reside. The study of the combination of mineral phases reveals information of the origin and history of the asteroid and constitutes its petrology. A discussion of the

possible mineralogy and petrology of materials which produce absorption features in the three general spectral regions (UV, visible and near-infrared) covered by measurements in this study follows. The effects of physical parameters are also considered.

Practically speaking, interpretation of visible reflectance spectra from 0.33-1.0 μm is limited to: (a) determining the presence or absence of mafic silicates based on an absorption band in the 0.9- μm region, (b) the chemistry in terms of high or low iron and calcium contents (Adams, 1974), (c) the presence or absence of opaque and metallic components which cannot be specifically diagnosed in all cases and (d) elimination of certain physical and mineral-chemistry combinations.

Absorptions in the UV-Visible

Absorptions in the UV-Visible region of the spectrum can be caused by four different phenomena: color centers (e.g., Kittel, 1976, Bill and Calas, 1978), conduction bands (Kittel, 1976, Hunt et al., 1971a), crystal field transitions (Burns, 1970) or intervalence charge transfer of ions (e.g., Burns, 1981).

Color Centers - Color centers arise from trapped electrons in crystal structure lattice defects. Naturally occurring color centers are commonly found in high symmetry crystals where it is easy to produce defects. When the presence of impurities result in a charge imbalance in a crystal lattice, electrons are bound by the crystal field of the surrounding ions to try to preserve electrical neutrality (Figure 6a). In this bound state the electron can be excited to higher energy levels and absorption bands can form (Figure 6a). Color centers can only be unambiguously identified upon the elimination of other types of absorptions and with independent evidence that conditions exist which would cause lattice defects. Such conditions include high radiation fields,

or possibly high degrees of shock. A test for the presence of color centers is to measure the spectrum at different temperatures. The absorption band disappears at high temperatures because the guest ion is driven from the lattice defect. This test has not been made for any asteroid to date. It is possible to test for color centers for some Earth-crossing asteroids as their surface temperatures vary by hundreds of degrees (a result of their eccentric orbits which place them at widely varying distances from the Sun). Identifying the geochemistry and type of color center cannot be done with reflectance spectroscopy alone (e.g., Bill and Calas, 1978). Color centers may be confused with crystal field bands and some charge transfer bands.

Conduction Bands - The energy required for transitions between some valence and conduction bands in semi-conductors is equivalent to photon energies in the UV-Visible (Figure 6b). The wavelength of the onset of the band is dependent on the particular semi-conductor (Figure 6b). The onset of the band which is extremely abrupt for pure semi-conductors, is reduced with an increase in impurity abundance. Conductivity is proportional to temperature (Kittel, 1976), therefore a decrease in temperature results in a lower conductivity and concurrent decrease in intensity of the band.

Metals - The valence and conduction bands overlap in conductors, therefore there is no forbidden gap and absorption is continuous (Figure 7a). Colored metal conductors have absorption edges at visible wavelengths which correspond to the plasma frequency of the conductor (Hecht and Zajac, 1976). This is the frequency below which the plasma density prevents absorption, the index of refraction is imaginary and the incident light is reflected (Figure 7b). The nature of a strong absorption edge (semi-conductor band edge or plasma frequency edge) cannot be determined from a reflectance spectrum alone.

Opagues - Opaque minerals are conductors or semi-conductors which totally absorb photons at all wavelengths of interest. The most common solar system opaques include elemental carbon, magnetite (spinel), and fine-grained metallic grains with oxide coatings. These minerals have a prominent effect on spectra which is disproportionate to their contribution by weight but important for information which reveals physical and chemical conditions of rock formation. One mechanism which results in total absorption is the formation of energy bands at ions instead of discrete energy level splitting. When anions with a full orbital energy state interact with cations with empty adjacent orbitals, they overlap and form energy bands and most of the light is absorbed at all optical wavelengths. This phenomenon occurs in oxides (e.g., Hunt et al., 1971). Some opaques are strong absorbers in which case the physical mechanism of absorption is a very strong charge transfer (as in the case of magnetite). The spectrum of elemental carbon and small (tens of microns) to large (centimeter) grained magnetite is featureless. Sub-micron-sized magnetite (and probably carbon) becomes transparent in the infrared. Unfortunately, existing techniques cannot discriminate between opaque types. It is theoretically possible to identify the presence of silicate opaques (magnetite and ilmenite) from vacuum ultra-violet (VUV) spectroscopy, however carbon and elemental metals have no features in this region (Wagner et al., 1980). It is important to pursue methods of remotely determining the mineralogy and chemistry of the opaques because of their value in determining formation conditions.

The addition of small amounts (1-5%) of an opaque component such as carbon or magnetite drastically reduces the strength of an absorption and its albedo (Figure 8, e.g., Singer, 1981, Clark, 1981, Johnson and Fanale, 1973). The general effects of shock are similar but the

addition of opaques reduces the albedo and spectral contrast at a faster rate than shock alone. For example, the spectral contrast of a silicate and opaque mixture would be lower at a given albedo than for a sample shocked to the same albedo. Different opaques probably behave differently in this manner as well.

Charge Transfer Absorptions - Charge transfer (CT) processes have been studied for many terrestrial and lunar materials (e.g., Smith and Strens, 1976, Loeffler et al., 1974). The absorptions originate from the transfer of electrons between two valence states of adjacent ions. Charge transfer absorptions are the strongest type of absorption (e.g., Burns, 1970). In certain cases and with additional knowledge of spectral parameters a charge transfer band can be assigned to specific ion interactions. Due to the short wavelength cutoff of Earth-based measurements, CT absorptions are usually only observed as absorption edges making it difficult or impossible to determine band centers. With a decrease in temperature (Smith and Strens, 1976) and an increase in pressure (Mao, 1976) CT bands increase in intensity (Figure 9a,b). A reflectance spectrometer on a spacecraft could measure the same area at different times of the day looking for spectral variations due to temperature, thereby unambiguously defining CT bands. Until this is possible, they are identified based on intensity, which is temperature and abundance dependent, and their apparent band width which often extends into the visible spectral region. The CT absorption is non-linear and has a characteristically concave shape (Figure 9). It should be noted that not all charge transfers extend beyond the ground-based observational limit of 0.33 μm , nor are they always extremely intense. High temperature, a low abundance of charge transferring species and an abundance of opaque material can reduce the intensity of the band. Band position is independent of pressure.

Crystal Field Absorptions - The most mineralogically diagnostic absorptions in reflectance spectra of dielectrics are intra-electronic transitions of d-orbital electrons in transition element-bearing minerals. Crystal structures containing cations with unfilled d-orbital electronic energy states set up electric fields which cause splitting of energy states schematically shown in Figure 10a. Absorptions in the 0.9- μm region are due to the transition of Fe^{2+} electrons between t_{2g} and e_g orbitals in cations in octahedral coordination (Figure 10b, Burns, 1970). The presence of an absorption at 2.0 μm in combination with the 0.9- μm band is diagnostic of the presence of pyroxene. Additional minerals have absorption bands in the 0.9- μm region which can be identified based on band position. Pyroxene, olivine, phyllosilicates and ferric oxides are the most cosmically abundant minerals with absorptions in this region.

The position, band width and band depth contain information about the type of transition (whether it is allowed or forbidden), chemistry of the mineral in which the transition occurs and the mineral structure in which the cation resides. Knowledge of the mineralogy of a solar system body places constraints on the original state and history of the body. Extensive laboratory investigations have aided in developing techniques to interpret reflectance spectra in terms of crystal field theory, especially for applications in remote sensing of planetary objects (e.g., Adams, 1974, Nash and Conel, 1974, Hazen et al., 1977, 1978, Singer, 1981, Sill, 1973, Fink and Burk, 1971, Adams and Goullaud, 1978, Hunt et al., 1970-1974). In most cases if there is one crystal field band, there are others which make identification of the presence of a mineral possible based on the appropriate combination of absorption bands. This analytical approach is valid only if the material is assumed crystalline and free of absorbing species which would mask

diagnostic absorptions. In the case of Mars for example, it seems that the soil is approaching an amorphous state as some diagnostic absorptions are present and others are absent (Singer, 1982). Interpretation of the absence of bands is not always unique as in the case of Mars.

Olivine chemistry - The position of the maximum visible reflectance in olivine spectra is sensitive to olivine chemistry. With increasing iron content the 1.0- μm bands shift to longer wavelength and the 0.65- μm band shifts to shorter wavelengths (Burns, 1970a). This causes the position of the maximum visible reflectance to shift. This behavior has not been well calibrated due to a preoccupation with the stronger crystal field bands in the 1.0- μm region. For example in a spectrum of Fo_{85} (Singer, 1981), the maximum reflectance is at 0.57 while for the olivine in Chassigny meteorite (Fo_{67} , Floran et al., 1978), the peak is at 0.66 μm (Figure 11a). These laboratory spectra are used in the following mineralogical interpretations to constrain olivine chemistry.

Vibrational bands - Because the new data reported in this study cover the spectral region between 0.33-1.0 μm , this discussion does not include vibration bands and their combinations and overtones as possible causes of absorptions. Features attributable to these phenomena are usually located beyond 1.0 μm . The overtones that do occur in the NIR (water) are shallow and not observable at the wavelength resolution of these data.

Factors Which Alter Absorption Bands

The existence and energy (position) of an absorption band is controlled by the mineralogy of the target object. The strength of the band is proportional to the abundance of the absorbing species in the mean optical path length. This is controlled by either crystallography, chemistry (e.g., oxidation state and abundance of the absorbing species

in the crystal structure), the addition of a mineral component or variations in physical parameters such as particle size, morphology, packing and viewing geometry. When surface processes alter the crystal structure and/or chemistry, the effects are seen in reflectance spectra. Interpretation of these variations is based on laboratory experiments with common solar system minerals, their mixtures and naturally occurring solar system assemblages such as meteorites (e.g., Gaffey, 1976, McFadden *et al.*, 1982) and lunar samples (e.g., Adams and Jones, 1970). Additional data sets such as albedo, polarization and radar properties are needed to constrain the interpretation (Gaffey and McCord, 1978).

The bi-directional reflectance at 0.56 μm relative to MgO (equivalent to albedo in this case because the albedo measurements of the asteroids have errors larger than the difference between bi-directional reflectance and geometric albedo) of low iron mafic silicates is higher than iron-rich mafic silicates (Figure 11b). The strength of absorption bands increases with increasing iron content and increasing particle size. Asteroids have albedos between 0.03 and 0.30. The band strength and albedo combined can place constraints on mineral chemistry and particle size assuming temporarily that there are no opaques present (which also lowers the albedo). In the absence of asteroids with albedos >0.30 the existence of pure olivine or pyroxene assemblages with particle sizes ranging from 5-74 μ can be eliminated. Large grained, low iron silicates cannot be ruled out as their albedo would be lowered as a result of the large mean optical path length.

In most cases mineralogy controls the primary spectral features. Physical effects alter the albedo predominantly over spectral features. With the spectral resolution and signal/noise of the asteroid spectra presented here, physical effects are considered but are not significant enough to effect the spectral interpretation. A review of the effects

of non-mineralogical parameters on reflectance spectra follows.

Physical Parameters - Experimental studies have shown that viewing geometry (Gradie et al., 1980), packing density, particle size (Adams and Felice, 1967), body shape (Gradie and Veverka, 1981), shock (Adams et al., 1979) and temperature (Singer and Roush, 1982) all affect reflectance spectra. Laboratory experiments have shown that the manifestation of these physical parameters in the UV region of reflectance spectra is no more than a 10% variation in the UV absorption band depth at the extremes that are expected to naturally occur in all cases except shock and particle size (Figure 12-17). Variations in spectra in the 0.9 μ m region will be discussed for each situation.

Viewing Geometry and Packing Density - The differences in reflectance of typical asteroidal material due to the range in viewing geometry at which these data were obtained (0° - 64°) (Figure 12) do not affect the mineralogical interpretation of the spectra. The situation is similar for different packing densities (Figure 13). The variations are of the same size or smaller than the errors of the observational data. At the extremes of viewing geometry, the reflectance in the 0.9 μ m region varies between 15-30% for different materials (Figure 12).

Particle Size - Variations in particle size are dominated by albedo changes and strength of the 1.0- μ m band (Figure 14) such that between <30- μ m and 150-250- μ m particle sizes the albedo changes by more than 100% at 0.56 μ m (Figure 14b) and the 0.9- μ m relative band depth changes by 100% (Figure 14c). The relative strength of the UV absorption edge changes by 50%. The appropriate combination of albedo and band depth must exist in order to constrain the effects of particle size over chemical mineralogy.

Body Shape - Body shape-dependent spectral differences result in spectral variations of 6% at the extremes of an ellipsoid with a major

to minor axis ratio, $a/b = 3$ (Figure 15, Gradie and Veverka, 1981). Most reasonable shape variations result in a small change in slope in the spectrum (Figures 15b,c). Anything but extreme shape differences would not be detectable in asteroid reflectance spectra. Figure 15d shows that the effects of shape are reduced slightly at higher phase angles.

Temperature - Temperature variations result in shifts of band position and band width (Sung et al., 1977, Singer and Roush 1982). The change in the UV absorption band is negligible and the position of the 1.0- μm band does not change as a function of temperature (Figure 16a). The width of the 1.0- μm band broadens with an increase in temperature. A spectrum might be incorrectly interpreted as an olivine pyroxene mixture when it is really a spectrum of a hot pyroxene (compare with Figure 16b).

Shock - The reflectance spectrum of shocked material is altered to the extent that the crystal structure is changed. Experiments by Adams et al. (1979) have shown that only slight changes in the reflectance of enstatite occur after shock pressures of 597 kbar, however the albedo is reduced by 33% at this pressure (Figure 17). Undulatory extinction is seen in thin section at these pressures. At lower pressures (250 and 298 kbar) the Fe^{2+} absorption bands in oligoclase and labradorite disappear. This indicates major reorganization of Fe-O bonds and the formation of diaplectic glass which can also be seen in thin section. The effects of shock are dependent on the strength of the bonds within each particular mineral. In a reflectance spectrum, the presence of pyroxene will dominate any signature of shocked plagioclase and/or olivine. In spectra of pyroxene-opaque mixtures, the effect of adding an opaque component to a pyroxene is to lower the albedo and reduce the spectral contrast, theoretically the same effect is seen in spectra of shocked

minerals. Detailed studies comparing these two effects have not yet been made.

A number of L-type ordinary chondrites that were classified into shock facies by Dodd and Jarosewich (1979) were measured in a survey of the reflectance properties of meteorites (Gaffey, 1976). These spectra have been examined for correlations of spectral properties with shock facies (Figure 18). The data show that the albedo and band depths decrease with increasing shock facies. It is possible that some other phenomenon, possibly varying trace amounts of opaques or glass, controls the observed spectral trend. There is presently insufficient data to test the significance of these observations however the suggestion is definitely there and follow-up experiments are warranted. There is some experimental evidence that these two conditions may be constrained on asteroids with vacuum-ultraviolet (VUV) spectra. Figure 19 shows that the position of the interband energy gap, E_g , shifts to higher energy when crystals have been shocked (Wagner *et al.*, 1980). However, the existing VUV asteroid spectra do not have adequate signal to noise to make this test for shock effects (Veeder, personal communication).

Mineralogical Interpretation of Asteroid Surfaces with Broad-band JHK Photometry

Broad-band JHK photometric measurements can often be made of near-Earth asteroids when they are too faint for higher wavelength resolution measurements. Some mineralogical constraints can be derived from JHK data. We have used the laboratory mixtures of Singer, (1981) and numerically integrated the data over JHK filter transmittance using the same technique as Clark, (1982).

Examination of Figures 20-22 shows that in an assemblage of binary silicate mixtures, JHK data can differentiate between the presence of

orthopyroxene and clinopyroxene mixed with olivine or with each other, and the presence of large proportions of olivine. The presence of spectrally dominant amounts of olivine is seen by a low relative reflectance at J and high relative reflectance at K. The presence of olivine is distinguished from a clinopyroxene (which also has a low relative reflectance at J) by the absence of a low relative K reflectance caused by the 2.0- μm band in clinopyroxene (Figure 22). Orthopyroxene and clinopyroxene mixed with olivine are distinguished by the different position of the 2.0- μm band and its effect on JHK data (Figures 20 and 21). If the K reflectance is less than the H reflectance, then clinopyroxene is present. When the spectrum of orthopyroxene dominates in a mixture it is not possible to identify the other component. For example, JHK data alone cannot differentiate between olivine or clinopyroxene when the orthopyroxene dominates the spectrum with 75% orthopyroxene present (Figures 20 and 22).

The addition of spectrally significant amounts of opaques would remove the mineralogically diagnostic features of these measurements and lower the albedo (Figure 8). Measurements of three component mixtures need to be made to determine what fraction of opaques erases the silicate signatures.

The addition of spectrally significant amounts of opaques would remove the mineralogically diagnostic features of these measurements and lower the albedo (Figure 10). Therefore, if JHK data of asteroids show diagnostic characteristics of the silicates with an albedo lower than expected for pure silicate mixtures of the particle size (45-90 μ) discussed here, then the cause of the reduced albedo is not due to the presence of material that is opaque in the IR.

MINERALOGICAL INTERPRETATION

The principles and experimental results of the previous section are used to determine the mineralogy and petrology of the 17 near-Earth asteroids observed to date. Because meteorites are fragments of small extra-terrestrial bodies, they are good asteroid-analogue material. For this reason we consider the mineralogy and spectral characteristics of each asteroid in terms of meteoritic analogues. This information will be used in a subsequent chapter to address the genetic relation between near-Earth asteroids and meteorite parent bodies.

433 Eros

The 0.9- and 2.0- μ m absorption bands and the UV absorption edge indicate the presence of mafic silicates (Figure 4) (e.g., Burns, 1970). Both olivine and pyroxene are present on the basis of the width of the 0.9- band (Figure 3), the high IR (infrared) relative reflectance and shallow 2.0- μ m pyroxene band. Due to the uncertainty in the IR slope inherent in fourier transform spectroscopy, the 2.0- μ m band position cannot be determined accurately to derive silicate chemistry quantitatively using the IR data of Feierberg *et al.* (1982) however, some compositions can be eliminated. The 2.0- μ m band position is at too long a wavelength to be due to the presence of orthopyroxene, and at too short

a wavelength to be a high-calcium clinopyroxene. This interpretation is based on the position of the pyroxene bands in mixtures measured by Singer (1981). The pyroxene is therefore a low-calcium clinopyroxene as determined by the approximate position of the 2.0- μm band. The composition of the olivine cannot be determined because the calibration has not been derived quantitatively yet. The albedo of this asteroid (Table III) and the depth of the 1.0- μm band are low for a pure crystalline olivine-pyroxene mixture.

The depth (10%) of the 0.9- μm band (reflectance maximum/minimum) may be controlled by four possible mechanisms: (1) the absence of absorbing species indicating that the silicates are low in iron, (2) a short mean optical path length which may be caused by small particle size, (3) the presence of an opaque component, (4) shock, or (5) reduced amounts of crystalline material. The first two possibilities are eliminated based on the low albedo of 433 Eros (0.125, Table III). A combination of the last three cases could create the characteristics of the observed spectrum. If the silicates and opaques are small particles such that the spectral contrast is reduced by the particle size of the silicates and the spectrum of the opaques becomes wavelength dependent in the IR, then the spectrum would have the observed features (low spectral contrast and high IR reflectance). An example of this phenomenon is seen in laboratory mixtures (Figure 23a) measured by Miyamoto *et al.* (1982). We speculate (Gaffey, personal communication but the authors don't state) that the unmeasured particle size of the carbon black used by Miyamoto *et al.* (1982) is small enough to produce a wavelength-dependent spectrum with a high IR reflectance.

Meteoritic analogues - The spectral features and albedo of 433 Eros were compared to spectra of classes of meteorites measured by Gaffey (1976, Figure 23b). The albedo of 433 Eros is too low and the

absorption bands too weak for this asteroid to be a high albedo achondrite analogue. The absorption bands are stronger and albedo lower than those of aubrites. The albedo is too high and bands too strong to be an ureilite analogue. The stony-irons that have been measured have higher IR reflectance and albedo. The ordinary chondrites have higher albedos for the most part and lower IR slopes and 0.9- μm absorption bands with minimum reflectance <1.0 relative to 0.56 μm in all cases. The low-Ca pyroxene composition is not consistent with the ordinary chondrites either. The UV absorption is more linear in 433 Eros than in ordinary chondrite spectra. The black chondrites have lower albedo and lower IR reflectance. The carbonaceous chondrites have lower albedos and weaker absorption bands than that of 433 Eros. The C30's have the appropriate albedo but lower IR reflectance and weaker absorption bands. There are therefore no meteoritic analogues to 433 Eros, contrary to previously published suggestions (Feierberg et al., 1982, Pieters et al., 1976), assuming that the reflectance of the surface of asteroids behave as powdered meteorites measured in the lab.

887 Alinda

The reflectance spectrum of 887 Alinda shown in Figure 3 was interpreted by Gaffey and McCord (1978) as a silicate and opaque assemblage. An interpretation of the spectral features indicates that the UV absorption edge is a CT band edge. The NIR absorption band in the spectrum of 887 Alinda is a spin-forbidden, Laporte allowed Fe^{2+} transition in a mafic silicate, probably olivine and pyroxene based on their cosmic abundance and bandwidth which is broader than that formed by pyroxene alone. The absorption band is weak for four possible reasons which result in a short mean optical pathlength: (1) low iron abundance, (2) small particle size, (3) presence of opaques, (4) shock effects. The

albedo of 0.18 (Morrison and Zellner, 1979) constrains these hypotheses. In the case of the first two possibilities, the albedo has to be high. The measured albedo contradicts the first two hypotheses. In the last two cases the albedo is reduced relative to a pure silicate spectrum. The presence of an opaque component is most likely by elimination of the shock hypothesis. The high degree of shock required to reduce the strength of absorption bands (Adams et al., 1979) is not expected from collisions of small bodies and from evidence in the meteorites. These conclusions based on the albedo of 887 Alinda are tentative because of the fact that the polarimetric and radiometric albedos are discordant (Morrison, 1977). It is possible that the standard radiometric model does not apply to 887 Alinda as has been discussed for some other small asteroids by Lebofsky et al. (1979).

Meteoritic analogues - The meteoritic analogue of an olivine-pyroxene assemblage with a small opaque component is a type 3 carbonaceous chondrite (Gaffey, 1976). Gaffey and McCord (1978) concluded that 887 Alinda is a C3 meteoritic analogue. A further interpretive step can be made by examining the spectra of C3V and C30 types (Gaffey and McCord, 1979, Figure 24). The spectrum of 887 Alinda has stronger 0.9- μm regions features, a higher albedo, and a break in slope at shorter wavelength than the C3V types. The spectral characteristics of 887 Alinda correlate with those of the C30 types, consistent with a higher chondrule/matrix ratio, higher molar iron content and abundance of olivine, and lower magnetite and carbon abundance than C3V's. These petrological differences are seen in reflectance as a higher albedo and stronger absorption bands. An initial interpretation of 887 Alinda as an H-type ordinary chondrite (Chapman, 1976) is incorrect mainly because of the linearity of the UV absorption in the spectrum of 887 Alinda which is not characteristic of H chondrites (Figure 23b).

1036 Ganymed

The 0.33-0.93 μ m spectrum of 1036 Ganymed (Figure 3) was presented by Chapman and Gaffey, (1979) but has not been interpreted previously. The UV CT and NIR crystal field absorption edges (Figure 3) are indicative of the presence of mafic silicates. The mineralogy of the silicate cannot be determined without further spectral coverage and an albedo measurement. The plateau between 0.63 and 0.80 could be a signature of a high calcium pyroxene (Figure 25) or a low iron olivine. If the 0.66- μ m band is real, it is consistent with the presence of a low iron olivine. Higher resolution spectra are needed to confirm this band. Without an albedo measurement the presence of opaques cannot be considered. With the available data only the presence of silicates is certain. The presence of additional components and the chemistry of the silicates is speculative.

Meteoritic analogues - With no albedo constraint, all meteorite types with UV and IR absorption bands are initially considered as analogues (Figure 23b). The basaltic achondrites, nakhlites, chassignites, and angrites are eliminated based on the depth of the NIR absorption at 0.93 μ m relative to the strength of the UV absorption edge. The NIR band is much stronger in these meteorite types than in the spectrum of 1036 Ganymed. Ureilites have less spectral contrast than 1036 Ganymed. The NIR absorption edge of ordinary chondrites is at shorter wavelengths than the spectrum of 1036 Ganymed. The shocked, black chondrites are eliminated on the basis of lack of spectral contrast as are the carbonaceous chondrites compared to 1036 Ganymed. There are therefore no meteoritical analogues to 1036 Ganymed. Additional wavelength coverage or an albedo determination is not expected to change this interpretation.

1566 Icarus

The surface composition of 1566 Icarus (Figure 3) as presented but not interpreted by Chapman and Gaffey (1979) and derived by Gehrels et al. (1970, Figure 26) appears to be mafic-silicate-rich based on the presence of the strong UV and NIR absorption edges. Because the NIR reflectance has not defined an absorption minimum at 1.0 μm (there is no upturn in reflectance), the band probably represents the presence of a significant olivine component. If the narrow band at 0.60 μm is real, this also indicates the presence of olivine. There is insufficient data to determine silicate chemistry or olivine/pyroxene ratios. There is no spectral evidence of an opaque, glass or metallic phase which would reduce the spectral contrast or result in significantly redder spectra than those observed. The albedo (0.30, Table III) indicates the presence of an opaque, shock effects or both. The orbit of 1566 Icarus crosses that of Mercury (Figure 1), the opaque component would probably not be a volatile such as carbon, but rather magnetite because carbon is not stable at very high temperature.

The difference in the two spectra indirectly calculated by Gehrels et al. (1970) in the NIR region (Figure 26) is consistent with changes in laboratory spectra of an L6 ordinary chondrite as a function of viewing geometry (Gradie et al. 1980, 1981). However, the data suggest there are additional factors affecting the spectra. If it is assumed that the mineralogical components of Icarus are similar to Bruderheim (olivine/pyroxene/metal assemblage), an assumption that initial mineralogical analysis supports, then the behavior of the two Gehrels et al. spectra are not totally consistent with spectral changes due to phase angle. The higher phase angle spectrum of the laboratory material remains redder until a cross-over point at 0.83 μm (Figure 12a). The spectra of Icarus have a cross-over point at 0.50 μm only where they are

scaled. In addition the increased relative reflectance at the larger phase angle below 0.50 μm is opposite to the phase relationship observed with Bruderheim (compare in Figure 12a, spectrum at 4° and 30° , this behavior is still seen at 60° (Gradie and Veverka, 1983) but by 120° the UV band is weaker than the rest). Therefore, there are factors in addition to viewing geometry responsible for the differences in the spectra of 1566 Icarus. When the spectrum of Chapman and Gaffey, 1979 (Figure 30) are considered with the Gehrels et al. spectra, the absence of a uniform variation with phase angle is additional evidence for non-viewing geometry variations. The observed changes may be attributed to particle size, body shape and/or compositional variation with rotation. Additional data are needed to constrain the cause of the observed differences.

Meteoritic analogues - The existing data are not adequate to place tight constraints on meteoritic analogues. Meteorite classes with low spectral contrast can be eliminated such as aubrites, enstatite chondrites, and irons. Without direct measurements of the 1.0- μm region any other class of meteorite is a potential candidate.

1580 Betulia

The spectrum of 1580 Betulia (Figure 3, Chapman and Gaffey, 1979) has the lowest spectral contrast of the measured near-earth asteroids to date. The featureless reflectance between 0.46 and 0.70 μm coupled with the low albedo (Table III) are diagnostic of a high abundance of opaques or large particle sizes of strongly absorbing material. Residual absorptions in the UV and NIR are diagnostic of mafic silicates. Because the band strength of both the UV and NIR band is weak (18 and 10% respectively) the silicates are likely to be low in Fe^{3+} iron. High iron phyllosilicates can be eliminated based on the position of the UV

absorption edge. Constraints between low iron phyllosilicates and low iron olivine and/or pyroxene are needed. There is an absence of a reddening agent implying large particle-sized opaques instead of fine-grained opaques which have a wavelength dependent spectrum with a high IR reflectance and large slope in the visible.

Meteoritic Analogues - All high albedo meteorites are eliminated from consideration as analogues. Only C1 and C2 carbonaceous chondrites have albedos as low as that of 1580 Betulia. The break in slope of the UV absorption edge at 0.56 μm in carbonaceous chondrites (Figure 23b) is not consistent with the break in slope at 0.43 μm in the spectrum of 1580 Betulia. Therefore, there are no meteoritic analogues to this asteroid.

1620 Geographos

The presence of mafic silicates are indicated by the UV and NIR absorption edge in the spectrum of 1620 Geographos (Figure 3, Chapman and Gaffey, 1979). With an albedo of 0.187 (Zellner and Gradie, 1976, Table III), the mafic silicate particle size could be large, there may be opaques present or the low albedo could be the result of shock. The large particle size can be ruled out due to the lack of a large NIR absorption edge slope (Hunt and Salisbury, 1970).

Meteoritic analogues - There are no meteoritic analogues to the spectrum of 1620 Geographos. None of the meteorite types has a relative reflectance increasing to 1.2 at 0.73 μm and then falling off in a NIR absorption edge.

1627 Ivar

There were data reduction problems with these data (Appendix A) which were not satisfactorily resolved. The interpretation of this

spectrum (Figure 3) is therefore tentative until confirmation of the spectrum can be made. The 8-color spectrum of Tedesco and Tholen (Figure 3, personal communication) do not agree in the NIR. The UV and NIR absorption edges in the 24-filter spectrum are indicative of the presence of mafic silicates most probably olivine and pyroxene. The strong inflection or plateau between 0.50 and 0.65 μm is characteristic of high-calcium pyroxene (Figure 25). The NIR absorption is poorly characterized but appears strong. This is consistent with the high albedo (0.23, Veeder, personal communication, Table III) of 1627 Ivar. The interpretation of this spectrum must remain inconclusive until confirmation data are available. The existing data suggest something unusual possibly a monomineralic differentiated fragment.

Meteoritic analogues - There are no meteoritic analogues based on these data or the 8-color photometry of Tedesco and Tholen.

1685 Toro

Chapman et al. (1973) interpreted the spectrum of 1685 Toro as an olivine-orthopyroxene assemblage. Additional data have become available since then (Table II and III). An interpretation of the spectrum measured in July, 1980 by Chapman (personal communication) combined with JHK data (Veeder et al., 1982) that are not tied into a simultaneously measured V magnitude is presented here (Figure 4). The broad NIR absorption band and strong non-linear UV absorption with an inflection at 0.50 μm and maximum reflectance at 0.66 μm (Figure 3) is indicative of the presence of olivine. The albedo of 0.14 (Dunlap et al., 1973, Table III) indicates the presence of opaques. However, recent radar measurements (Ostro et al. 1983) indicate that the albedo is closer to 0.30, in which case there would be a smaller opaque component present. Large particle-size, monomineralic olivine is eliminated as an interpretation

because the NIR absorption band is not strong enough. The composition of the olivine in 1685 Toro is between Fa_{15} and Fa_{33} based on the position of the reflectance maximum (Figure 3) compared to laboratory measurements of olivines of this composition (Figure 11a). If there is a pyroxene component, it has to be present in amounts <25% based on the slope of the visible edge of the NIR band (compare with Figures 20, 21 from Singer, 1981). With a 75/25 mixture of olivine and pyroxene, the 1.0- μ m absorption edge slope is more negative due to the influence of the pyroxene band, than that in the spectrum of 1685 Toro based on comparisons with laboratory mixtures (Singer, 1981). At higher proportions of pyroxene the position of reflectance maximum shifts to longer wavelengths as well. These features indicate a pyroxene component <25% by weight.

The JHK data (Veeder et al., 1982) place some constraints on the mineralogical interpretation. If 1685 Toro were a pure olivine assemblage, the J/H ratio would be much lower relative to H and K (Clark, 1982) due to the presence of the 1.3- μ m band. The H ratio would still be in the wing of the 1.3- μ m band and the K/H ratio would be higher in the absence of a 2.0- μ m band. The JHK ratios of 1685 Toro do not support the existence of a pure olivine assemblage. These data indicate the presence of clinopyroxene because the K reflectance is slightly less than the H reflectance. According to Figure 20, in an orthopyroxene and olivine mixture, the K reflectance is never less than the H reflectance regardless of how much orthopyroxene is present, indicating that the pyroxene in 1685 Toro is not orthopyroxene. The surface of 1685 Toro consists predominantly of low-iron olivine and low-calcium clinopyroxene.

The difference between the spectra of 1685 Toro measured at two apparitions (Figure 27 bottom) may be attributed to a difference in viewing geometry, aspect angle or mineralogical or textural

heterogeneity across its surface. The observed differences are larger than those observed in laboratory measurements of an olivine-pyroxene assemblage as a function of viewing geometry (Figures 12 a,d, Gradie et al., 1980) in light of the fact that the phase angles were 60 ° and 40 ° in 1972 and 1980 respectively. The variations expected as a function of irregular body shape according to the laboratory measurements of Gradie et al., 1981 (Figure 15c) would be of smaller magnitude and different wavelength dependence than observed for 1685 Toro. The change in reflectance as a function of olivine/pyroxene alone is not similar to the observed spectral differences (compare Figures 27 bottom and 16b). The differences in the observed spectrum are therefore only attributable to gross compositional variations as a function of rotational phase angle or variation in aspect angle at the time of observation. These differences must be verified and studied in more detail. If they are real compositional variations, they are larger than any seen on any asteroid previously (Gaffey, personal communication).

Meteoritic analogues - Chapman et al. (1973) point out that L-type ordinary chondrites are predominantly olivine-orthopyroxene assemblages and that the spectrum of 1685 Toro is similar to L-type ordinary chondrites. The spectral features of this asteroid are not consistent with L-type ordinary chondrites (Figure 27 top) in a manner indicating mineralogical differences between the asteroid and ordinary chondrites. The visible reflectance maximum is at longer wavelengths in L-type ordinary chondrites indicating a different olivine composition. If the albedo of Dunlap et al. (1973) is correct, then it is too low for an ordinary chondrite. The albedo reported by Ostro et al. (1983) however does not contradict the ordinary chondrite interpretation. If the JHK data are correct in indicating that the pyroxene is a clinopyroxene, then the mineralogy is not that of ordinary chondrites. The spectrum of

1685 Toro is not an ordinary chondrite analogue on the basis of olivine and pyroxene chemistry. An olivine rich meteorite type, chassignites, have absorption bands almost a factor of two stronger (Figure 23b) and an albedo higher than either of the two albedo calculations of 1685 Toro. If 1685 Toro were to have a chassignite composition of different particle size than exist for the laboratory measurements, then the albedo would be higher and the band depths less than the asteroid if the particles were smaller. Or, if the asteroid were to have a larger particle size than the meteorite type, the albedo would be lower and absorption bands deeper than the meteorite reflectance. The observed combination of different spectral features precludes a particle size difference between 1685 Toro and chassignites. The 0.9- μ m band in C30's and ureilites (Figure 23b) which have albedos consistent with the albedo determination of Dunlap et al. (1973) are 20-30% weaker. These factors eliminate these meteorite types as analogues. There are no meteoritic analogues to 1685 Toro.

1862 Apollo

The NIR band, UV absorption and inflection in the visible reflectance spectrum of 1862 Apollo (Figures 3 and 4) are diagnostic of the presence of mafic silicates. In this spectrum both olivine and pyroxene are present based on the width of the band. The strength of the NIR absorption is low for a pure olivine-pyroxene mixture. This can be caused by four phenomena as discussed in the interpretation of 433 Eros. The first two possibilities, low iron composition with moderate to small particle size and small particle size independent of composition, are eliminated due to constraints provided by the average albedo measurement of 0.21 \pm 0.02 (Lebofsky et al., 1981). However, the surface could be composed of low iron mafic silicates of large particle sizes

(>250 μ) (Hunt and Salisbury, 1970) which have an albedo consistent with that of 1862 Apollo. The albedo could also be reduced by the presence of opaques, which are present in small enough quantities to reduce the albedo but not eliminate the spectral contrast. Metallic particles are a candidate for this type of material (Gaffey, unpublished). The pyroxene is a low-calcium clinopyroxene based on the relative reflectance at 1.65 and 2.2 μ m (compare Figure 4 to Figures 20-22). The mineralogical components are therefore olivine, low-calcium clinopyroxene and a small quantity of opaques, and/or fine-grained metal.

Meteoritic analogues - The absorption bands are too strong for a C30 or C3V analogue (Figure 24). The high albedo (0.21) supports elimination of this identification. The absorption bands are too weak and albedo too low for it to be a high albedo achondrite with strong 1.0- μ m absorptions. The UV absorption edge slope and lower albedo of ureilites eliminate this assignment. LL4 ordinary chondrites have both the same albedo, strength of absorption bands, UV absorption edge shape and position of reflectance maximum as the visible spectrum of 1862 Apollo. If the JHK data are correct in indicating a clinopyroxene composition then 1862 Apollo is not an ordinary chondrite analogue. High resolution IR spectra will resolve this issue.

The low reflectance at 1.25 μ m relative to 0.56 μ m is not characteristic of any known mineralogy. It is possible that the V-band measurements should be corrected for the large light curve variations of 1862 Apollo (0.6 magnitudes, Harris personal communication). If this is the case, then the vertical scale in Figure 4 should be floated for 1862 Apollo too, the most appropriate meteoritic analogue.

1865 Cerberus

The spectrum of 1865 Cerberus measured with 8-color filters and 24-filter photometry do not agree in the NIR (Figure 3). There were problems with the data reduction (Appendix A) which, though not well understood, may account for the differences. Additional measurements should be made when the asteroid can be observed again. A tentative interpretation is made knowing that remeasurement may prove it wrong.

The strong UV and NIR absorption are indicative of the presence of mafic silicates, probably olivine and pyroxene. Opaques are a minor component based on the high spectral contrast. There is no albedo measurement so constraints on particle size versus opaque content cannot be made.

1915 Quetzälcoat1

The narrow-band photometry and 8-color spectrum of 1915 Quetzälcoat1 shown in Figure 3 do not agree within the errors of the measurement. Since the higher resolution measurements were made when the asteroid was 13.5 magnitudes versus 19.0 magnitude when 8-color measurements were made, the discrepancy is attributed to measurement error as a function of signal to noise. For the purposes of mineralogical interpretation, only the narrow -band photometry is used. The datum point at 0.70 μm has a large error due to fluctuations in the telluric O_2 emission which could not be accurately calibrated for this run.

The UV absorption in the spectrum of 1915 Quetzälcoat1 (Figure 3) is a CT band. The mid-visible absorption band in the 0.6- μm region is a spin-forbidden crystal field transition of a transition element other than iron. The 0.9 μm band is a spin-allowed, laporte forbidden crystal field transition of ferrous iron in a low Ca, low Fe pyroxene. There is little to no evidence of opaques, metals or olivine (Figure 4).

The UV absorption edge assignment is based on the non-linear nature of the absorption (Gaffey and McCord, 1979), its strength relative to unity at 0.56 μm and the position of the band center being at a wavelength $\leq 0.35 \mu\text{m}$. The mid-visible absorption band at approximately 0.60 μm is commonly attributed to olivine, however the 0.9- μm band is not broad enough or positioned at the appropriate wavelength to indicate the presence of olivine. In laboratory spectra of some eucrites (e.g., Figure 28) there is a similar band which must be attributed to a transition element in pyroxene (possibly chromium, although the abundance of transition elements has not been systematically correlated with this spectral feature). There is no such absorption feature in lunar pyroxenes measured by Hazen et al. (1978) nor in spectra of pure plagioclase, the other component in eucrites. Additional evidence is needed to constrain the assignment of a specific cation in a specific crystal structure.

The position of the 0.9- μm band in the spectrum of Quetzàlcoatl eliminates all minerals except low Ca, low Fe pyroxene and ferric oxides. The band position is in the region of overlap between these two crystal structures. This spectrum also has additional features commonly found in ferric oxide minerals, notably an absorption in the mid-visible and a strong UV absorption. The distinguishing characteristics between ferrous and ferric iron, are the relative strengths of these bands and the slope of the UV absorption. Figure 29 shows comparisons of the spectrum of 1915 Quetzàlcoatl with ferric oxide spectra, clays and mixtures of ferric oxides and clay minerals (Singer, 1982). Examination of Figure 29 shows that the UV absorption is stronger, the slope is higher, and the 0.9- μm absorption is weaker in ferric oxide-bearing minerals than in the spectrum of 1915 Quetzàlcoatl. If the particle size of the ferric iron-bearing minerals were to be larger than samples (<38

microns) measured by Singer (1982), then the spectral contrast and the specular component would be reduced because particle sizes $<38\mu\text{m}$ produce the greatest spectral contrast in these minerals. Larger ferric iron particle size would reduce the slope of the UV absorption, perhaps bringing it into agreement with that of Quetzàlcoatl, but at the same time the depth of the $0.9\text{-}\mu\text{m}$ band would be reduced. This is not consistent with the observations of 1915 Quetzàlcoatl. If a spectrally opaque material were added to a ferric oxide, the UV absorption slope would be reduced but so would the intensity of the other absorption bands. In conclusion, the spectral signature of 1915 Quetzàlcoatl is not that of a ferric iron-bearing mineral in an octahedral crystal site. Furthermore, ferric iron-bearing minerals can be distinguished from ferrous iron-bearing minerals based on the relative intensity of the absorption bands and the UV slope even when they both have absorptions in the $0.9\text{-}\mu\text{m}$ region. This is contrary to the inference of Morris and Neely (1981) that absorptions previously interpreted as ferrous iron bands may indeed be ferric-iron absorptions. Because the band position in the spectrum of 1915 Quetzàlcoatl is at the short wavelength end of the range observed in pyroxenes, the composition of the pyroxene is low Fe and low Ca orthopyroxene as determined from the pyroxene calibration of Adams (1974). The JHK data (Veeder et al., 1982, Table III, Figure 4) are consistent with an orthopyroxene-dominated assemblage because the reflectance at 1.6 and $2.2 \mu\text{m}$ are the same within the errors of the measurements (Figures 20-22). This is not the case when significant amounts of clinopyroxene are present (Figures 21,22). The JHK data also indicate that there is an olivine component present of less than 50% by weight (Figure 20). This interpretation is based on the fact that the relative reflectance at $1.25 \mu\text{m}$ is less than at 1.6 and $2.2 \mu\text{m}$. In pure orthopyroxene assemblages this would not be the case. Therefore, if

olivine is the IR reddening agent, it is present in amounts less than 50% by weight. A third or totally different component must be present to account for the albedo of 1915 Quetzàlcoatl.

The spectrum of 1915 Quetzàlcoatl does not have the characteristics of a laboratory sample of pure orthopyroxene ground to particle sizes ranging from <30 - 150-250 microns measured at room temperature (Figures 14 b,c). The bandwidth is narrower and the depth is less than laboratory spectra of pure orthopyroxenes. Possible factors affecting these parameters include particle shape, packing, viewing geometry, temperature, size, the presence of additional components and shock. Consideration of these factors leads to the conclusion that the spectrum of 1915 Quetzàlcoatl is that of a shocked orthopyroxene assemblage by elimination of other possibilities.

Discussion: Particle shape and packing - 1915 Quetzàlcoatl has the reduced albedo expected from increased internal reflections of spherical particles (Adams and Felice, 1967), however the spectral contrast is not enhanced with respect to powders of orthopyroxenes which normally have prismatic morphology. Therefore particle sphericity is not the cause of the observed differences. For the same reason that particle shape differences don't account for the differences between the spectra under discussion, particle packing also cannot explain the differences.

Phase angle - Because both the laboratory sample and the asteroid spectrum were taken near 0° phase (Table I) there are no viewing geometry differences to attribute to the spectral differences between pure orthopyroxene and 1915 Quetzàlcoatl.

Temperature - The temperature at the surface of Quetzàlcoatl is calculated to be about 252K with an albedo of 0.23 (calculated from the standard radiometric model, Morrison, 1977). Therefore some bandwidth reduction can be expected relative to room temperature spectra (Sung et

al., 1977). The reduction in band depth with temperature (Figure 16a) is not large enough (Singer and Roush, 1982) to account for the reduced band depth in the spectrum of Quetzàlcoat1 relative to pure orthopyroxene.

Particle size - The albedo of 1915 Quetzàlcoat1 (0.23, Veeder, personal communication, Table III) is not high enough to be a pure orthopyroxene assemblage unless the particle size is large (Figure 14b). The reflectance of large particles (150-250 μm) in the bottom of the band is not high enough to be attributed to larger particle sizes (Figure 14b). When scaled to unity at 0.56 μm (Figure 14c) the relative band depth of large particle sizes is larger than 1915 Quetzàlcoat1.

Additional components - The relative strength of the spin forbidden absorption compared to the 0.9- μm band depth indicates that there is no additional component reducing the spectral contrast of the spectrum. A non-specific opaque material would reduce spectral contrast in both the UV and IR regions. A small phyllosilicate component would effectively mask the NIR absorption band while at the same time contribute to the UV absorption. The spectra of carbonaceous chondrites serve as an analogue for a phyllosilicate dominated spectrum with a ferro-magnesian silicate component (Gaffey, 1976). Such spectra (Figure 23b) retain the UV absorption, and have a shallow 0.9- μm band. However, the albedo of a mixture of pyroxene and phyllosilicates cannot be reduced to 0.23 and retain the necessary spectral contrast. The JHK data support the presence of an olivine component but do not explain the albedo, narrow band width and reduced band depth relative to pure orthopyroxene.

Shock - From a comparison of the spectra of shocked and unshocked enstatite orthopyroxene (Adams et al., 1979, Figure 21) with that of 1915 Quetzàlcoat1, it looks like this mechanism could produce a spectrum with the observed features. Shock-diagnostic features remain to be

determined. This interpretation is based on elimination of other possible causes and a general agreement between observed and laboratory measurements of shocked minerals. The surface of 1915 Quetzàlcoat1 is most likely a shocked assemblage of predominantly orthopyroxene with some olivine.

Meteoritic analogues - Based on interpretation of the visible reflectance spectrum alone, the meteoritic analogue to 1915 Quetzàlcoat1 is a diogenite, a monomineralic orthopyroxene assemblage. The JHK data do not support this interpretation because the reflectance at 1.25 μm is lower than at 1.6 and 2.2 μm (see Figure 20). A diogenite assemblage has a higher reflectance at 1.25 μm than at 1.6 and 2.2 μm (see Gaffey, 1976). There are no known meteorite types with olivine present in abundances between the trace amounts found in diogenites (which is not evident in reflectance spectra of diogenites) and ordinary chondrites. The spectrum of 1915 Quetzàlcoat1 cannot be interpreted as an ordinary chondrite assuming that the spectrum of the parent body and laboratory meteorite sample are to be similar.

1943 Anteros

The 8-color data for two days (Figure 3) and JHK spectrum of 1943 Anteros was published by Veeder et al. (1981, Figure 4). The UV and NIR absorption edges are consistent with the presence of mafic silicates, predominantly olivine as evidenced by the position of the NIR maximum reflectance at 0.82 μm , the band minimum beyond 1.06 μm and the fact that the reflectance at J relative to H is low. Pure plagioclase also has an absorption band centered at about 1.25 μm , but the albedo (0.80) is much higher than 1943 Anteros (Table III). The lower reflectance of K relative to H is a low resolution expression of a 2.0- μm clinopyroxene band. The clinopyroxene component ranges from 0-25% based on

laboratory data of Singer (1982) (Figures 20-22) and the measurement errors. The albedo (0.18, Veeder et al., 1981, Table III) indicates that either the particle size is very large, an opaque is present or the asteroid has been severely shocked. The spectral contrast is high which would eliminate the presence of a significant opaque component. The contribution of shock cannot be evaluated with the existing data. Further constraints are needed to discriminate between shock and particle size effects.

Meteoritic analogues - Meteorite classes composed of predominantly olivine and clinopyroxene include ureilites, nakhlites, winonaites (Prinz et al. 1980), and the type exemplified by ALHA77005. Higher resolution data are needed to discriminate between these meteorite types. The question of a meteoritic analogue remains open.

2100 Ra-Shalom

The spectrum of 2100 Ra-Shalom (Figure 3) has the same spectral characteristics as that of 887 Alinda. However, there are differences between the two. The albedo is lower (0.05 Lebofsky and Veeder, personal communication, Table III), the 0.9- μm band is weaker and less well defined and the UV absorption edge is weaker. These differences are consistent with the presence of more opaques relative to 887 Alinda. The strength and position of the edge of the UV absorption as compared to 1580 Betulia for example, implies the presence of phyllosilicates which have a UV absorption that persists when other absorptions are masked (e.g., compare with C2 carbonaceous chondrites in Figure 23). The surface composition is therefore a mafic silicate, olivine and/or pyroxene and phyllosilicates. The limited IR data which are not tied into a V magnitude (Figure 4) are consistent with this interpretation.

Meteoritic analogues - The low albedo of 2100 Ra-Shalom (0.05) limits the possible meteoritic analogues to carbonaceous chondrites. The C3 carbonaceous chondrites are brighter and contain smaller amounts of phyllosilicates than C2's. The C2's are generally darker than 2100 Ra-Shalom, due to the presence of more opaque carbonaceous material. 2100 Ra-Shalom has spectral features and albedo intermediate between the C2's and C3's of the meteorite types.

2201 1947XC

The available data (Figures 3 and 4) on this asteroid are difficult to interpret due to an eclectic set of data and no albedo determination. The conventional interpretation is as follows: the NIR absorption band is indicative of the presence of mafic silicates. The short wavelength position of the reflectance maximum at $0.60\mu\text{m}$ is indicative of a spectrally dominant olivine component with a fayalite content intermediate between Fa_{15} and Fa_{1a3} (Figure 13). From here the interpretation encounters contradictions. The UV reflectance is greater than unity relative to the reflectance at $0.56\mu\text{m}$. This feature is not seen in any known, common rock-forming mineral. To confuse matters, the UVB photometry of this asteroid measured by Bowell and Harris (IAUC3436) 12/16-17/79 (Figure 3) does not indicate any unusual behavior for an asteroid. The NIR band looks like the first of the three olivine bands if the point to point scatter is considered noise. Because the standard deviation of the data from an average of 50 spectra measured on two days is smaller than the difference between data points, it is difficult to call the results noise (see Appendix A). The JHK data are not consistent with a dominant olivine component because the J reflectance is similar to that at H and K (Figure 4). Instead, the JHK data alone are consistent with a dominant orthopyroxene or a mafic silicate and opaque

assemblage (Figures 8, 20-22). The IR data with 1.5% wavelength resolution (Soifer et al., personal communication) are consistent with this suggested interpretation (Figure 4). However, the UV, VIS and NIR data contradict the IR data.

The possibility of interpreting this spectrum in terms of features from low level cometary activity is considered for four reasons. The first being the difficulty interpreting the spectrum in terms of asteroidal material, secondly the orbit of 2201 1947XC has a high eccentricity and is therefore more comet-like than asteroid-like, and Drummond (1982) finds a possible association between a meteor stream and this asteroid. The fourth possible hint of a cometary source is that the rotation period has been reported to be a multiple of 24 hours (Harris, personal communication). A long rotation period can be explained by outgassing forces which could reduce the angular momentum of the object. This explanation is by no means unique.

Three comets (Comet Bennett 1969i, Johnson et al., 1971, Comet Arend-Rigaux, Chapman personal communication, and Comet Kobayashi-Berger-Milon 1975H, Chapman and Gaffey, personal communication) at varying stages of activity have been measured with the same instrument used for measurements of 2201 1947XC. These spectra are shown in Figure 30. Comet Ashbrook-Jackson (Newburn et al., 1981) was measured with the same instrument using filters with band centers and bandwidths coincident with cometary emission bands. Danks and Dennefeld (1981) report a near-infrared spectrum of 19791, Comet Bradfield. None of these spectra have features identical to 2201 1947XC. There is no definitive cometary spectral signature as can be seen from the diversity of the spectra in Figure 30. Instead we look for individual features seen in comet spectra and in that of the asteroid. There is no CN or C₃ emission in 2201 1947XC. These strong bands are located at 0.388 and 0.405 μ m

respectively, (Wurm, 1963). A high relative reflectance in Comet 1975H (Figure 30) at these wavelengths indicate their presence. An NH emission band occurs at $0.336\mu\text{m}$. A test of the presence of this molecule as a cause of the high UV reflectance in 2201 1947XC could be made knowing the conditions under which this emission is seen compared to the observing conditions of 2201 1947XC. Other cometary emission bands which might be seen in this asteroid are forbidden lines of oxygen at 0.56 and $0.63\mu\text{m}$ and additional NH_2 bands in the near-infrared. At present the spectral features seen in 2201 1947XC cannot be attributed to any cometary activity. It is worth pursuing this question further.

The discrepancy between the UBV photometry of Bowell and Harris (Figure 3) could be explained by the absence of cometary activity at the time of their observations when the asteroid was further from the sun (1.2 AU) than it was on 12/28-29/79 (1.07 AU) when spectral reflectance measurements were made.

Based on the available data of this asteroid, the spectrum does not show common rock-forming mineral signatures. Further applications of cometary physics will be made in the future to address the possible connection between weak cometary emission and the surface of this asteroid. Additional data should be collected in June, 1983, when the asteroid can be observed again.

1979VA

An interpretation of the data of 1979VA is made because there is both 8-color (Tedesco and Tholen, personal communication) and JHK photometric measurements (Hartmann et al., 1982). Unfortunately, there is no albedo determination. The flat spectrum with a break in slope at $0.43\mu\text{m}$ is indicative of either large grains of mafic silicates, the presence of opaques or a low abundance of iron in silicate(s). An

albedo measurement will differentiate between the first two and the third possibility. The JHK data show a rapid increase in reflectance between 1.6 and 2.2 μ m. This may be due to the presence of high-iron olivine (Figure 11b, Hunt et al., 1970), small grains of magnetite (Hunt et al., 1970), or carbon (Miyamoto et al., 1982) that are transparent in the IR.

Meteoritic analogues - If the surface of this asteroid is large-grained fayalite, then there is no meteoritic analogue. There is no meteorite spectrum with the observed spectral features through the VIS and IR. Most meteorites have a lower slope in the IR.

1980AA

The 0.9- μ m band and the UV absorption are characteristic of the presence of mafic silicates (Figure 3). The inflection in the visible seen in 1685 Toro, 1862 Apollo and 1915 Quetzàlcoatl is not present in this spectrum. The observed spectral contrast indicates the presence of opaques or a low abundance of iron in the silicates. There is no albedo measurement to constrain these two interpretations. A high albedo would support the low iron interpretation, while a low albedo supports the presence of abundant opaques.

Meteoritic analogues - The strength of the 0.9- μ m and UV absorption bands eliminates all but two types of achondrites as possible meteoritic analogues (Figure 23b). These two possible analogues are eliminated on additional criteria. Aubrites are eliminated because their absorption bands are too weak, and ureilites are eliminated on the basis of the presence of the prominent inflection in the visible (0.50 μ m) which is not seen in the spectrum of 1980AA. Future observations should verify the absence of this feature. Carbonaceous chondrites types C1 and C2 are eliminated because the 0.9- μ m band of 1980AA is too strong. The C3's

are eliminated because the slope of the UV absorption is too low in 1980AA. absorption significantly to be a possible explanation of the Particle size could be a possible explanation of the differences between 1980AA and C3's (Figure 14) based on the strength of the UV absorption alone. The NIR band is not strong enough to support a large particle size interpretation. The slope of the UV absorption edge also eliminates ordinary chondrites which have distinctly non-linear UV slopes. Additionally, the depth of the 0.9 μ m band also eliminates the higher metamorphic grade ordinary chondrites. Enstatite chondrites have a weaker 0.9- μ m absorption band and stronger UV band than 1980AA. The only meteoritic analogue is shocked, black chondrites which have a linear UV absorption edge and a moderate to weak 0.9- μ m absorption band (Figure 23b). If the 0.70- μ m band in 1980AA is real however, then black, shocked chondrites are not appropriate analogues. Another test of this interpretation is that the albedo should be between 5 and 10%.

1981QA

1981QA has similar spectral features as 2100 Ra-Shalom and 887 Alinda (Figure 3). The UV absorption is stronger than 2100 Ra-Shalom but the position of the break in slope and the 0.9- μ m region reflectance are similar. The petrologic assemblage therefore consists of a mafic silicate with either an opaque or metallic component. An albedo measurement would constrain these two possibilities, however there is none available to the best of my knowledge. 8-color photometry of this asteroid (Tedesco and Tholen, personal communication) indicates the presence of possibly shocked olivine or low-Fe olivine. Additional measurements are needed.

Meteoritic analogues - The meteoritic analogue based on narrow band reflectance measurements is either a C3 or E6 chondrite. An aubrite and

stony-iron analogue is eliminated because the NIR relative reflectance is not as high as in these meteorites (Gaffey, 1976). According to the 8-color photometric measurements (Tedesco and Tholen, personal communication) alone, there is no meteoritic analogue.

Bias Considerations

Is it possible to relate the significance of these results to the real population of near-Earth asteroids? This poses some formidable problems. One possible factor in the apparent albedo bias of near-Earth asteroids is the use of the standard radiometric model (Morrison, 1977). This model fails for some asteroids and results in an erroneously high albedo. More accurate modelling of the surface properties of 433 Eros (Lebofsky and Rieke, 1979) and 2100 Ra-Shalom (Lebofsky, personal communication) result in lower albedos than derived from the standard radiometric model. Some of the high albedos measured for near-Earth asteroids are real, however, because the results of 10- and 20- μ m radiometry and polarimetry are in agreement (e.g., 1862 Apollo). The contribution of thermal properties to the apparent albedo bias is resolvable with measurements at 10- and 20- μ m and polarimetry.

The question of brightness bias cannot be addressed without some indication of their source region. For example, if many of the near-Earth asteroids originate from the inner asteroid belt, then the observed predominance of bright objects would be real, as the inner belt is dominated by bright asteroids (e.g., Gradie and Tedesco, 1982). However, this determination cannot be made with the benefit of bias correction. Therefore, there is no reason to assume any proportion of bright objects to dark objects.

Is there any observational selection as a function of orbital elements other than semi-major axis? There are presently 66% more known

objects in low inclination or low eccentricity orbits than in orbits with inclinations $>10^{\circ}$ or eccentricity >0.50 . Clearly, high inclination and eccentric orbits have shorter observing windows from Earth. Corrections for this bias must await discovery of more asteroids in high eccentricity and high inclination orbits.

Bias correction methods used by Zellner (1979) are not applied to near-Earth asteroids because their bias is a function of discovery circumstances. Perhaps corrections for observational bias can be made based on discovery circumstances. Zones of distance from the Earth at the time of discovery can be defined in 0.01 A.U. bins. A correction to the known population can be made by calculating a bias factor as the number of discovered asteroids present in that zone relative to the total number of near-Earth asteroids of known surface composition. This correction assumes that the bias is a function of size only. Such a bias is suspected, as only three known near-Earth asteroids have albedos below 0.06. A look at the known population as a function of distance from the Earth at discovery and albedo will determine whether or not the albedo bias is size dependent. This approach will be more accurate than binning the asteroids according to the discovery magnitude, as such magnitudes are not photometrically determined and there is considerable personal bias in these estimates.

As of November, 1982, 25% of each group of the known Apollo, Amor and Aten asteroids have been mineralogically characterized. Upon addressing some of the questions discussed above we will have a better idea of how well the observed population represents the true population. I would not be surprised if compositionally dark objects in the near-Earth population are truly unusual.

Population Characterization

A summary of the mineralogical components of the observed near-Earth asteroid population is presented in Table IV. The present data base does not reveal any significant differences in mineralogy or petrology between the Apollo, Amor and Aten asteroids as individual dynamical groups. The presence of rare or unusual minerals does not have to be invoked to interpret the spectra except in a few cases in which there is considerable observational uncertainty. With the possible exception of 2201 1947XC, these objects are composed of cosmically abundant minerals commonly found on asteroid surfaces and in meteorite assemblages. The proportions of these minerals and their chemistry that combine to form these assemblages and the physical nature of their surfaces, are for the most part different from most main belt asteroids and meteorite assemblages that have measured reflectance spectra.

Mafic silicates dominate all but three spectra of near-Earth asteroids measured to date (1580 Betulia, 1979VA and probably 2201 1947XC). This dominance of mafic silicates is interpreted from the presence of strong UV and NIR absorption bands and/or albedos usually higher than 0.010 (2100 Ra-Shalom has a lower albedo but a strong UV absorption band). This is contrary to the situation existing among the observed main belt asteroids (Chapman and Gaffey, 1979). Possible explanations for this include: mineralogical or textural differences, surface weathering processes (or lack thereof) or observational bias. Each of these possibilities will be discussed.

The spectra can be interpreted as having larger proportions of mafic silicates than main belt asteroids. However, they are not pure silicates as evidenced by the fact that the albedo and NIR absorption band strengths are lower than laboratory mixtures of pure silicates. One way to produce an apparently larger proportion of silicates is to have less opaques present. It is difficult to invoke a mechanism in

which opaques are preferentially lost from main belt parent bodies in the process of near-Earth asteroid formation, assuming near-Earth asteroids are fragments from main belt objects. If the particle size alone were larger on near-Earth asteroids, then the albedo would be lower in the presence of strong absorption bands. Smaller particle size would result in higher albedo but lower spectral contrast compared to main belt asteroids. Particle shape, packing and porosity result in differences much smaller than the observed differences between near-Earth asteroids and the majority of the observed main belt asteroids. The observed enhanced spectral contrast is analogous to the observed higher spectral contrast in younger craters on the Moon. Therefore, the near-Earth asteroids may exhibit higher spectral contrast and albedo by virtue of their being fresh, unweathered material. This observation is consistent with the dynamical calculations of short mean life times of near-Earth asteroids and the assumption that these asteroids are younger fragments of parent bodies that have or had weathered or protected surfaces prior to the event that brought them into near-Earth orbit. If the orbital change took an evolutionarily significant period of time, surface maturation is precluded in this time interval.

None of these asteroids have reflectance spectra dominated by the signature of large grains of unoxidized metal. These spectra would have a reflectance increasing with wavelength throughout the observed spectral range and low contrast absorption bands. The absence of large-grained metal assemblages implies that these asteroids are not fragments representing the boundary between the core and mantle of differentiated bodies. The presence of fine-grained metal with an oxide coating cannot be distinguished from other opaques. Such metal grains may be present but cannot be discriminated from other opaques.

The composition of 1915 Quetzàlcoat1 indicates that at least one of these asteroids is a fragment of a differentiated body. This is the second basaltic achondrite analogue found among the asteroids. It fills a gap in the observed size range of these objects. Dynamical mechanisms are now needed to connect basaltic achondrites, 1915 Quetzàlcoat1 and 4 Vesta. If a dynamical connection cannot be made then the presence of 1915 Quetzàlcoat1 would indicate that the basaltic achondrite parent body is now the size of this 0.14 km body. Objects of this size are usually below our detection limits. Whether or not other members of this population are undifferentiated or differentiated cannot be answered presently. Perhaps the presence or absence of a shallow mid-visible absorption band might address this question. Further study is needed.

Assuming that meteorite analogues would have the same spectral characteristics as meteorites measured in the lab, there is considerably more compositional diversity among the near-Earth asteroids compared to the meteorite population. The presence of only two ordinary chondrite analogues among the observed near-Earth asteroids is disproportionate to the number of ordinary chondrite meteorites. This supports the hypothesis that the ordinary chondrite parent bodies are few in number. It is also probable that the asteroids supplying the ordinary chondrites have not been found. The orbital elements of 1980AA are not similar to those calculated for the Farmington meteorite, also a black chondrite (Levin et al., 1976). The orbit of 1862 Apollo, the other ordinary chondrite analogue, does not have an aphelion near Jupiter, a criterion for an ordinary chondrite orbit (Wetherill, 1969).

If future measurements of 2201 1947XC indicate that it does show signs of weak cometary activity, the hypothesis and dynamical arguments indicating that some near-Earth asteroids are cometary nuclei will have some observational support. Presently the data are only suggestive and

further attempts to explain the observed features in terms of the physics of a cometary phenomenon will be made in the future.

References

Adams, J.B. (1974). Visible and near-infrared diffuse reflectance of pyroxenes as applied to remote sensing of solid objects in the solar system. **J. Geophys. Res.**, **79**, 4829-4836.

Adams, J.B. and Felice, A.L. (1967). Spectral reflectance 0.4 to 2.0 microns of silicate rock powders. **J. Geophys. Res.**, **72**, 5705-5715.

Adams, J.B. and Jones, R.L. (1970) Spectral reflectivity of lunar samples. **Science**, **167**, 737.

Adams, J.B. and Goullaud, L.H. (1978) Plagioclase feldspars: Visible and near infrared diffuse reflectance spectra as applied to remote sensing. **Proc. Lunar Planet. Sci. Conf. 9th**, 2901-2909.

Adams, J.B., Horz, F., and Gibbons, R.V. (1979) Effects of shock-loading on the reflectance spectra of plagioclase, pyroxene and glass. **Lunar and Planet.**, **X**, 1-2.

Arnold, J.R. (1964) The origin of meteorites as small bodies. In Isotopic and Cosmic Chemistry, ed., H. Craig, S.L. Miller, and G.J. Wasserburg, North-Holland Publ. Co., Amsterdam, 347-364.

Bill, H. and Calas, G. (1978) Color centers, associated rare-earth ions and the origin of coloration in natural fluorites. **Phys. Chem. Minerals**, **3**, 117-131.

Bowell, E., Gehrels, T., and Zellner, B. (1979) Appendix VII. Magnitudes, colors, types and adopted diameters of the asteroids. In Asteroids, T. Gehrels, ed. The University of Arizona Press, Tucson, 1108-1129.

Burns, R.G. (1970) Mineralogical applications of crystal field theory, Cambridge University Press, Cambridge.

Burns, R.G. (1970a) Crystal field spectra and evidence of cation ordering in olivine minerals. **Am. Mineral.**, 55, 1608-1632.

Burns, R.G. (1981) Intervallence transitions in mixed-valence minerals of iron and titanium. **Ann. Rev. Earth Planet. Sci.**, 9, 345-383.

Chapman, C.R. (1976) Asteroids as meteorite parent bodies: The astronomical perspective, **Geochim. Cosmochim. Acta**, 40, 701-719.

Chapman, C.R. and Morrison, D. (1976) J,H,K photometry of 433 Eros and other asteroids, **Icarus**, 28, 91-94.

Chapman, C.R. and Gaffey, M.J. (1979) Reflectance spectra for 277 asteroids. In Asteroids, T. Gehrels, ed., The University of Arizona Press, Tucson, 655-687.

Chapman, C.R., McCord, T.B., and Pieters, C. (1973) Minor planets and related objects. X. Spectrophotometric study of the composition of (1685) Toro. **Astron. J.**, 78, 502-505.

Chapman, C.R., Morrison, D., and Zellner, B. (1975) Surface properties of asteroids: A synthesis of polarimetry, radiometry and spectrophotometry. *Icarus*, **25**, 104-130.

Clark, R.N. (1980) A large scale interactive one dimensional array processing system. *Publ. Astron. Soc. Pacific*, **92**, 221-224.

Clark R.N. (1981) The spectral reflectance of water-mineral mixtures at low temperatures. *J. Geophys. Res.*, **86**, B4, 3074-3086.

Clark, R.N. (1982) Implications of using broadband photometry for compositional remote sensing of icy objects. *Icarus*, **49**, 244-257.

Danks, A.C. and Dennefeld, M. (1981) Near-infrared spectroscopy of comet Bradfield 19791. *Astron. J.*, **86**, 314-317.

Degewij, J., Cruikshank, D.P., and Hartmann, W.K. (1980) Near-infrared colorimetry of J6 Himalia and S9 Phoebe: A Summary of 0.3- to 2.2 μm reflectances. *Icarus*, **44**, 541-547.

Dodd, R.T. and Jarosewich, E. (1979) Incipient melting in and shock classification of L-group chondrites. *Earth and Planet. Sci. Lett.*, **44**, 335-340.

Drummond, J.D. (1982) Theoretical meteor radiants of Apollo, Amor, and Aten asteroids. *Icarus*, **49**, 143-153.

Dunlap, J.L. (1974) Minor planets and related objects. XV. Asteroid (1620) Geographos. **Astron. J.**, **79**, 324-332.

Dunlap, J.L., Gehrels, T., and Howes, M.L. (1973) Minor planets and related objects. IX. Photometry and polarimetry of (1685) Toro. **Astron. J.**, **78**, 491-501.

Eaton, N., Green, S.F., McCheyne, R.S., Meadows, A.J., and Veeder, G.J. (1982) Observations of asteroids in the 3-4 μm region.

Feierberg, M.A., Larson, H.P., and Chapman, C.R. (1982) Spectroscopic evidence for undifferentiated S-type asteroids. **Astrophys. J.**, **257**, 361-372.

Fink, U. and Burk, D. (1973) Reflection spectra, 2.5-7 μ , of some solids of planetary interest. **Comm. LPL no. 185**, **10**, 8-20.

Floran, R.J., Prinz, M., Hlava, P.F., Keil, K., Nehru, C.E., and Hinthorne, J.R. (1978) The chassigny meteorite: a cumulate dunite with hydrous amphibole-bearing melt inclusions. **Geochim. Cosmochim. Acta**, **42**, 1213-1229.

Gaffey, M.J. (1976) Spectral reflectance characteristics of meteorite classes. **J. Geophys. Res.**, **81**, 905-920.

Gaffey, M.J. and McCord, T.B. (1978) Asteroid surface materials: Mineralogical characterizations from reflectance spectra. **Space Sci. Rev.**, **21**, 555-628.

Gaffey, M.J. and McCord, T.B. (1979) Mineralogical and petrological characterizations of asteroid surface materials. In Asteroids, T. Gehrels, ed., The University of Arizona Press, Tucson, 688-723.

Gehrels T., Roemer, E., Taylor, R.C., and Zellner, B.H. (1970) Minor Planets and related objects. IV. Asteroid (1566) Icarus. **Astron. J.**, 75, 186-195.

Gradie, J. and Veverka, J. (1983) The wavelength dependence of phase coefficients. **Icarus**, Submitted for publication.

Gradie, J. and Veverka, J. (1981) Effects of body shape on disk-integrated spectral reflectance. **Proc. Lunar Planet. Sci.**, 12B, 1769-1779.

Gradie, J. and Tedesco, E. (1982) Compositional structure of the asteroid belt. **Science**, 216, 1405-1407.

Gradie, J., Veverka, J. and Buratti, B. (1980) The effects of scattering geometry on the spectrophotometric properties of powdered materials. **Proc. Lunar Planet. Sci. Conf. 11th**, 799-815.

Hardorp, J. (1981) The sun among the stars V. A search for solar spectral analogs. **Astron. and Astrophys.**, 105, 120-132.

Hartmann, W.K., Cruikshank, D.P., and Degewij, J. (1982) Remote comets and related bodies: VJHK colorimetry and surface materials. **Icarus**, 52, 377-408.

Hazen, R.M., Mao, H.K., and Bell, P.M. (1977) Effects of compositional variation on absorption spectra of lunar olivines. **Proc. Lunar Sci. Conf. 8th**, 1081-1090.

Hazen, R.M., Bell, P.M., and Mao, H.K. (1978) Effects of compositional variation on absorption spectra of lunar pyroxenes. **Proc. Lunar Planet. Sci. Conf. 9th**, 2919-2934.

Hecht, E., and Zajac, A. (1976) Optics, Addison-Wesley, Reading, MA.

Hunt, G.R. and Salisbury, J.W. (1970) Visible and near-infrared spectra of mineral and rocks: I. Silicates minerals. **Modern Geol.**, 1, 283-300.

Hunt, G.R., Salisbury, J.W., and Lenhoff, C.J. (1971) Visible and near-infrared spectra of minerals and rocks: III. Oxides and hydroxides. **Mod. Geol.**, 2, 195-205.

Hunt G.R., Salisbury, J.W., and Lenhoff, C.J. (1971a) Visible and near-infrared spectra of minerals and rocks: IV. Sulphides and sulphates. **Mod. Geol.**, 3, 1-14.

Hunt, G.R., Salisbury, J.W., Lenhoff, C.J. (1972) Visible and near-infrared spectra of minerals and rocks: V. Halides, phosphates, arsenates, vanadates and borates. **Mod. Geol.**, 3, 121-132.

Hunt, G.R., Salisbury, J.W., and Lenhoff, C.J. (1973) Visible and near infrared spectra of minerals and rocks: VI. Additional silicates. **Mod. Geol.**, 4, 85-106.

Hunt, G.R., Salisbury, J.W., and Lenhoff, C.J. (1974) Visible and near infrared spectra of minerals and rocks: IX. Basic and ultrabasic igneous rocks. **Mod. Geol.**, 5, 15-22.

Johnson, T.V. and Fanale, F.P. (1973) Optical properties of carbonaceous chondrites and their relationships to asteroids. **J. Geophys. Res.**, 78, 8507-8518.

Johnson, T.V., Lebofsky, L.A., and McCord, T.B. (1971) Comet Bennett 1969i: Narrow-band filter photometry 0.3-1.1 microns. **Pub. Astron. Soc. Pac.**, 83, 93-94.

Kittel, C. (1976) Introduction to Solid State Physics, John Wiley and Sons, New York.

Larson, H.P. and Veeder, G.J. (1979) Infrared spectral reflectances of asteroid surfaces. In Asteroids, T. Gehrels, ed., the University of Arizona Press, Tucson, 724-744.

Lebofsky, L.A. and Rieke, G.H. (1979) Thermal properties of 433 Eros. **Icarus**, 40, 297-308.

Lebofsky, L.A., Veeder, G.J., Lebofsky, M.J., and Matson, D.L. (1978) Visual and radiometric photometry of 1580 Betulia. **Icarus**, 35, 336-343.

Lebofsky, L.A., Lebofsky, M.J., and Rieke, G.H. (1979) Radiometry and surface properties of apollo, amor and aten asteroids. **Astron. J.**, 84, 885-888.

Lebofsky, L.A., Veeder, G.J., Rieke, G.H., Lebofsky, M.J., Matson, D.L., Kowal, C., Wynn-Williams, C.G. and Becklin, E.E. (1981) The albedo and diameter of 1862 Apollo. *Icarus*, **48**, 335-338.

Levin, B.J., Simonenko, A.N. and Anders, E. (1976) Farmington meteorite: A fragment of an Apollo asteroid. *Icarus*, **28**, 307-324.

Loeffler, B.M., Burns, R.G., Tossell, J.A., Vaughan, D.J., and Johnson, K.H. (1974) Charge transfer in lunar materials: interpretation of ultra-violet-visible spectral properties of the moon. *Proc. Lunar Sci. Conf. 5th*, 3007-3016.

Mao, H.K. (1976) Charge-transfer processes at high pressure. In The Physics and Chemistry of Minerals and Rocks, ed. R.G.J. Strens, Wiley and Sons, New York, 573-581.

Mao, H.K., and Bell, P.M. (1974) Crystal-field effects of trivalent titanium in fassaite from the Pueblo de Allende meteorite. *Carnegie Inst. of Wash. Yearbook*, 488-492.

McCord, T.B. (1968) A double beam astronomical photometer. *Appl. Opt.* **7**, 475-478.

McFadden, L.A., Gaffey, M.J., Takeda, H., Jackowski, T.L., and Reed, K.L. (1982) Reflectance spectroscopy of diogenite meteorite types from antarctica and their relationship to asteroids. *Proc. 7th Symp. Antarctic Meteorites*, ed. T. Nagata, National Institute of Polar Research, Tokyo, 188-206.

McSween, H.Y., Taylor, L.A., and Stolper, E.M. (1979) Allan Hills 77005: A new meteorite type found in Antarctica. **Science**, **204**, 1201-1203.

Miyamoto, M., Mito, A., Takano, Y. (1982) An attempt to reduce the effects of black material from the spectral reflectance of meteorites or asteroids. **Proc. 7th Symp. Antarctic Meteorites**, ed. T. Nagata, National Institute of Polar Research, Tokyo, 291-307.

Morris, R.V. and Neely, C. (1981) Diffuse reflectance spectra of pigmentary-sized iron oxides, iron oxyhydroxides and their mixtures: Implications for the reflectance spectra of Mars. **Lunar and Planet. Sci. XII**, 723-725.

Morrison, D. (1977) Asteroid sizes and albedos. **Icarus**, **31**, 185-220.

Morrison, D. and Zellner, B. (1979) Appendix V. Polarimetry and radiometry of the asteroids. In Asteroids, T. Gehrels, ed. The University of Arizona Press, Tucson, 1090-1097.

Nash, D.B. and Conel, J.E. (1974) Spectral reflectance systematics for mixtures of powdered hypersthene, labradorites, and ilmenite. **J. Geophys. Res.**, **79**, 1615-1621.

Newburn, R.L., Bell, J.F., and McCord, T.B. (1981) Interference-filter photometry of periodic comet Ashbrook-Jackson. **Astron. J.**, **86**, 469-475.

Ostro, S.J., Campbell, D.B., and Shapiro, I.I. (1983) Radar observations of asteroid 1685 Toro. **Astron. J.**, Submitted for publication.

Pieters, C., Gaffey, M.J., Chapman, C.R., and McCord, T.B. (1976) Spectrophotometry (0.33-1.07 μ m) of 433 Eros and compositional implications. **Icarus**, **28**, 105-115.

Prinz, M., Waggoner, D.G., and Hamilton, P.J. (1980) Winonaites: A primitive achondritic group related to silicate inclusions in IAB irons. **Lunar and Planet. Sci.**, **XI**, 902-904.

Shoemaker, E.M., Williams, J.G., Helin, E.F., and Wolfe, R.F. (1979) Earth-crossing asteroids: orbital classes, collision rates with Earth, and origin. In Asteroids, T. Gehrels, ed., The University of Arizona Press, Tucson 253-273.

Sill, G.T. (1973) Reflection spectra of solids of planetary interest. **LPL Comm.**, no. 184, 10, 1-7.

Singer, R.B. (1981) Near-infrared spectral reflectance of mineral mixtures: Systematic combinations of pyroxenes, olivine, and iron oxides. **J. Geophys. Res.**, **86**, 7967-7981.

Singer, R.B. (1982) Spectral evidence for the mineralogy of high-albedo soils and dust on Mars. **J. Geophys. Res.**, Submitted for publication.

Singer, R.B. and Roush, T.L. (1982) Effects of temperature on mafic mineral crystal-field absorptions, 0.4-2.6 μ m. **B.A.A.S.**, **14**, 727.

Smith, G., and Strens, R.G.J. (1976) Intervalence transfer absorption in some silicate, oxide and phosphate minerals. In The Physics and Chemistry of Minerals and Rocks, ed. R.G.J. Strens, Wiley and Sons, New York, 583-612.

Sung, C., Singer, R.B., Parkin, K.M., Burns, R.G., and Osborne, M. (1977) Temperature dependence of Fe^{2+} crystal field spectra: Implications to mineralogical mapping of planetary surfaces. **Proc. Lunar Sci. Conf. 8th**, 1063-1079.

Tedesco, E., Drummond, J., Candy, M., Birch, P., and Nikoloff, I. (1978) 1580 Betulia: An unusual asteroid with an extraordinary light curve. **Icarus**, 35, 344-359.

Veeder, G.J., Matson, D.L., Bergstralh, J.T., and Johnson, T.V. (1976) Photometry of 433 Eros from 0.65 to 2.2 μ m. **Icarus**, 28, 79-85.

Veeder, G.J., Tedesco, E.F., Tholen, D.J., Tokunaga, A., Kowal, C., Matthews, K., Neugebauer, G., and Soifer, B.T. (1981) The Diameter and albedo of 1943 Anteros. **Icarus**, 46, 281-284.

Veeder, G.J., Matson, D.L., and Kowal, C. (1982) Infrared (JHK) photometry of asteroids. **Astron. J.**, 87, 834-839.

Wagner, J.K., Cohen, A.J., Hapke, B.W., and Partlow, W.D. (1980) Vacuum ultraviolet reflectance spectra of groups L, LL, and E chondrites and of achondrites. **Proc. Lunar Planet. Sci. Conf. 11th**, 775-797.

Wetherill, G.W. (1969) Relationships between orbits and sources of chondritic meteorites. In Meteorite Research, ed., P.M. Millman, D. Reidel, Dordrecht, 573-589.

Wurm, K. (1963) The physics of comets. In The Moon Meteorites and Comets, eds., B.M. Middlehurst and G.P. Kuiper, The University of Chicago Press, Chicago, 573-617.

Zellner, B. (1979) Asteroid taxonomy and the distribution of the compositional types. In Asteroids, ed., T. Gehrels, The University of Arizona Press, Tucson, 783-808.

Zellner, B. and Gradie, J. (1976) Minor planets and related objects. XX. Polarimetric indications of albedo and composition for 94 asteroids. **Astron. J.**, **81**, 262-280.

Zellner, B., Wisniewski, W., Andersson, L. and Bowell, E. (1975) Minor Planets and related objects XVIII. UBV Photometry and Surface Composition. **Astron. J.**, **80**, 986-995.

Zellner, B., Andersson, L., and Gradie, J., (1977) UBV photometry of small and distant asteroids. **Icarus**, **31**, 447-455.

Table I

OBSERVING PARAMETERS

Name	Date	Observatory	Voltage	Aperture (")	β°
433 Eros	8/25-26/81	MKO 2.2m	1900	18	38
1627 Ivar	11/4-7/80	MKO 2.2m	1800	12	11
1685 Toro ^a	7/15/80	KPNO 2.1m	2000	b	40
1862 Apollo	11/15-17/80	MKO 2.2m	1800	12	62-78
1865 Cerberus	11/4-7/80	MKO 2.2m	1800	12	10-12
1915 Quetzàlcoatl	3/5-6/81	MKO 2.2m	1800	12	5-7
2100 Ra-Shalom	8/25-26/81	MKO 2.2m	1800	12	29-30
2201 1947XC	12/28-29/79	MKO 2.2m	1700	18	64
1980AA	1/26/80	MKO 2.2m	2000	20	6
1981QA	8/27-28/81	MKO 2.2m	1900	18	25

^aChapman, personal communication. ^bnot recorded.

Table II

PHOTOMETRY OF 17 NEAR-EARTH ASTEROIDS CONVERTED TO FLUX RELATIVE TO V

Name	$R_{U/V}$	$R_{B/V}$	$R_{J/V}$	$R_{H/V}$	$R_{K/V}$
433 Eros	0.54 \pm .01 ^a	0.79 \pm .01 ^a	1.3 \pm 0.1 ^m	1.5 \pm 0.1 ⁿ	1.7 \pm 0.1 ⁿ
887 Alinda	0.59 \pm .05 ^b	0.80 \pm .04 ^b			
1036 Ganymed	0.61 \pm .01 ^a	0.83 \pm .01 ^a			
1566 Icarus	0.56 \pm .05 ^c	0.86 \pm .04 ^c			
1580 Betulia	0.83 \pm .03 ^d	0.97 \pm .03 ^d			
1620 Geographos	0.54 \pm .03 ^e	0.80 \pm .02 ^e			
1627 Ivar	0.45 \pm .03 ^f	0.86 \pm .03 ^g			
1685 Toro	0.55 \pm .03 ^g	0.79 \pm .02 ^g	0.84 \pm .05 ^o	1.00 \pm .05 ^o	0.96 \pm .05 ^o
1862 Apollo	0.65 \pm .01 ^h	0.86 \pm .01 ^h	0.82 \pm .02 ^p	1.12 \pm .07 ^p	0.99 \pm .02 ^p
1865 Cerberus	0.72 ^h	0.87 ^h			
1915 Quetzâlcoat1	0.60 \pm .03 ⁱ	0.83 \pm .05 ⁱ	0.87 \pm .05 ^o	1.00 \pm .05 ^o	1.06 \pm .10 ^o
1943 Anteros	0.69 \pm .03 ^h	0.85 \pm .03 ^h	1.06 \pm .13 ^q	1.44 \pm .11 ^q	1.32 \pm .16 ^q
2100 Ra-Shalom	0.72 \pm .04 ^j	0.9101 ^j		1.00 \pm .05 ^r	1.05 \pm .04 ^r
2201 1947XC	0.36 \pm .03 ^k	0.84 \pm .02 ^k	1.03 \pm .06 ^s	1.00 \pm .07 ^s	0.97 \pm .06 ^s
1979VA	0.95 \pm .01 ^h	1.01 \pm .01 ^h	0.99 \pm .17 ^p	0.98 \pm .05 ^p	1.19 \pm .05 ^p
1980AA	0.64 \pm .01 ^l	0.85 \pm .02 ^l			
1981QA	0.66 \pm .03 ^h	0.87 \pm .03 ^h			

^aBowell et al., 1979.^bZellner et al., 1975.^cGehrels et al., 1970.

avg. of better observations.

^dTedesco et al., 1978.^eDunlap, 1974.^fZellner et al., 1977.^gDunlap et al., 1973.^hTedesco and Tholen, pers. comm.ⁱBinzel, pers. comm.^jBowell, IAUC3264.^kBowell and Harris, IAUC3436.^lHarris, IAUC3450.^mChapman and Morrison, 1976.ⁿVeeder et al., 1976.^oVeeder et al., 1982.^pHartmann et al., 1982.^qVeeder et al., 1981.^rLebofsky et al., 1978.^sSoiffer, et al., pers. comm.

Table III

PHYSICAL PARAMETERS OF 17 NEAR-EARTH ASTEROIDS

Name	$P_V(\text{rad})$	$P_V(\text{pol})$	d (km)	a	e	i
433 Eros	$0.125_{\pm}0.025^a$	0.20^b	39.3×16.1^a	1.458	0.219	10.77
887 Alinda	0.166^c	0.21^b	3.6^b	2.50	0.55	9.19
1036 Ganymed				2.66	0.54	26.45
1566 Icarus		0.30^d	1.04^d	1.08	0.83	22.91
1580 Betulia	0.03^e	0.046^f	6.3^f	2.19	0.49	52.04
1620 Geographos		0.16^g	2.4^g	1.24	0.34	13.33
1627 Ivar	0.23^h		6.2^h	1.86	0.40	8.44
1685 Toro		0.14^i	5.6^i	1.36	0.44	9.37
1862 Apollo	$0.21_{\pm}0.02^j$		$1.2-1.5_{\pm}0.1^j$	1.47	0.56	6.26
1865 Cerberus				1.08	0.47	16.09
1915 Quetzàlcoat1	0.23^h		0.14^h	2.53	0.58	20.5
1943 Anteros	0.18^k		2.0^k	1.43	0.26	8.7
2100 Ra-Shalom	0.05^l	$<0.06^m$	$>1.4^l$	0.83	0.44	15.7
2201 1947XC				2.18	0.71	2.5
1979VA				2.5	0.61	2.7
1980AA				1.86	0.43	4.1
1981QA				2.35	0.49	8.95

^aLebofsky and Rieke, 1979.

^bZellner and Gradie, 1976.

^cMorrison, 1977.

^dGehrels et al., 1970.

^eLebofsky et al., 1978

^fTedesco et al., 1978.

^gDunlap, 1974.

^hVeeder, pers. comm.

ⁱDunlap et al., 1973.

^jLebofsky et al., 1981.

^kRevised from Veeder et al., 1981, pers. comm.

^lLebofsky, pers. comm.

^mTedesco, pers. comm.

Table IV

MINERALOGICAL-PETROLOGICAL CHARACTERIZATION OF NEAR-EARTH ASTEROIDS

Name	Surface Type	Met. Anal.	Tax. Type
433 Eros	low-Ca pyx-ol shocked? opaque? N		S
887 Alinda	ol-pyx-opaque	C30	S
1036 Ganymed	mafic sil- opaque?	N	S
1566 Icarus	mafic sil	?	S
1580 Betulia	low-Fe sil-opaque	N	F
1620 Geographos	mafic sil-opaque	N	S
1627 Ivar	hi-Ca pyx?	N	S
1685 Toro	ol-pyx >75/25	N	S
1862 Apollo	ol-low-Ca-cpx-opaque or metal	LL4	S
1865 Cerberus	mafic sil?	?	S
1915 Quetzàlcoatl	opx shocked?	diogenite	S
1943 Anteros	ol>pyx	N	S
2100 Ra-Shalom	ol-pyx-phyllo-sil	C2-C3	C
2201 1947XC	?	N	U
1979VA	sil-opaque	N	C
1980AA	mafic sil-opaque?	Black chondrite	S
1981QA	mafic sil-opaque or metal	C3 or E6	PSM

pyx = pyroxene
 ol = olivine
 sil = silicate
 cpx = clinopyroxene
 opx = orthopyroxene
 phyllo-sil = phyllosilicate

Met. Anal. = meteoritic analogue
 N = none
 Tax. = taxonomic

Figure Captions

Figure 1: Plan view of some orbits of near-Earth asteroids. 1979XA=2201 1947XC.

Figure 2: 2100 Ra-Shalom via two calibrations. Data represented by solid boxes were reduced with 16 Cyg B as the standard star. Solid crosses connected with a solid line data were reduced with α Equ and an α Lyr/Sun ratio.

Figure 3: Compilation of available visible (0.33-1.0 μm) reflectance of near-Earth asteroids. Large, solid crosses represent UVB photometry converted to flux relative to V magnitude (references in Table II). When solid crosses extend beyond 0.55 μm , the data are 8-color photometry of Tedesco and Tholen. Reflectance is scaled to 1.0 at 0.56 μm .

Figure 4: JHK photometry is converted to flux relative to V for 433 Eros, 1979VA and 1862 Apollo and plotted with visible spectra. All other JHK reflectance is arbitrarily scaled to 1.0 at H since simultaneous V photometry was not obtained. The vertical scale can therefore be anywhere for these asteroids relative to the visible spectra. Broken vertical lines indicate a floating vertical scale for data to the right of the broken line.

Figure 5: Data representing four groups with similar spectral features. These data are presented for descriptive purposes only. 1627 Ivar 8-color data (Tedesco and Tholen) only shown.

Figure 6: a: Schematic representation of a point defect in a cubic

crystal lattice site, Kittel, 1976. b: Reflectance spectra of some color centers in fluorite, Hunt et al., 1972. c: Energy level schematic of a semi-conductor, Kittel, 1976. d: Reflectance spectra of sulphur showing the strong band edge characteristic of a semi-conductor, Hunt et al., 1971a.

Figure 7: (a) Spectrum of nickel powder showing continuous absorption of a metal conductor and a component of NiO which tends to lower the reflectance and flatten the spectrum, T.V.V. King, personal communication. (b) The plasma frequency edge of colored conductors. This phenomenon mimics the behavior of semi-conductors but the physics is different, Hecht and Zajac, 1976.

Figure 8: Mixtures of olivine and magnetite (Singer, 1981) and integrated to JHK bandpasses. Small amounts of opaque lowers the albedo drastically.

Figure 9: Top: Transmission spectra of biotite. Vertical scale is optical density, higher value means stronger absorption in a reflectance spectrum. Horizontal scale is frequency, the absorption band is at $0.73\mu\text{m}$. Decreasing temperature makes charge transfer absorptions stronger, Smith and Strens, 1976. Bottom: Transmission spectrum of polycrystalline pyroxene. Increasing pressure increases the strength of charge transfer bands, Mao and Bell, 1974.

Figure 10: Top: Energy level diagram of d-orbital electrons in three different fields, Burns, 1970. Bottom: Spectral reflectance of orthopyroxene. An expression of the splitting of d-orbital energy levels in an octahedral crystal field.

Figure 11: (a) Reflectance spectra of olivines. With increasing iron, the 0.60- μm band shifts to shorter wavelength, causing a shift in the position of maximum visible reflectance. Fa_{15} from Singer, 1981. Fa_{33} measured in this study. (b) A general trend of decreasing albedo with increasing iron abundance is illustrated in these olivine spectra, Hunt et al., 1970.

Figure 12: The effects of viewing geometry of four types of asteroidal material, Gradie et al., 1980. (a) If effects of phase were mistakenly ignored the mineralogical interpretation of these spectra would be the same at all phase angles. (b) Higher phase angle spectra would be interpreted as containing more sub-micron sized opaques or metallic component (which is probably what is happening as the path length increases on a basalt). (c) same interpretation as for a basalt. (d) At $d=120$ an increase in sub-micron-sized opaques would be invoked based on a mineralogical interpretation alone.

Figure 13: Reflectance spectra of different packing densities, Adams and Felice, 1967. If a mineralogical interpretation were made ignoring the physical differences, there would be no effect on the interpretation.

Figure 14: (a) The specular reflectance component has a significant effect on band depth compared to any discrete range of particle sizes, Gaffey, personal communication. (b) The range in albedo as a function of particle size is shown here, note the band is saturated at sizes ranging from 150-250 μ T.V.V. King, personal communication. (c) Scaled spectra from b. The largest difference in band depth occurs for smaller particle sizes, when the albedo is higher (b). If particle-size were

ignored, the 30- μ spectrum might be incorrectly interpreted as a lower iron pyroxene spectrum. However, the band position already indicates that the iron content is about as low as it can be in a pyroxene.

Figure 15: Effects of body shape for different materials, Gradie and Veverka, 1981. $\Delta M = \Delta \% \text{ Reflectance}$ for small values. (a) A difference in small-sized opaque abundance might be invoked to explain differences due to extreme body shape effects. (b) There would be no effect on the mineralogical interpretation due to body shape. (c) Mineralogical interpretation would not be effected.

Figure 16: (a) With increasing temperature the long-wavelength band edge gets broader, Singer and Roush, 1982. The band position does not change. (b) A condition mimicking a change in temperature is the addition of specific amounts of olivine (data from Gaffey, personal communication). Only these ratios mimic the temperature change in orthopyroxene. Comparisons were not made in the IR which probably eliminates the ambiguity.

Figure 17: Effects of shock on different silicates. The crystal structure is altered at different pressures for different minerals.

Figure 18: Shock criteria (Dodd and Jarosewich, 1979) L-group ordinary chondrites. (a) olivine fractured; plagioclase wholly or chiefly undeformed. (b) olivine fractured; undulose extinction, plagioclase wholly or chiefly undeformed. (c) same as for b but plagioclase largely to wholly deformed. (d) olivine fractured and mosaic extinction; plagioclase wholly deformed and/or maskelynite. (e) olivine fractured, with mosaic extinction and granulation; plagioclase largely or wholly

maskelynite. (f) olivine recrystallized; plagioclase maskelynite.

Figure 19: Shift in plagioclase peak with shock in VUV spectrum, Wagner et al., 1980 (peak at 200 nm is the epoxy in which the plagioclase was mounted.)

Figure 20: Olivine-Orthopyroxene mixtures (Singer, 1981) integrated to JHK transmission characteristics. The 2.0- μ m orthopyroxene band is centered between the H and K filter.

Figure 21: Olivine-Clinopyroxene mixtures (Singer, 1981) integrated to JHK transmission characteristics. The 2.0- μ m band appears as a low K reflectance relative to H. The reflectance of J remains less than H because of the longer wavelength position of clinopyroxene relative to orthopyroxene.

Figure 22: Clinopyroxene-orthopyroxene mixtures (Singer, 1981) integrated to JHK transmission characteristics. Clinopyroxene can be detected in amounts as low as 25% by the lower K reflectance relative to J and H.

Figure 23: (a) The effect of adding an opaque that is transparent (probably sub-micron-sized), Miyamoto et al., 1982. (b) Reflectance spectra of meteorite types from Gaffey, published in Chapman et al., 1975. Left: Chondrites: Ordinary chondrites: L6, LL, H, L4,5, L3, Black. Enstatite chondrites: E, Abee. Carbonaceous chondrites: C4, C3V, C2. Right: Achondrites: Diogenite: Diog. Howardite: How. Eucrite: Euc. Aubrite: Aub. Nahklite: Nak. Chassignite: Chas. Ureilite: Urei. Angrite: Ang. Stony-Iron: Mes. (mesosiderite).

Figure 24: Differences between spectra of C3V and C30 meteorites reflecting different chondrule-matrix ratio, opaque abundance and silicate chemistry, Gaffey, 1976.

Figure 25: Reflectance spectrum of diopside. The low iron abundance results in the charge-transfer band edge shifting to shorter wavelengths. The high calcium content expands the M2 octahedral site and results in the 0.9- μm band shifting to longer wavelengths. Therefore, there is a plateau in the mid-visible reflectance.

Figure 26: Derived spectra of Icarus (Gehrels *et al.*, 1970) (small points) and spectrum measured by Chapman and Gaffey, 1979 (squares) and UVB photometry Bowell *et al.*, 1979 (crosses). The variation in the spectrum as a function of phase angle is not the same as measured in the laboratory. However, since these were different apparitions, perhaps body shape or other factors contribute to the differences. More measurements should be made in the future.

Figure 27: Spectrum of 1685 Toro compared to L-type chondrites. The 0.9- μm band edge or band minimum is not characteristic of these meteorite types.

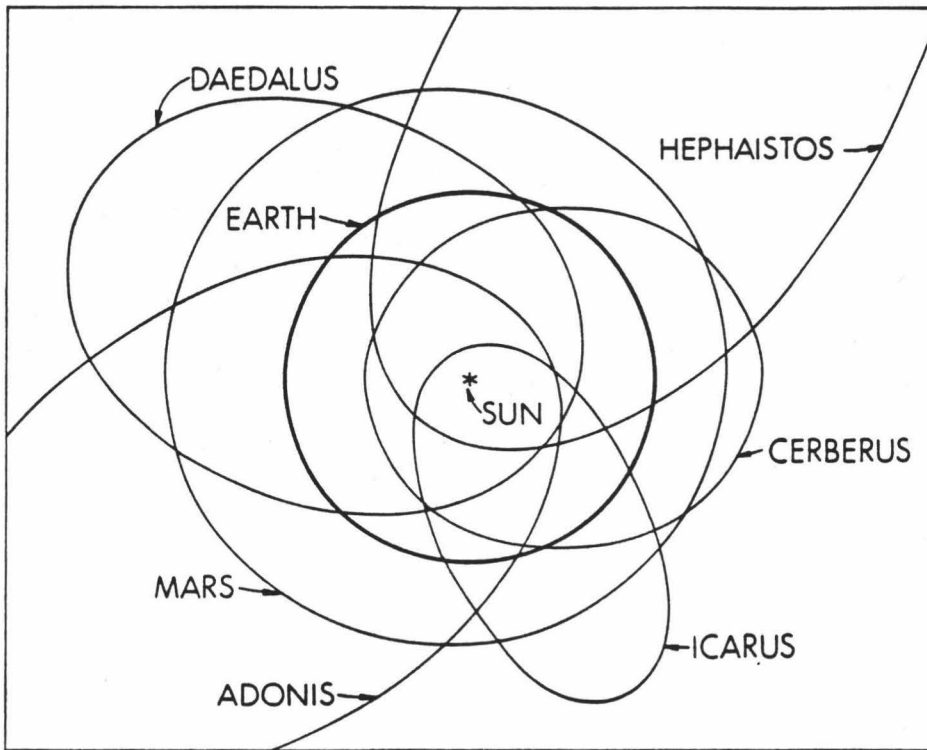
Figure 28: Two pyroxene-plagioclase assemblages with a 0.60- μm absorption band attributed to a transition element cation other than iron.

Figure 29: Ferric iron-bearing minerals have absorption band strengths different from those of 1915 Quetzalcoatl.

Figure 30: Reflectance of 2201 1947XC and comets measured and reduced

in the same manner.

EARTH, MARS, AND FIVE APOLLOS A



EARTH, MARS, AND SIX APOLLOS B

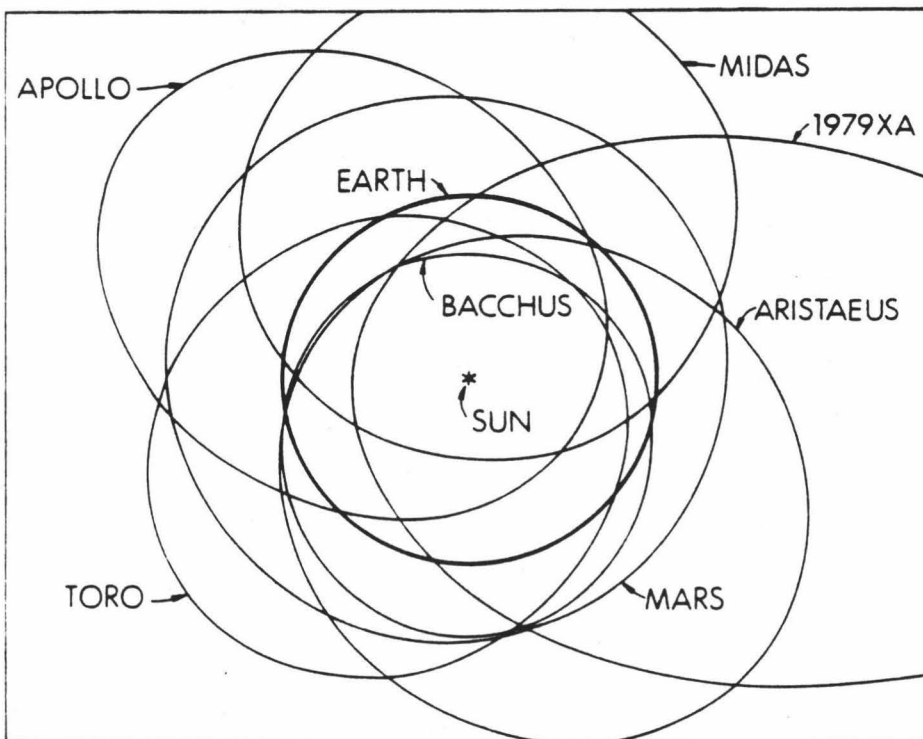


Figure 1

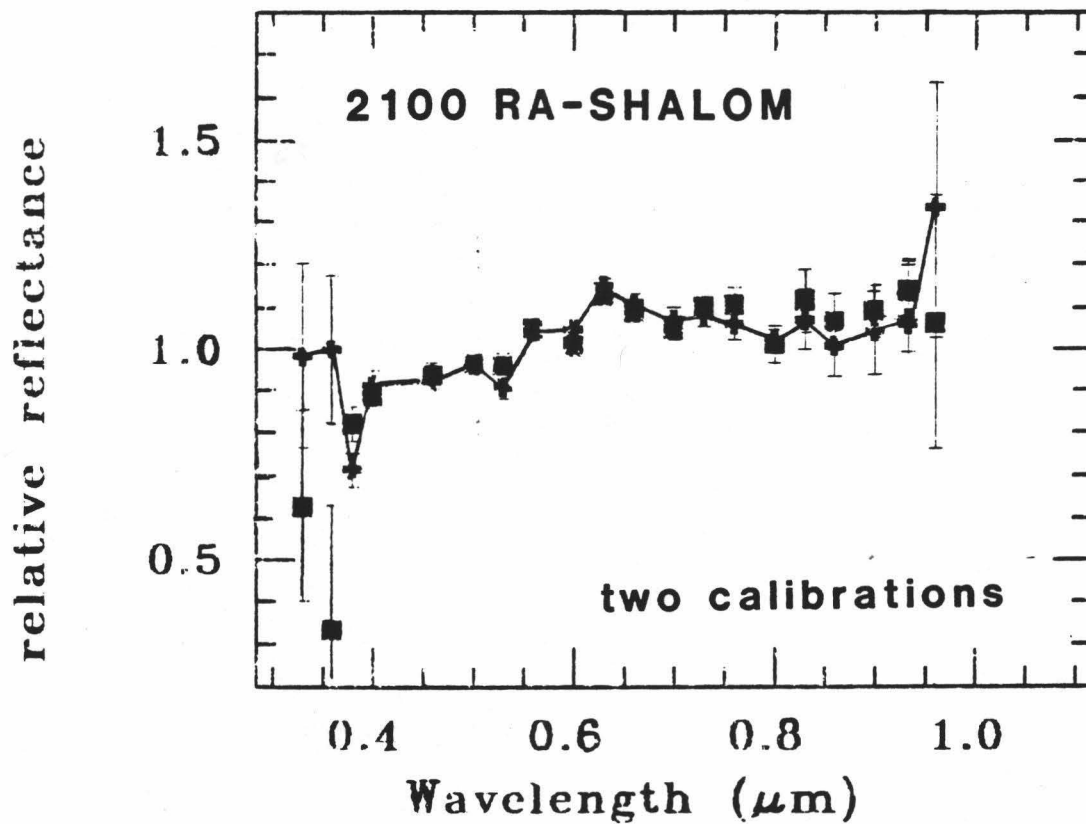


Figure 2

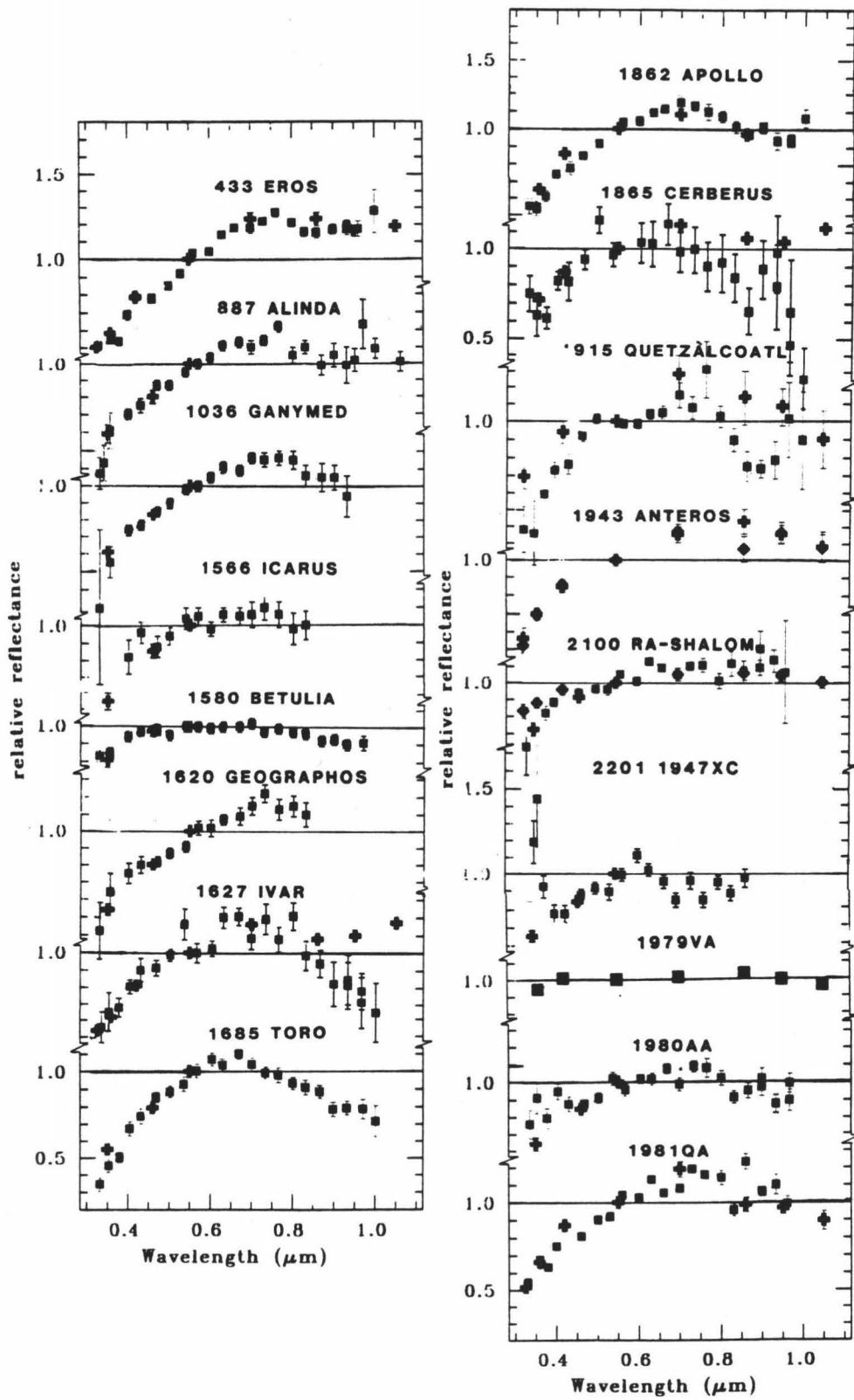


Figure 3

VISIBLE and JHK SPECTRA

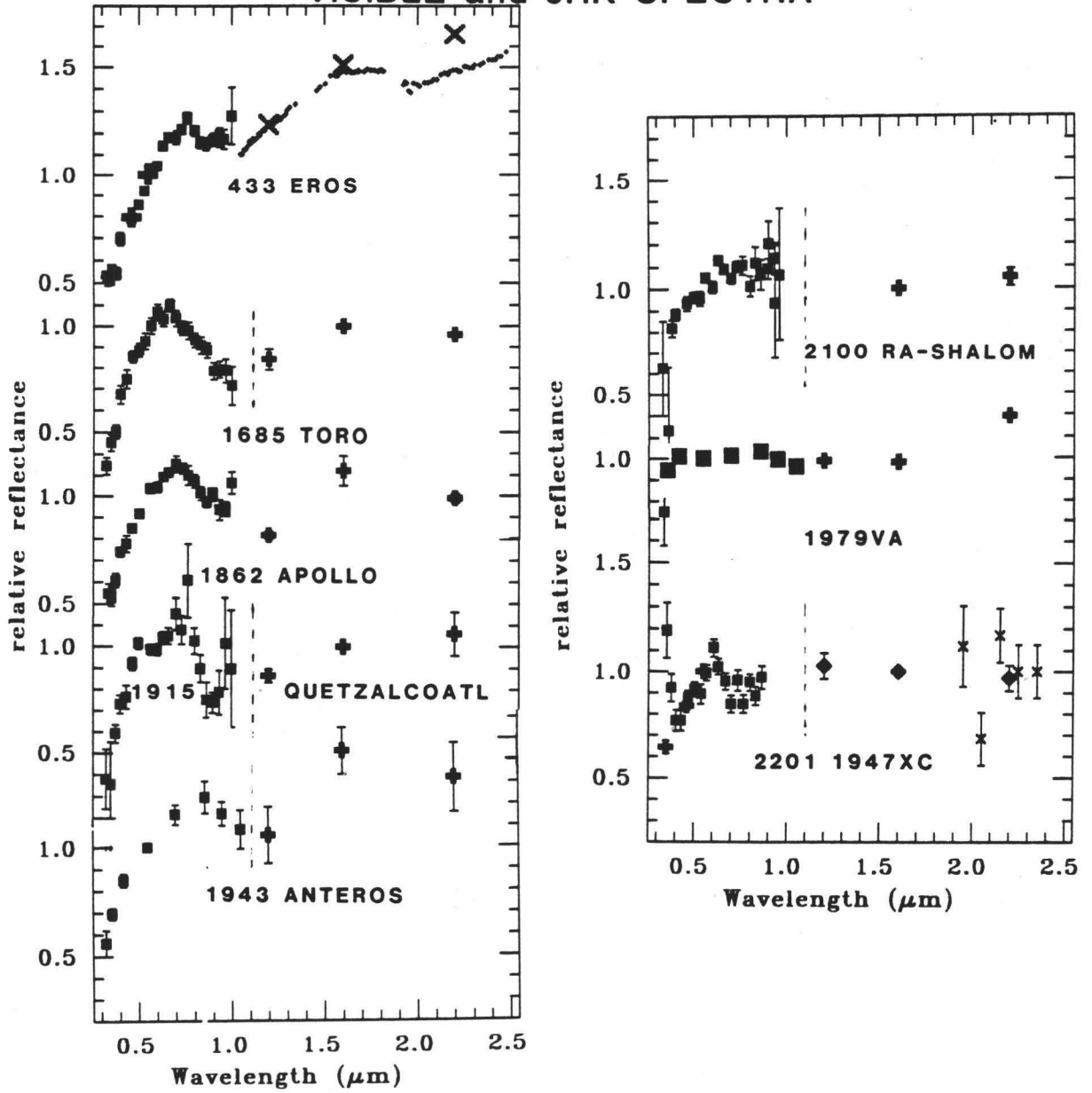


Figure 4

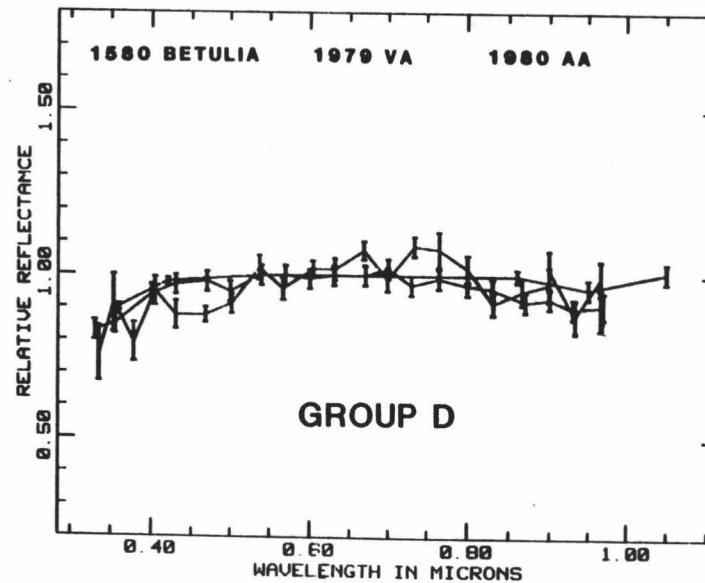
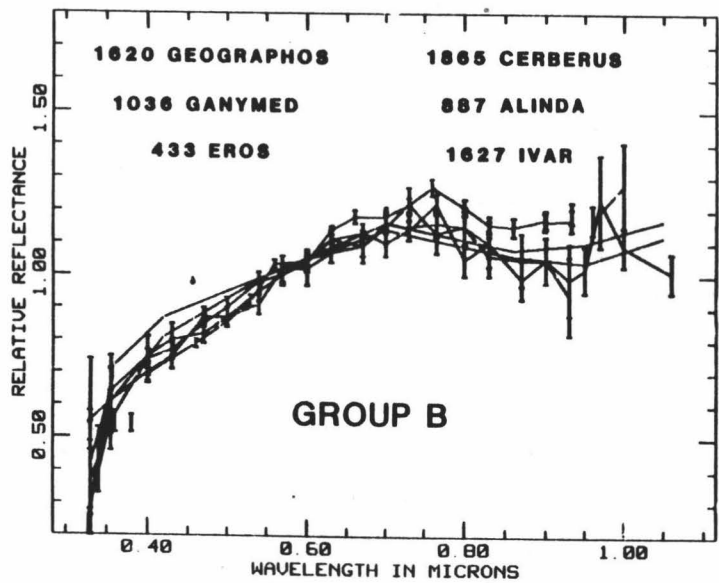
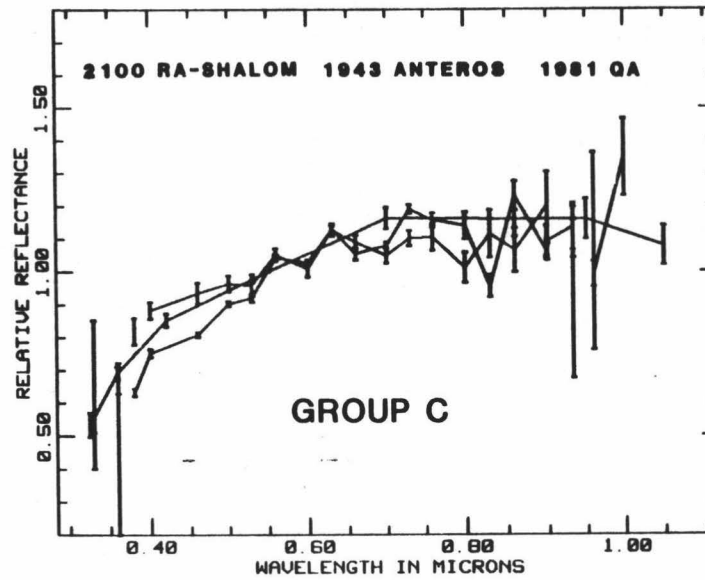
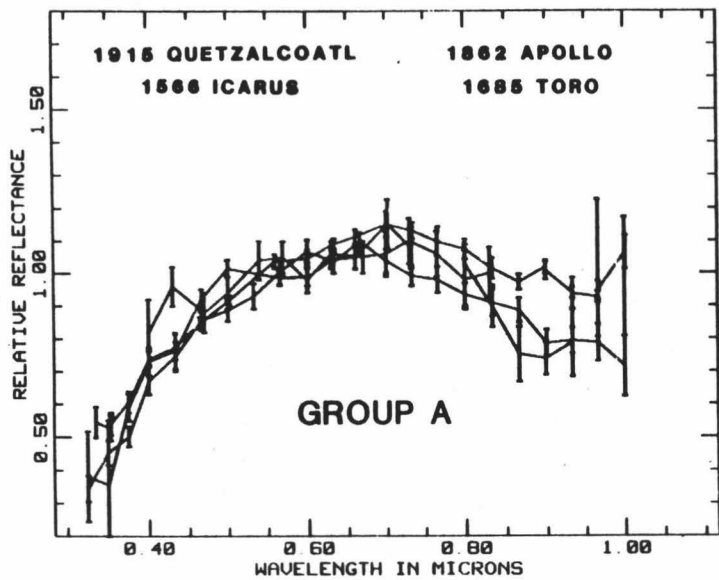
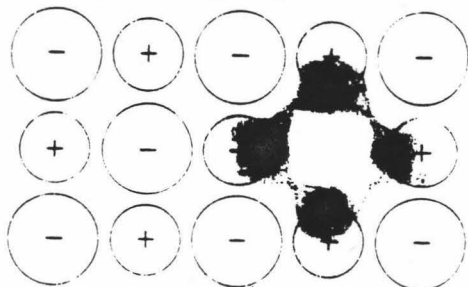


Figure 5
- 77 -

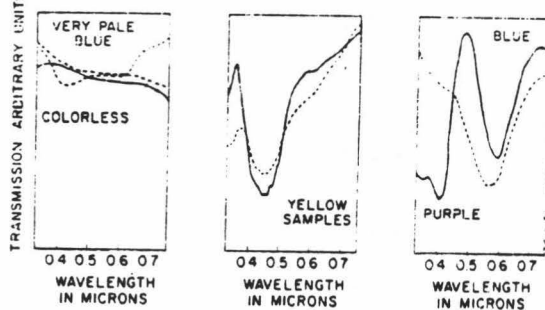
COLOR CENTERS

a schematic



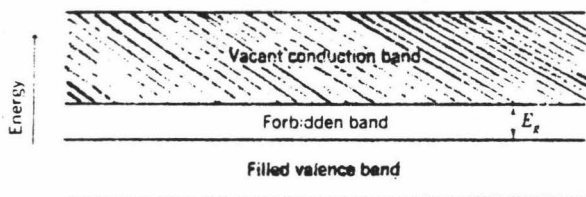
b

FLUGRITE RCSICLARE ILL.



SEMI-CONDUCTOR

c



d

SULPHUR 49 WINNEMUCCA, NEV.

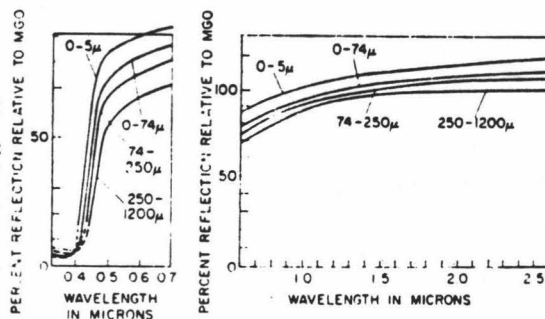


Figure 6

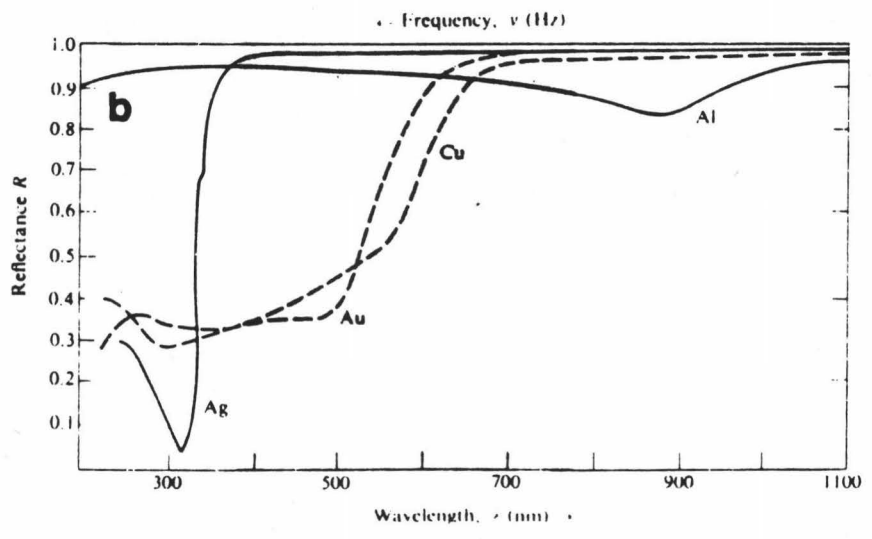
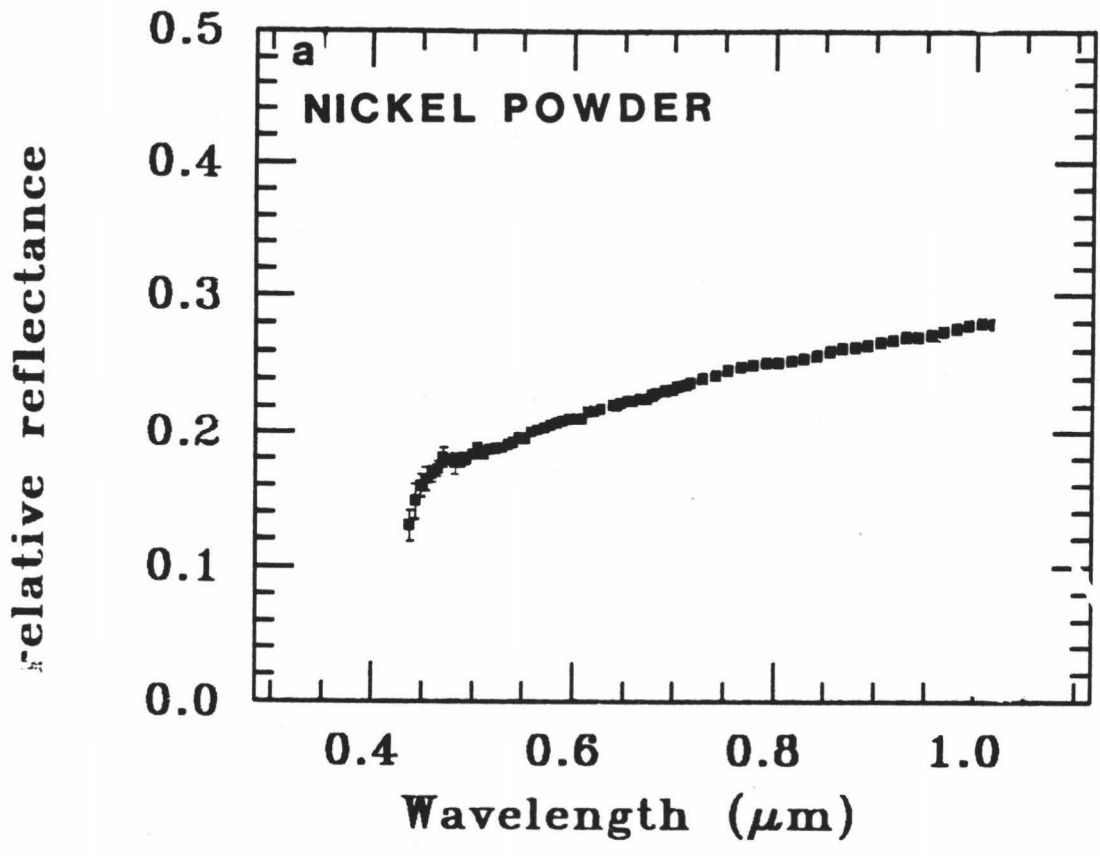


Figure 7

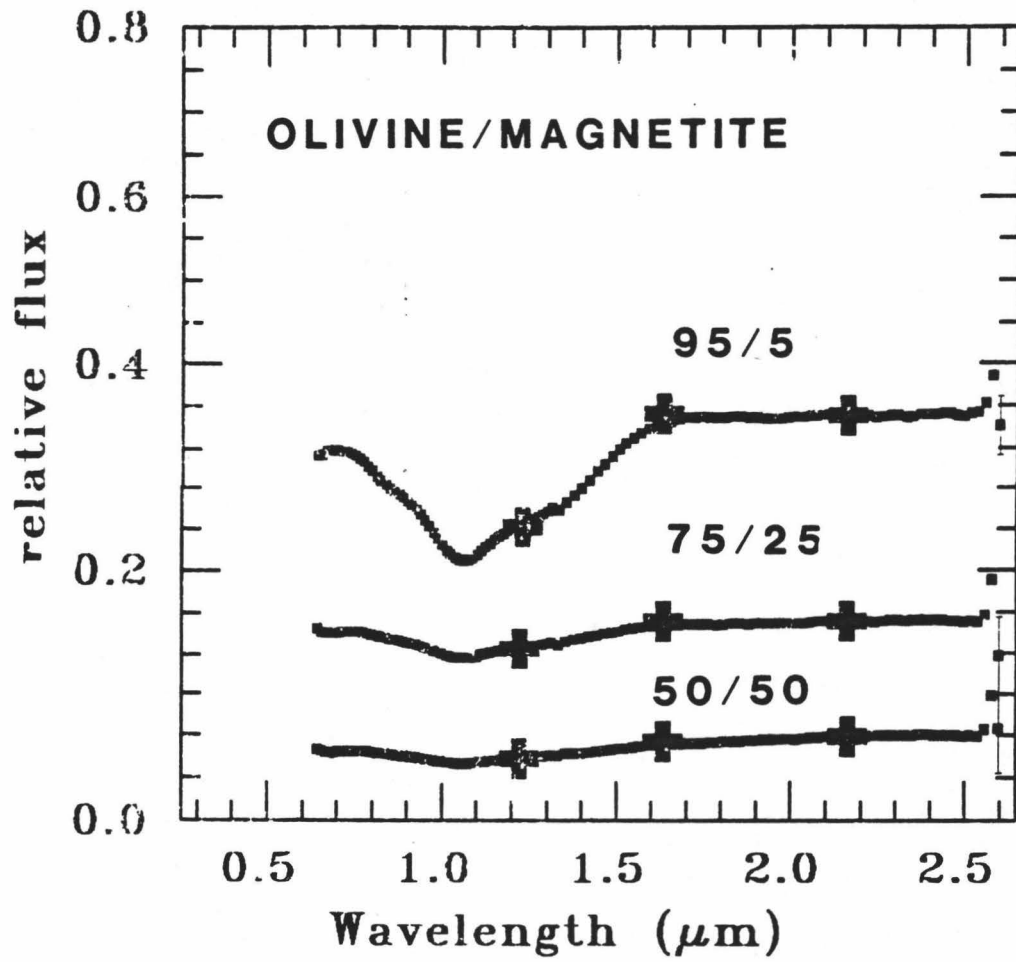


Figure 3

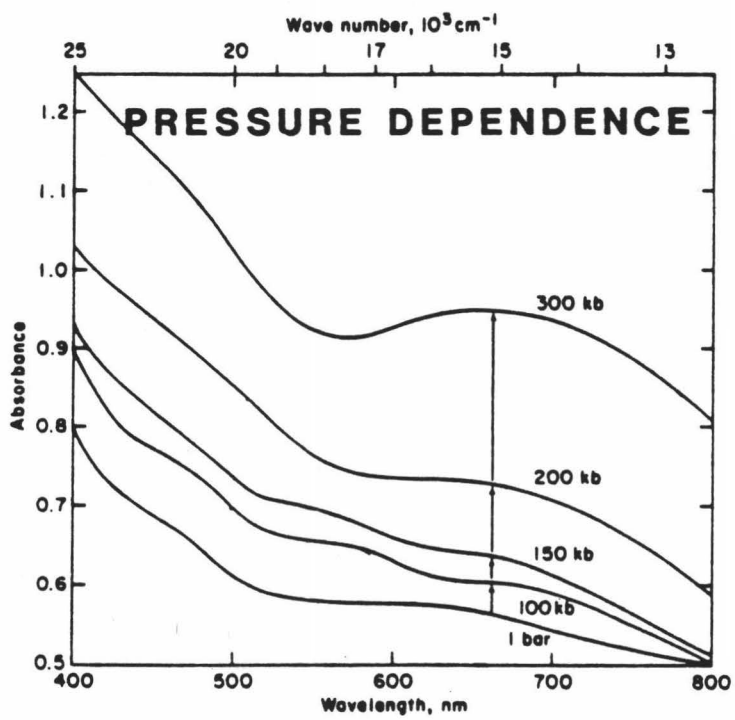
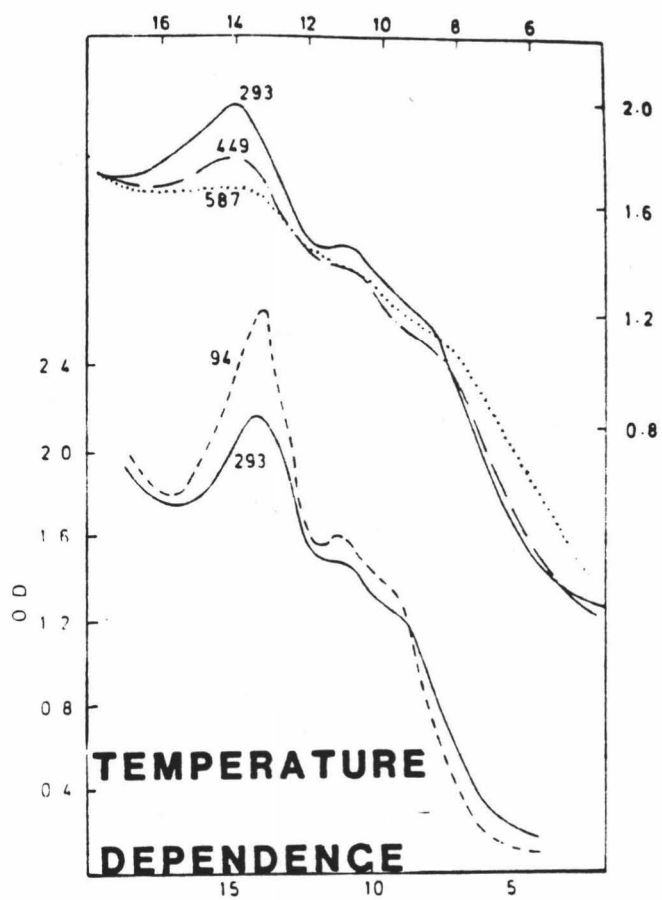


Figure 9

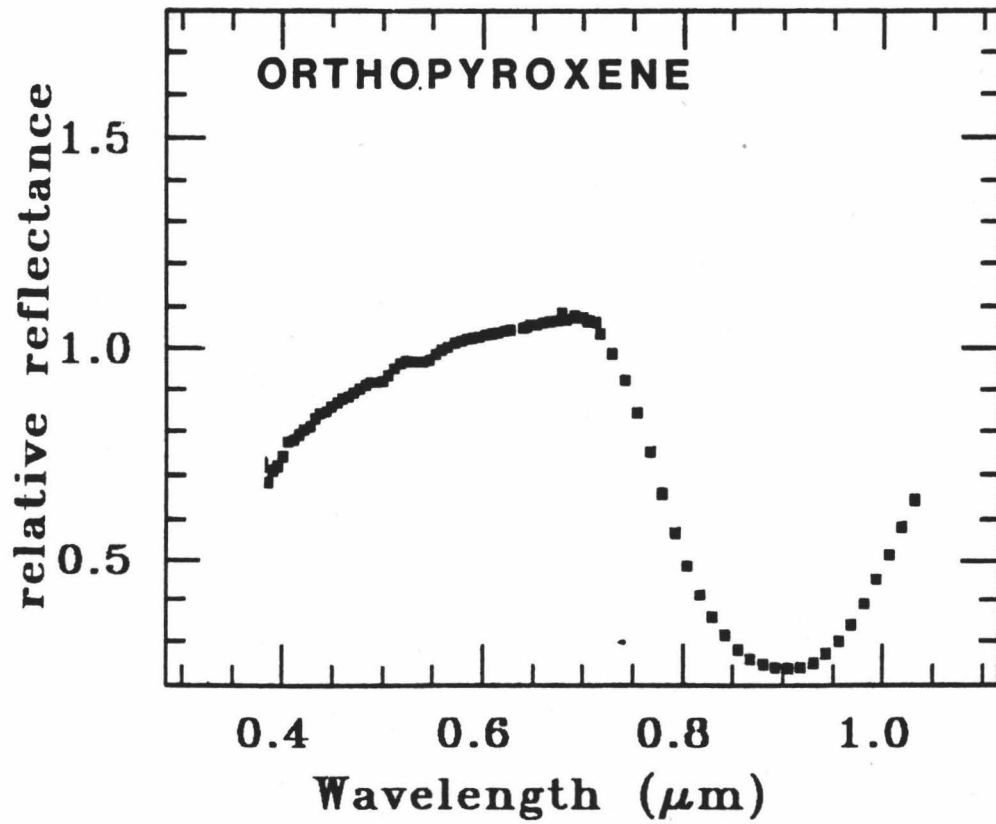
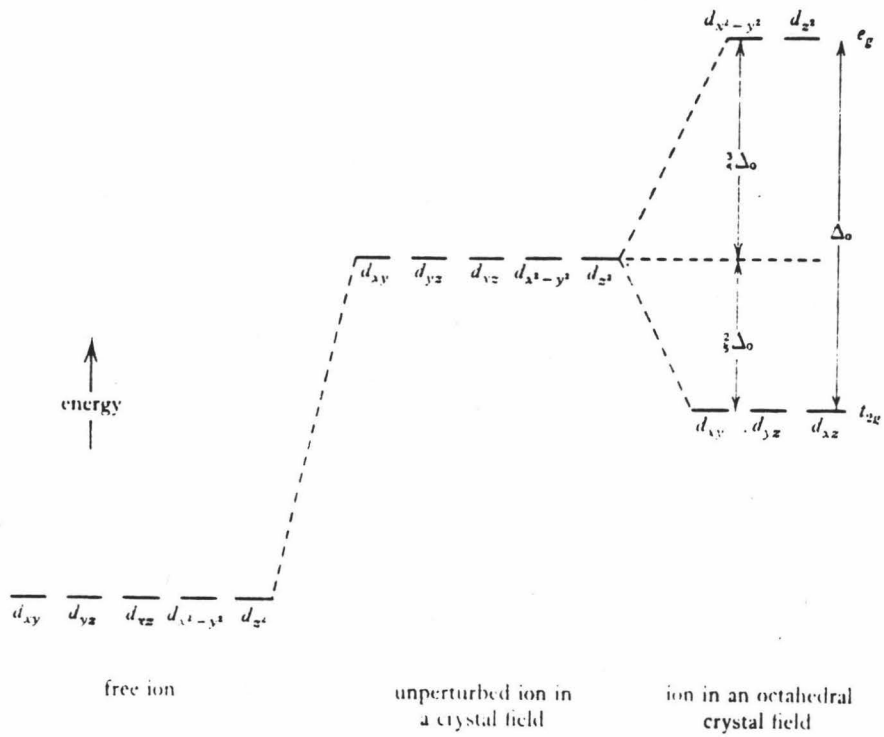


Figure 10

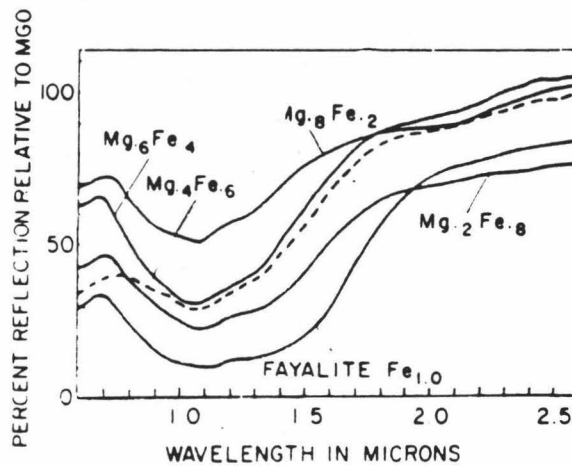
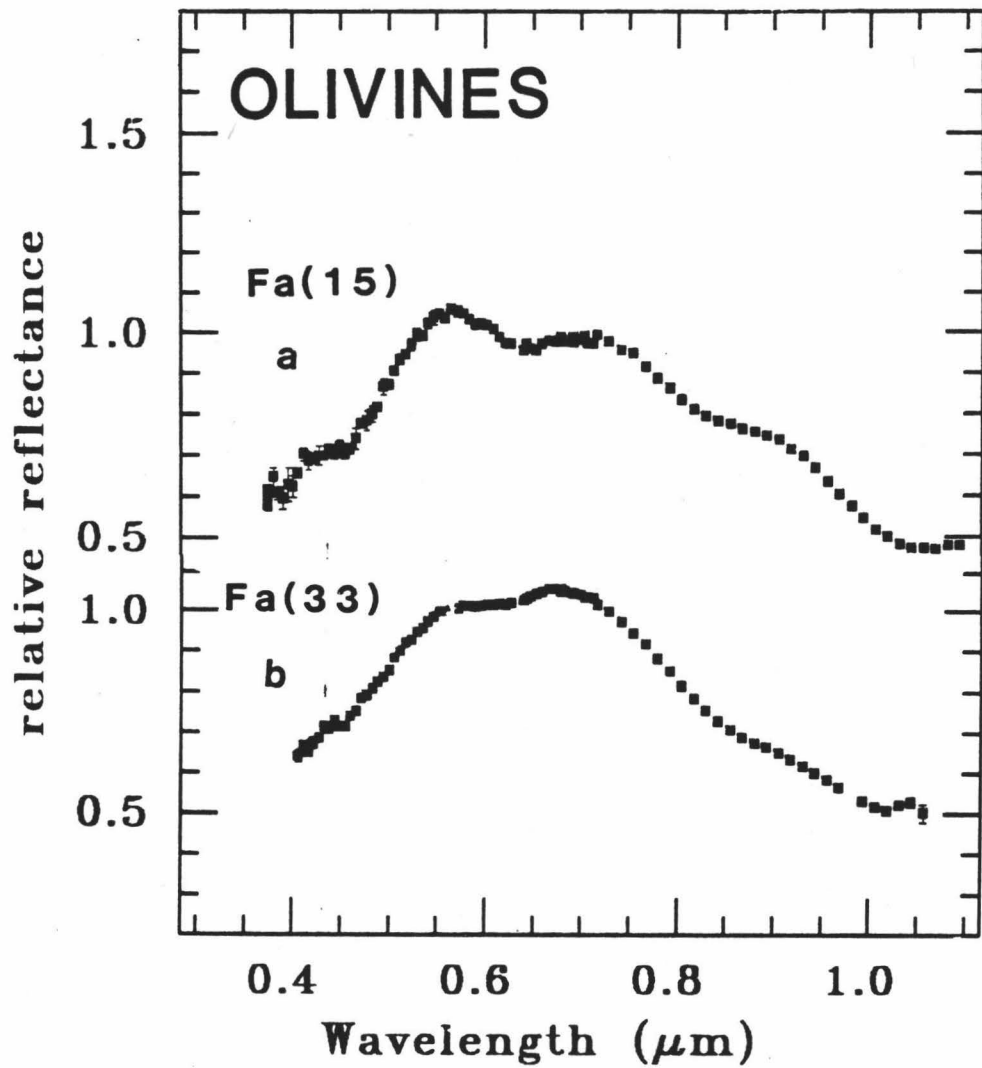


Figure 11

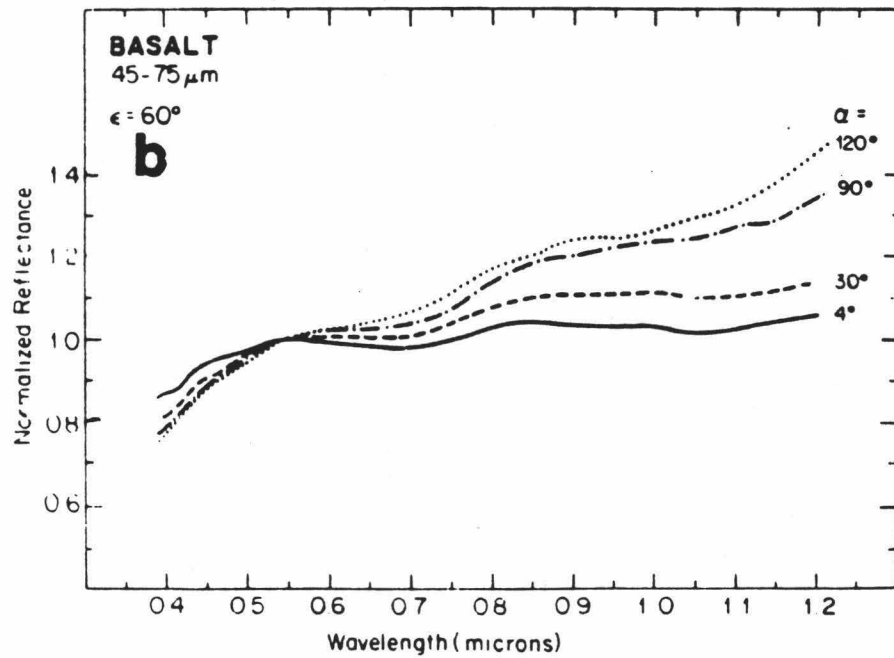
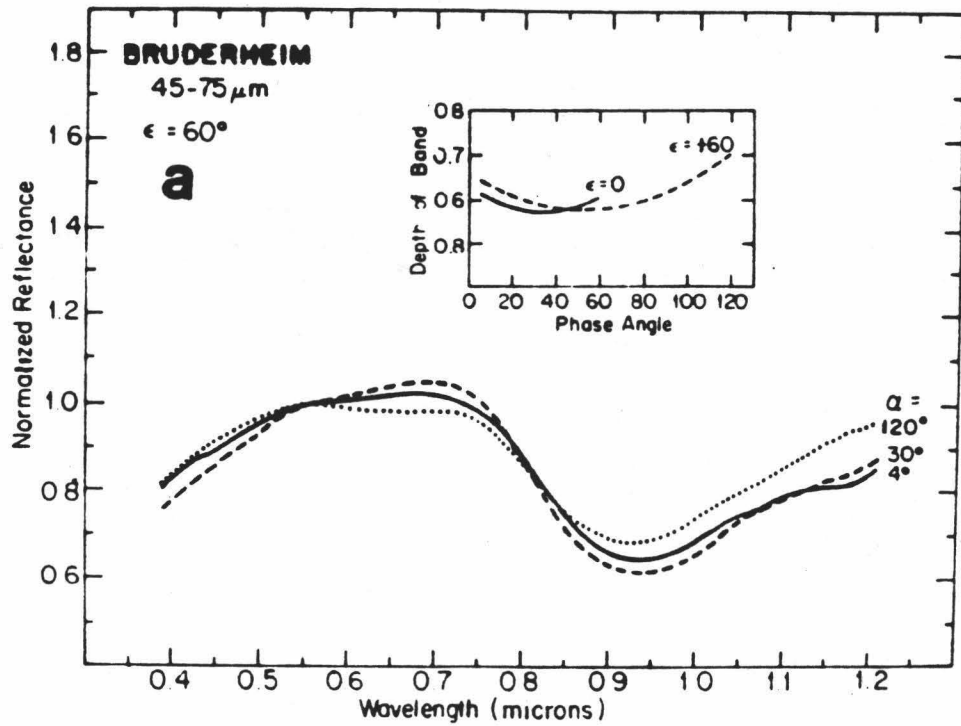


Figure 12a-b

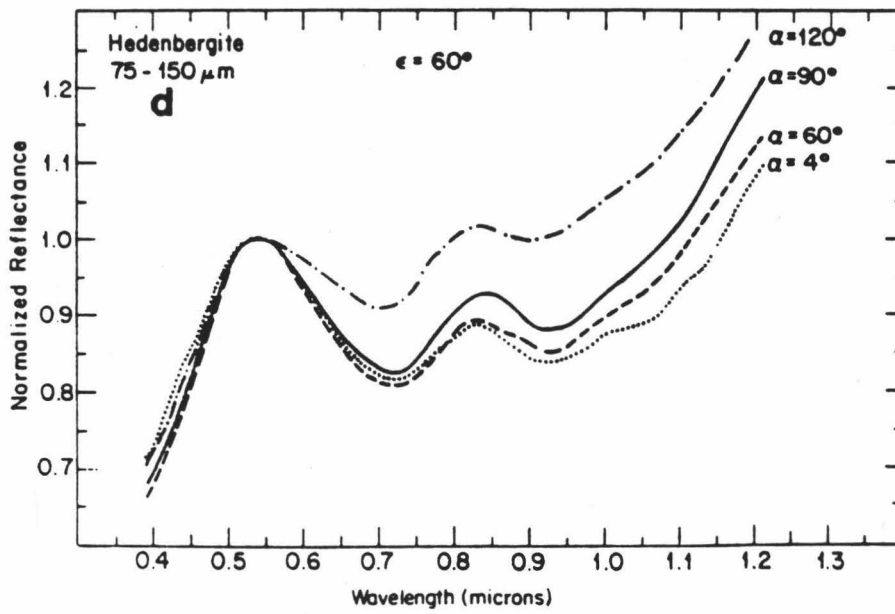
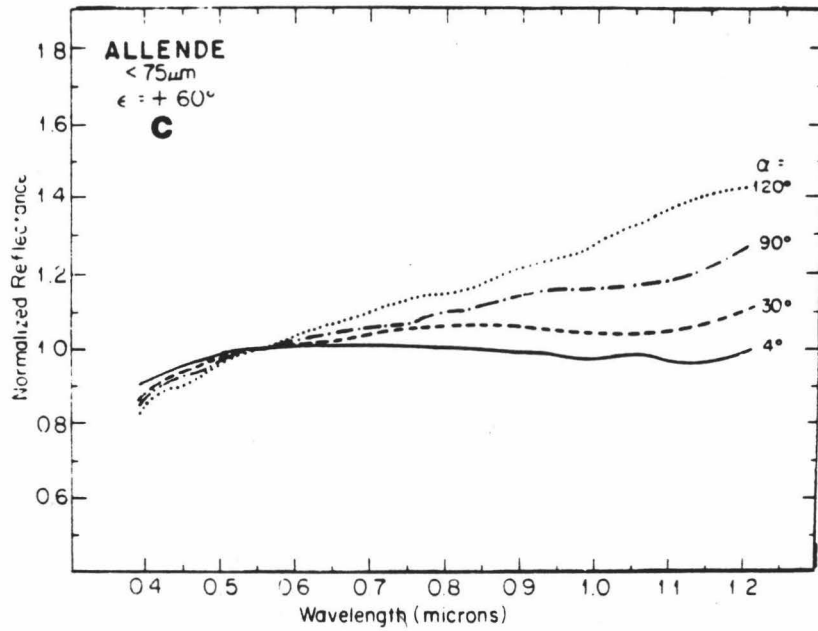


Figure 12c-d

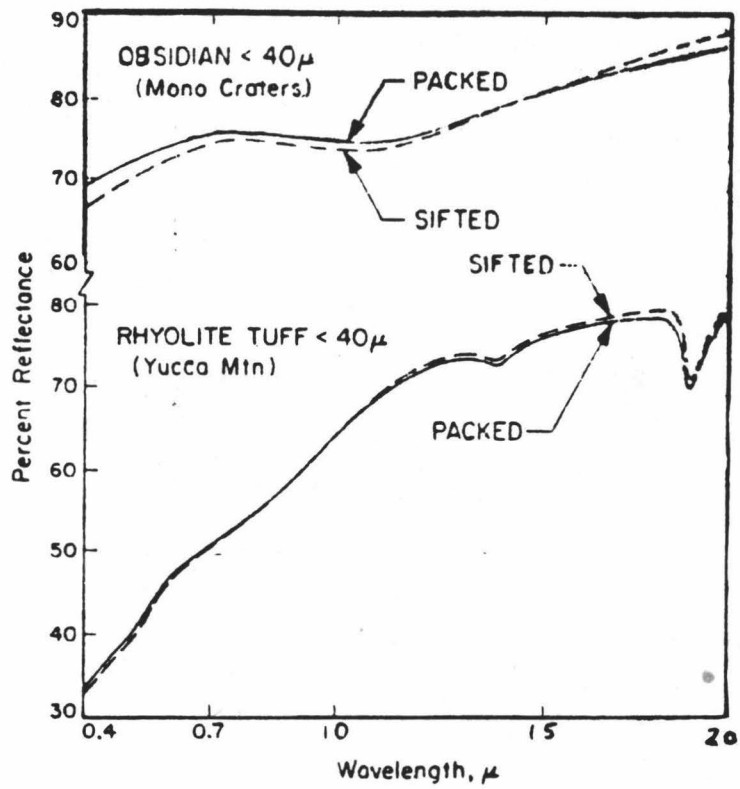


Figure 13

ENSTATITE

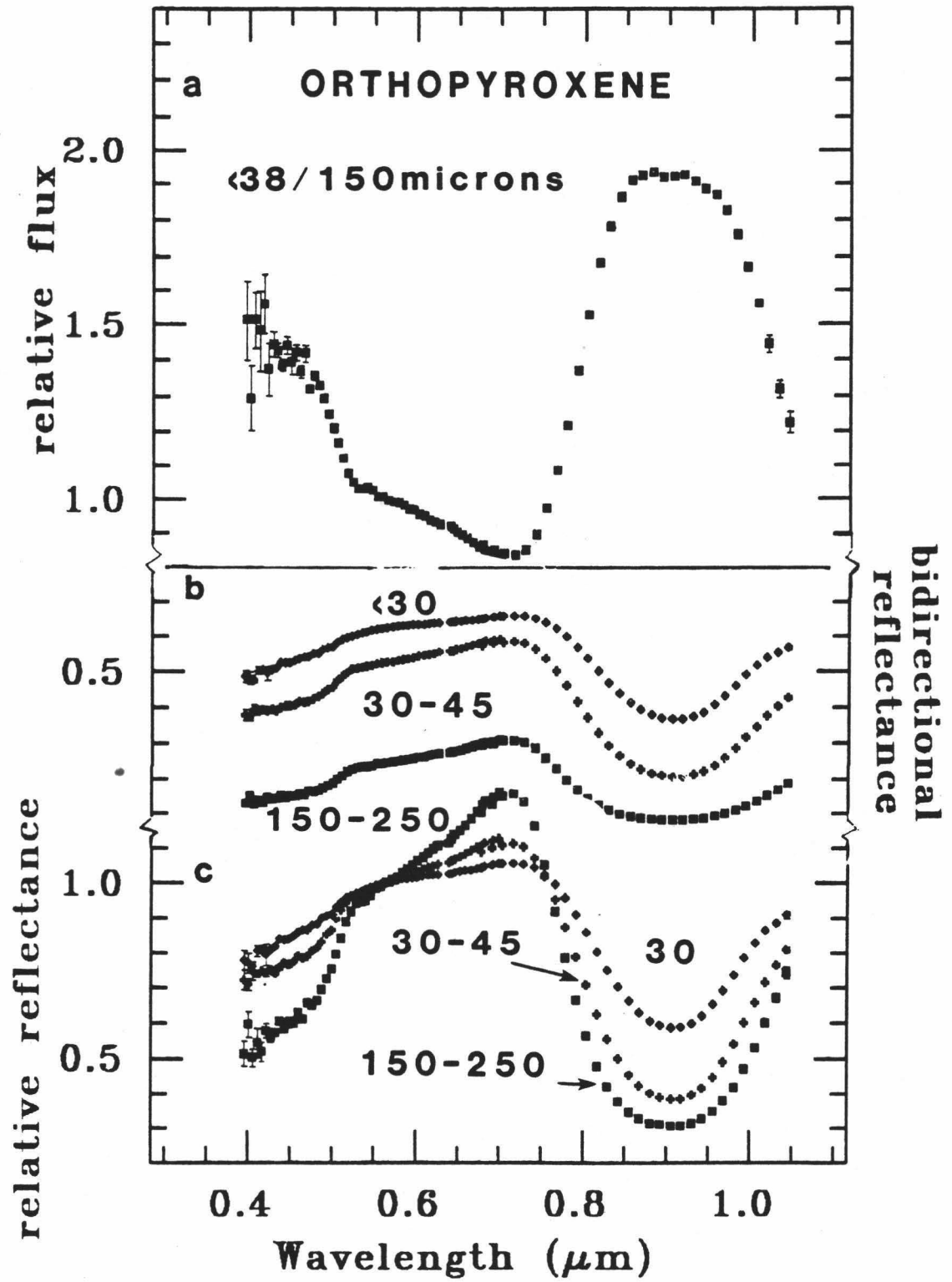


Figure 14

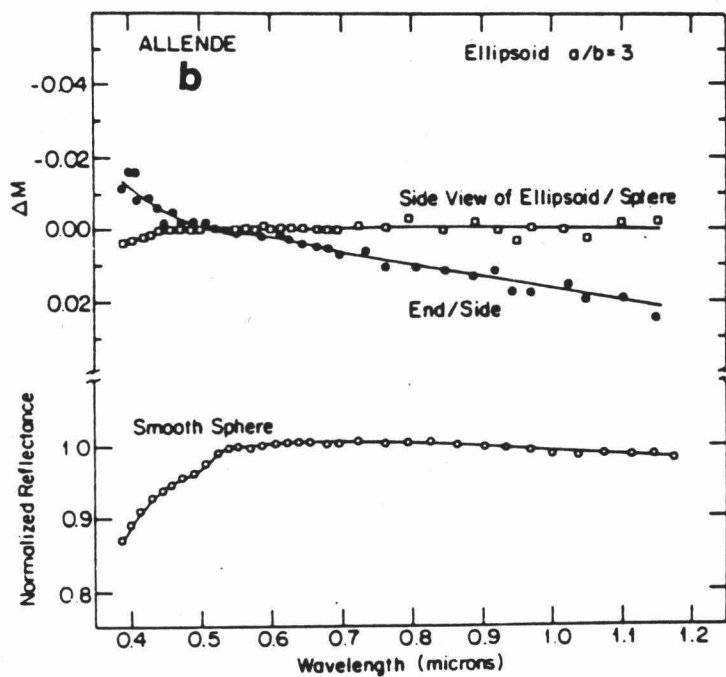
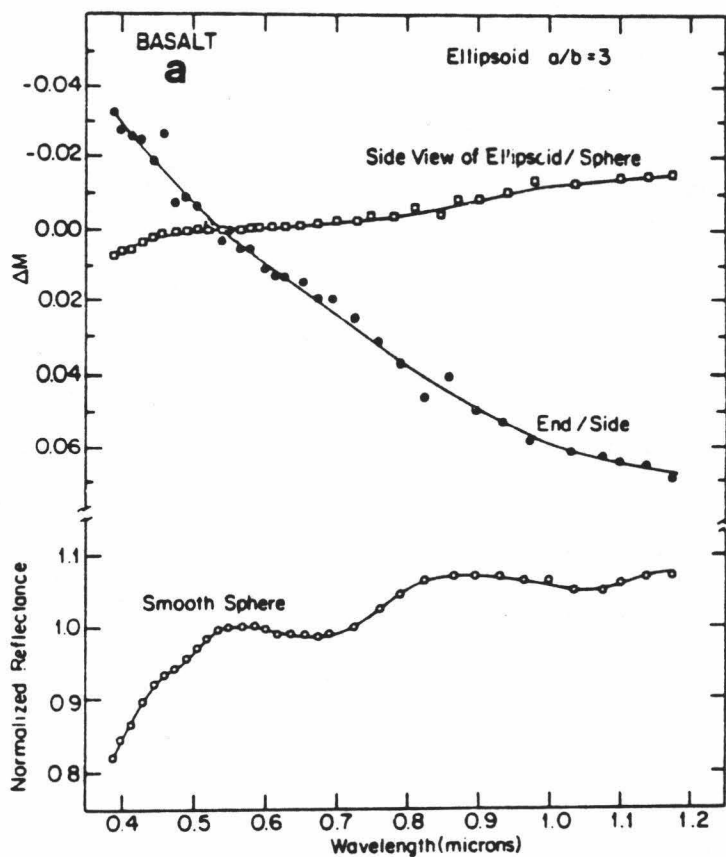


Figure 15a-b

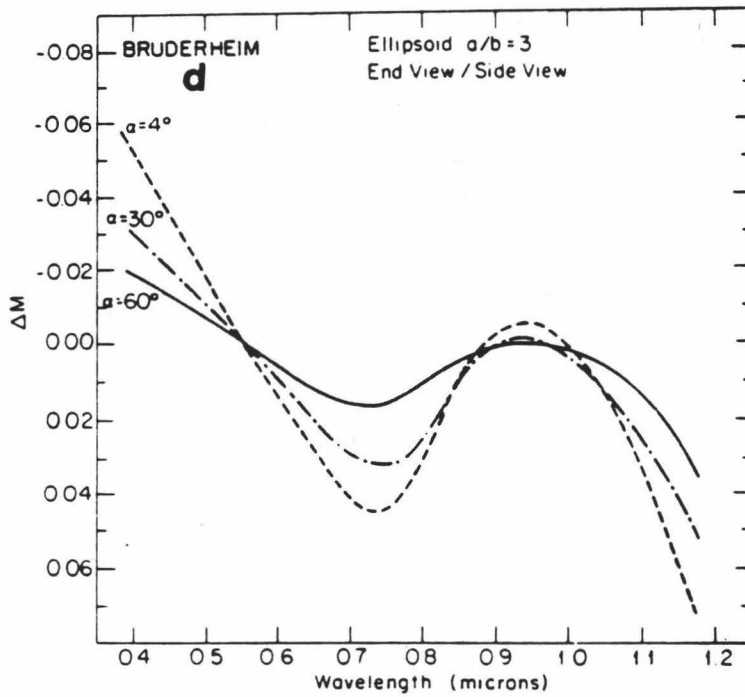
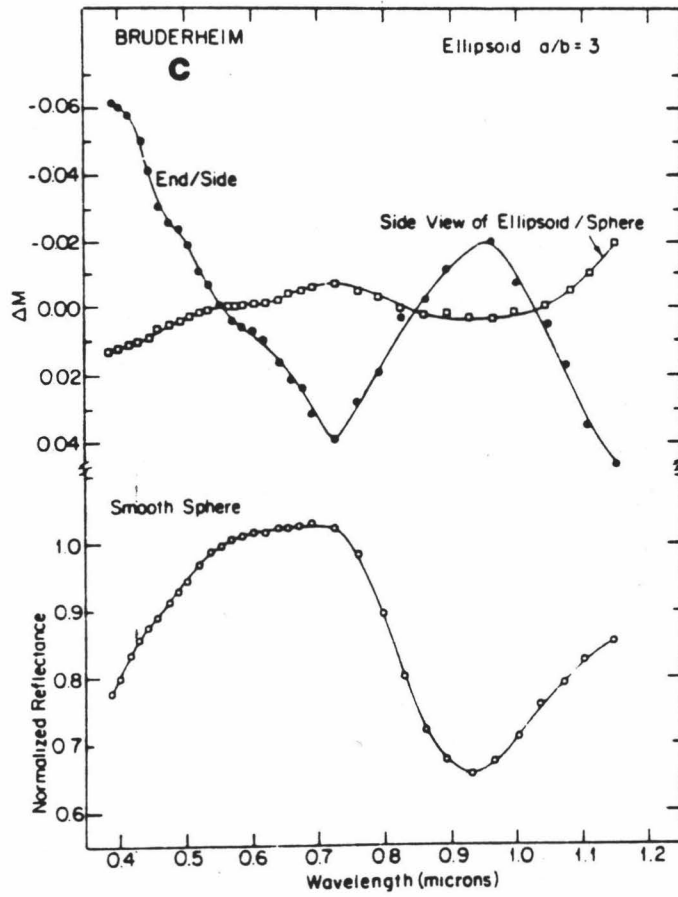


Figure 15c-d

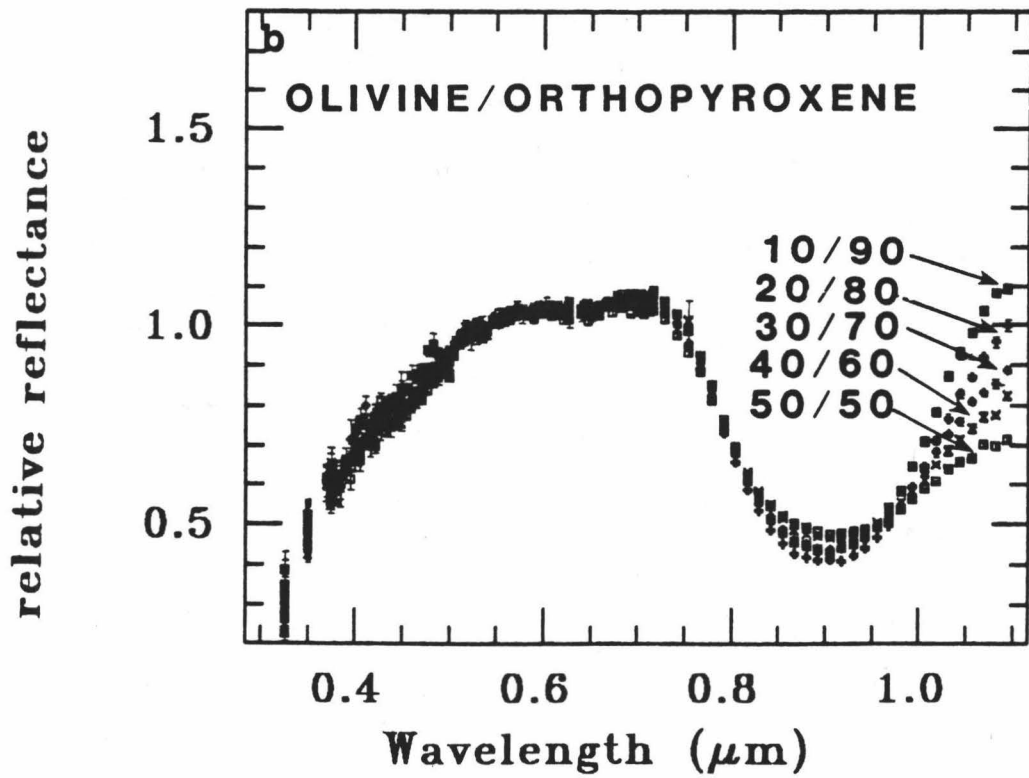
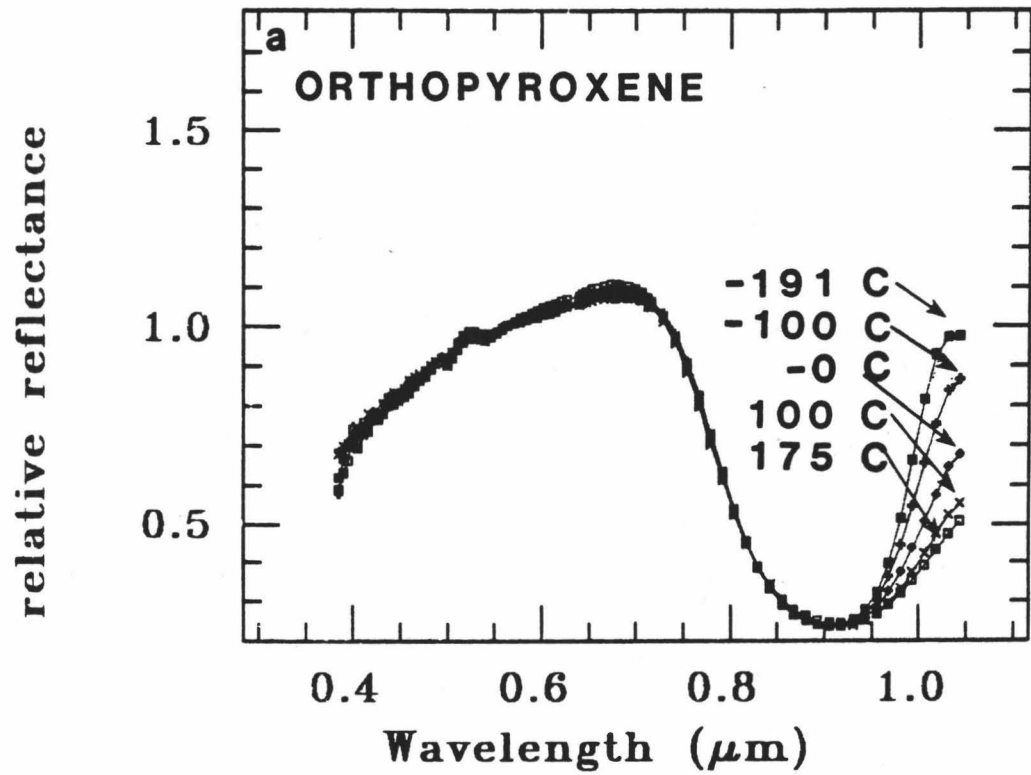


Figure 16

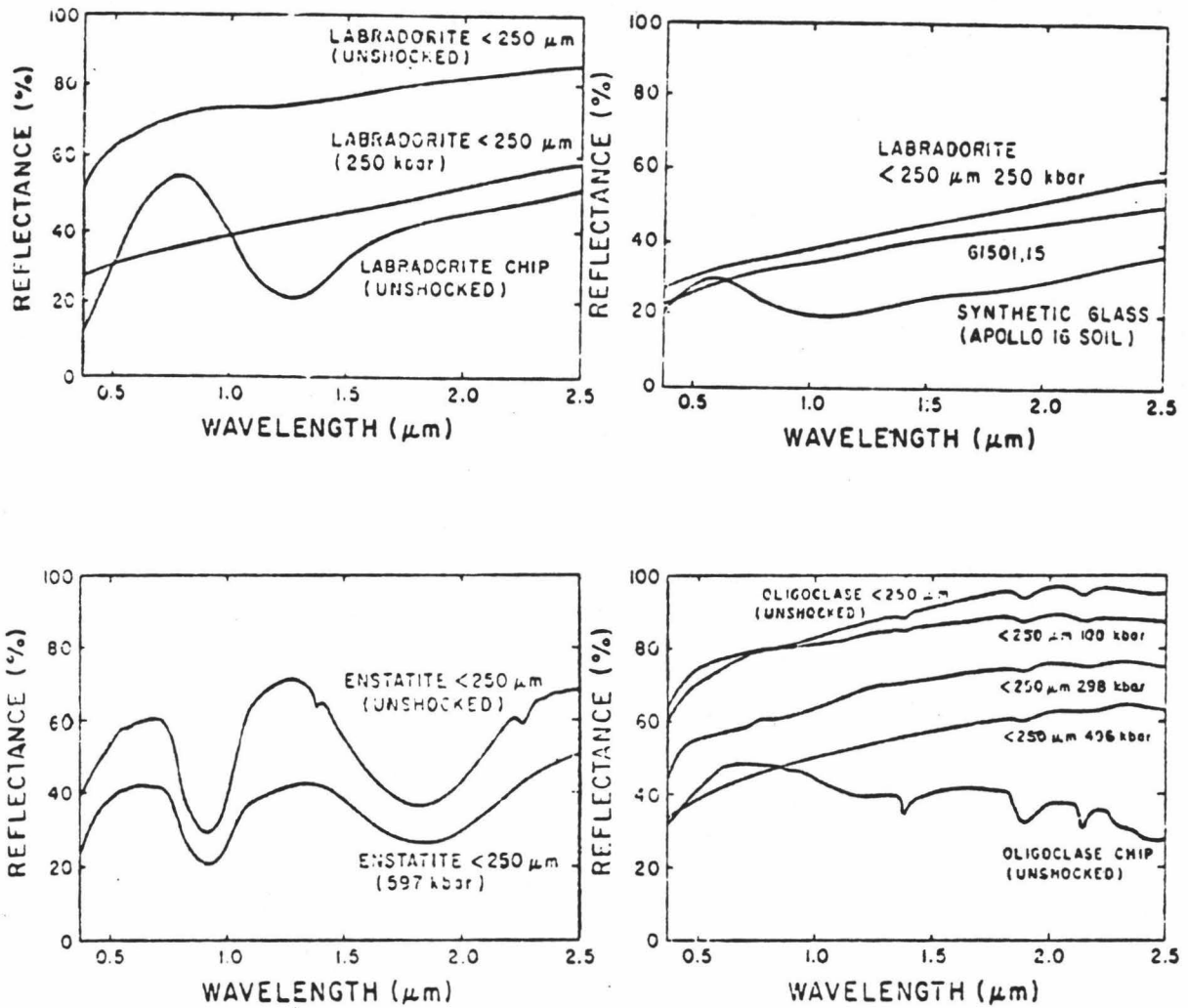


Figure 17

SHOCK FACIES

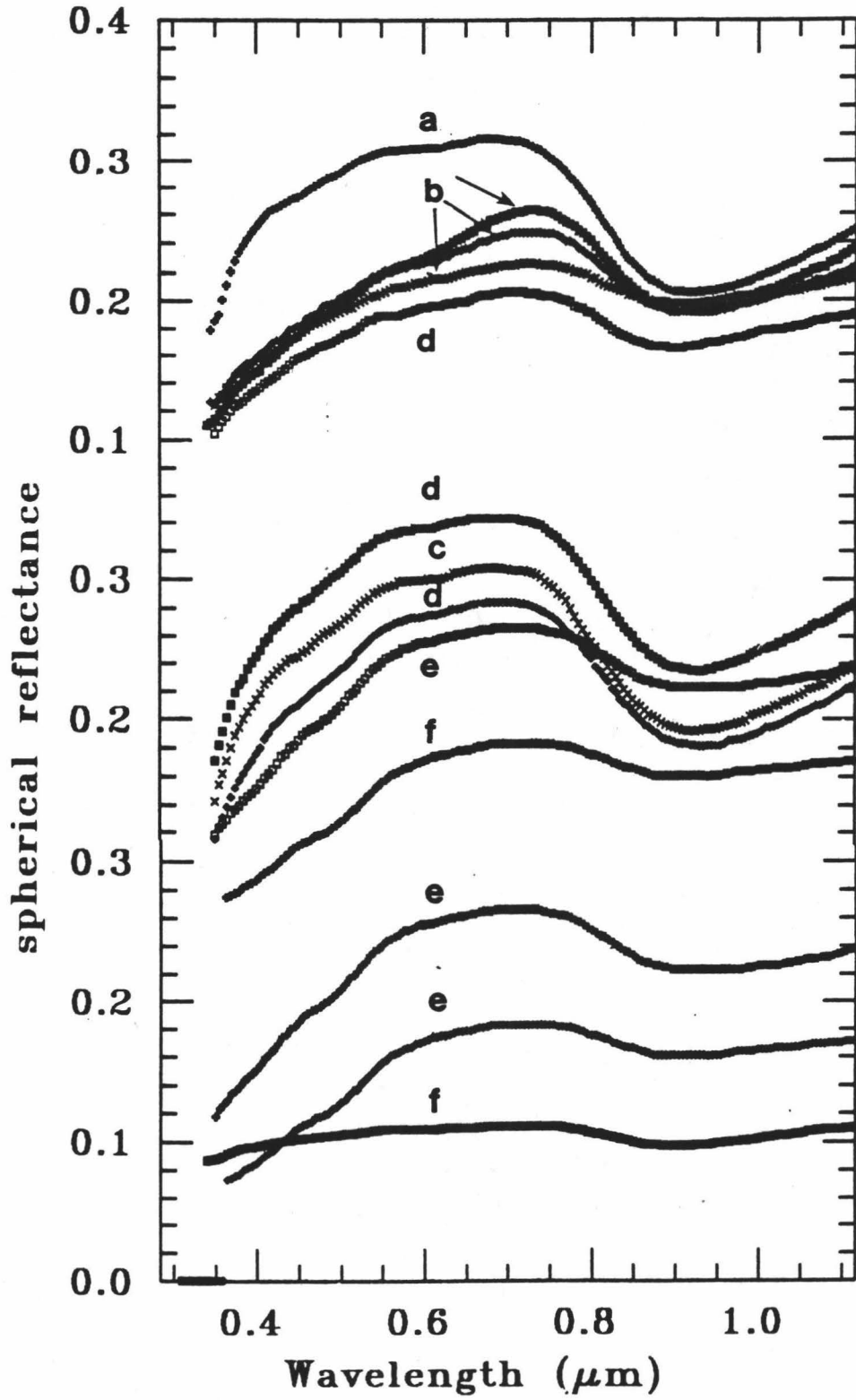


Figure 18

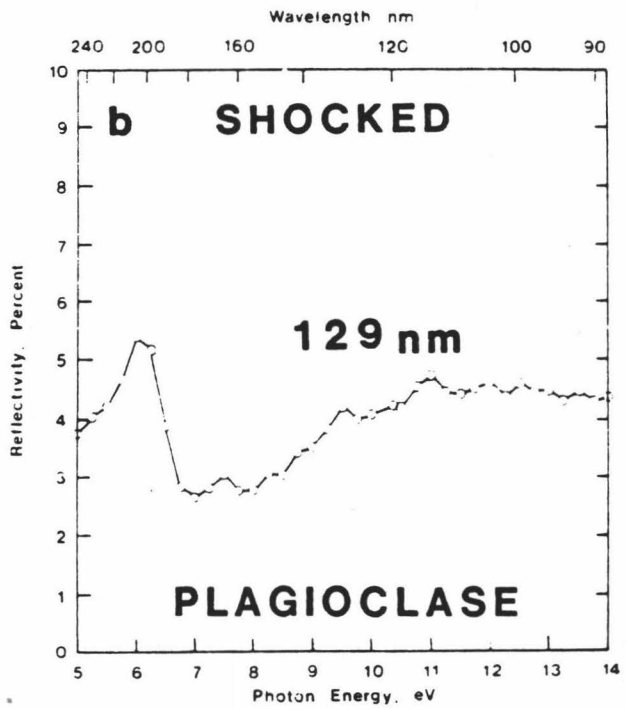
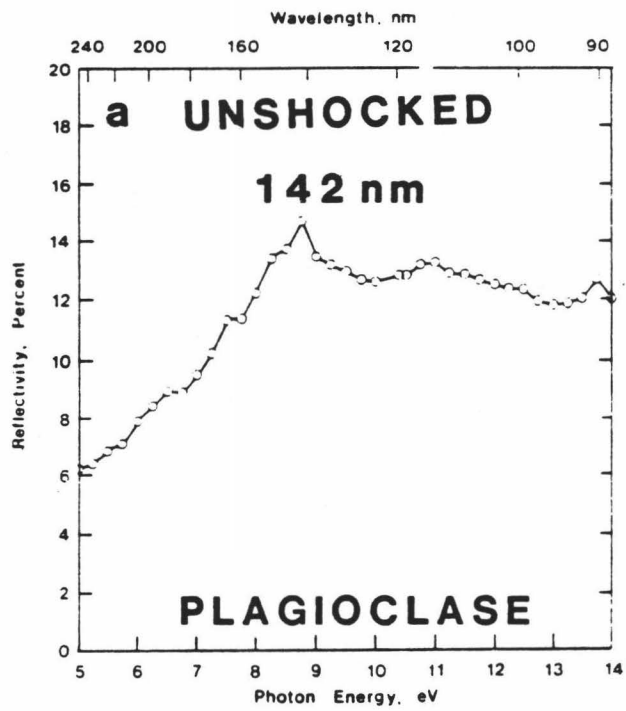


Figure 19

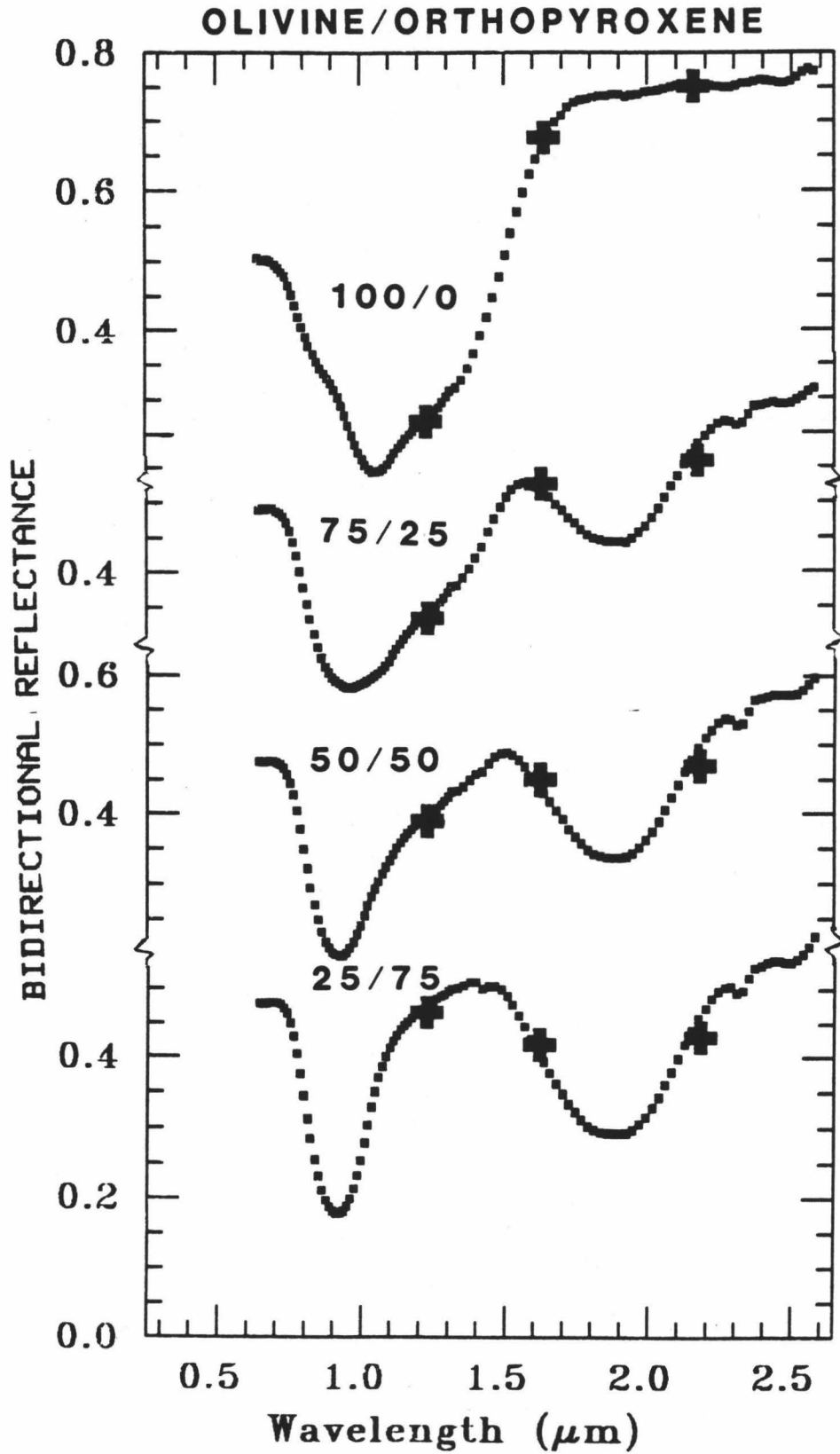


Figure 20

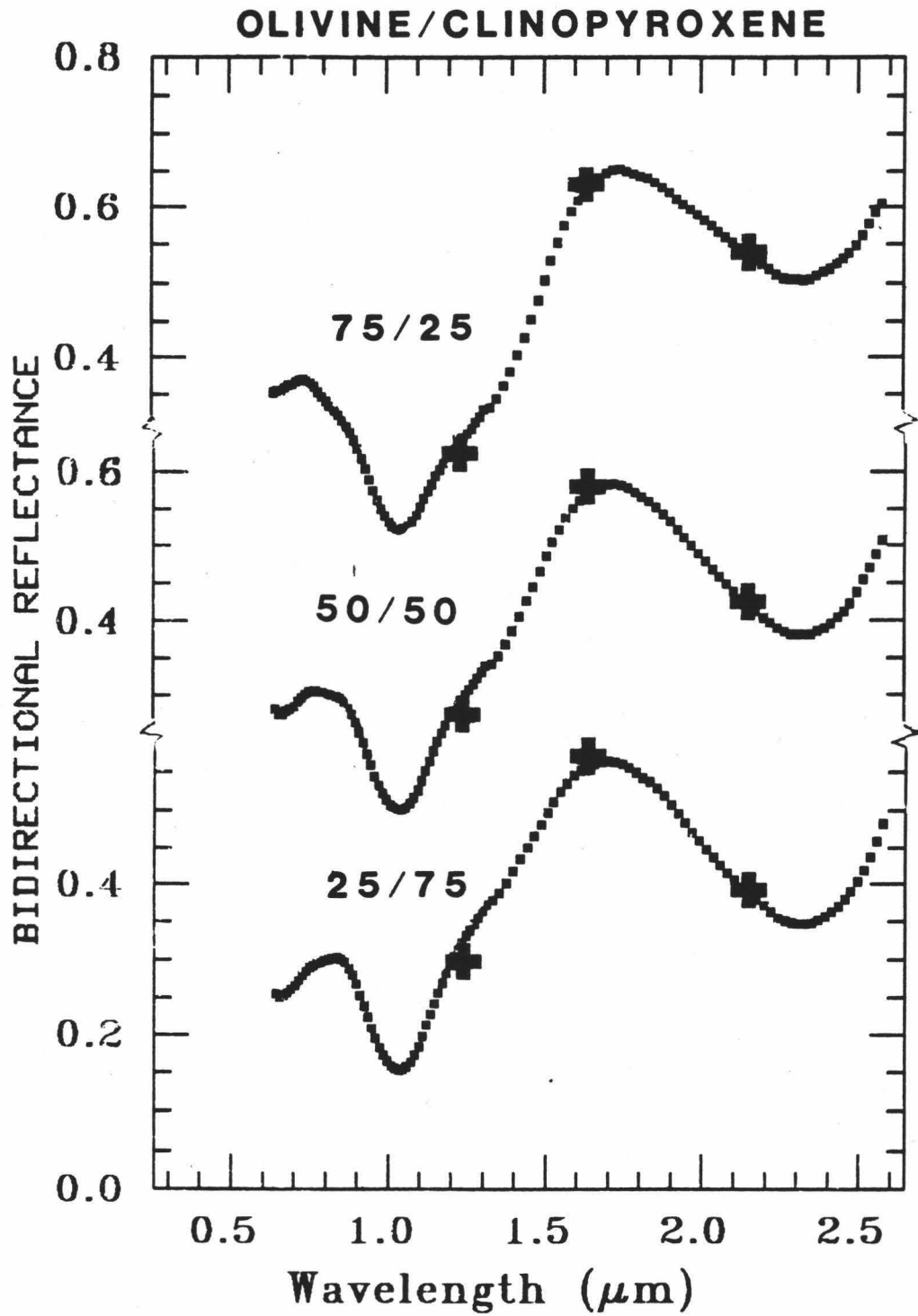


Figure 21

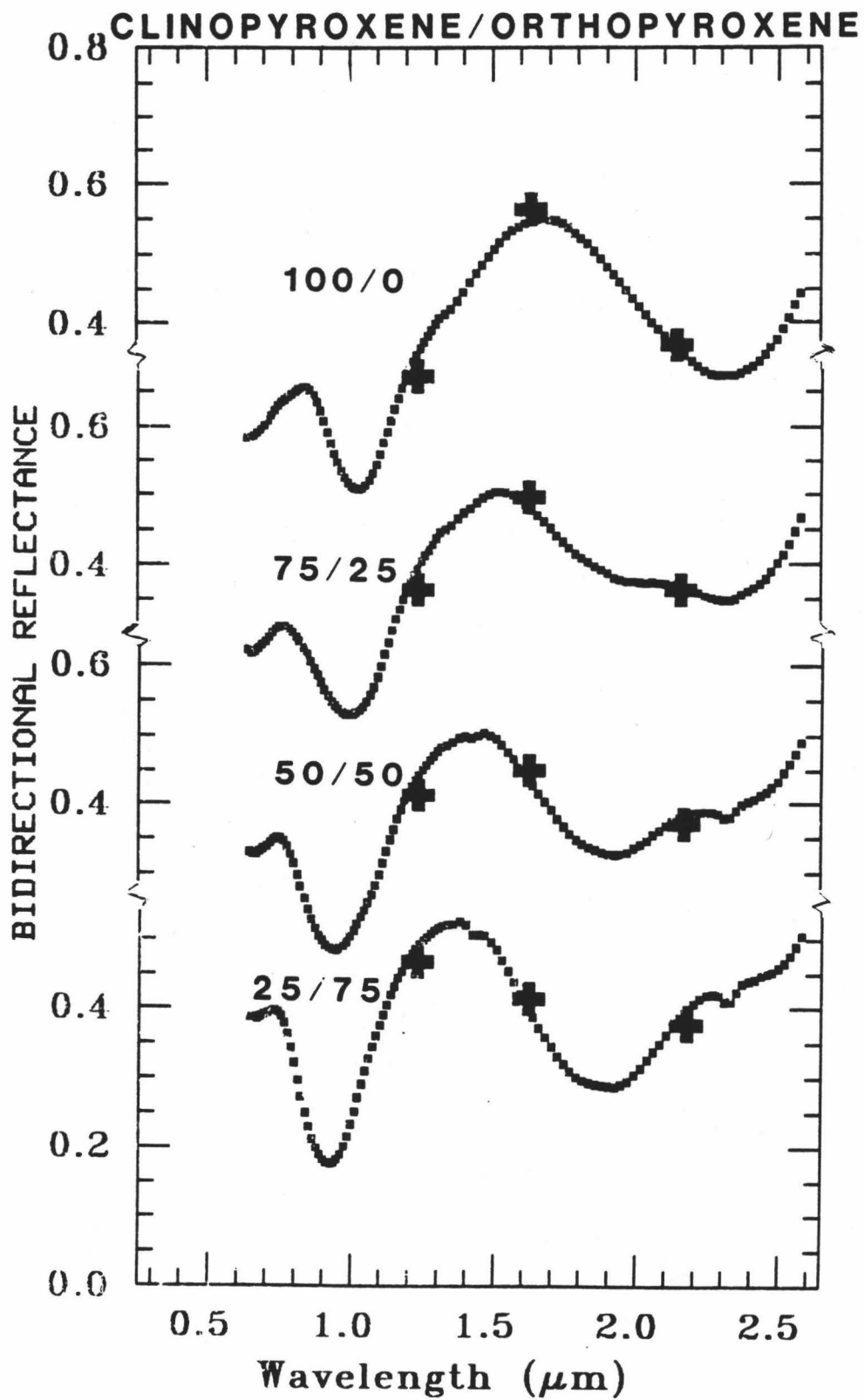
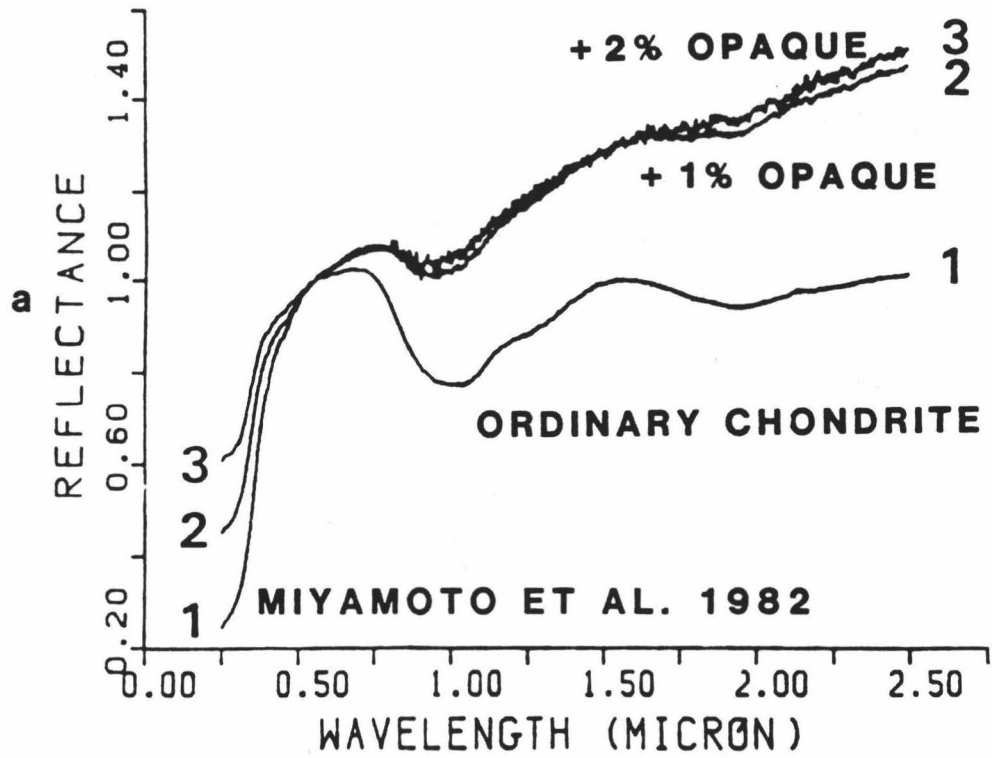


Figure 22



METEORITE TYPES

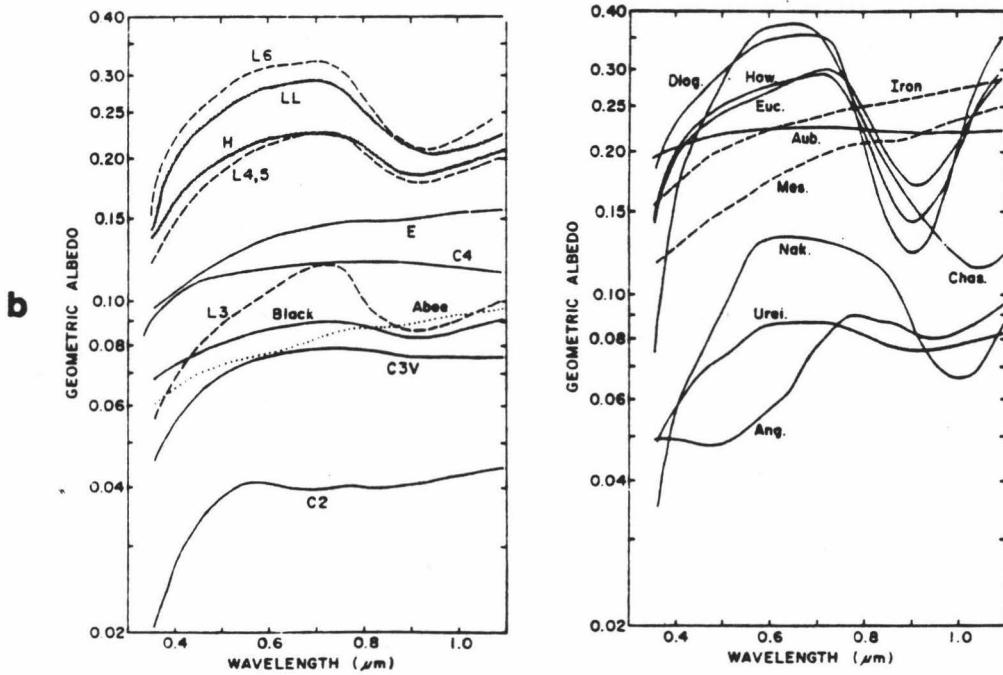


Figure 23

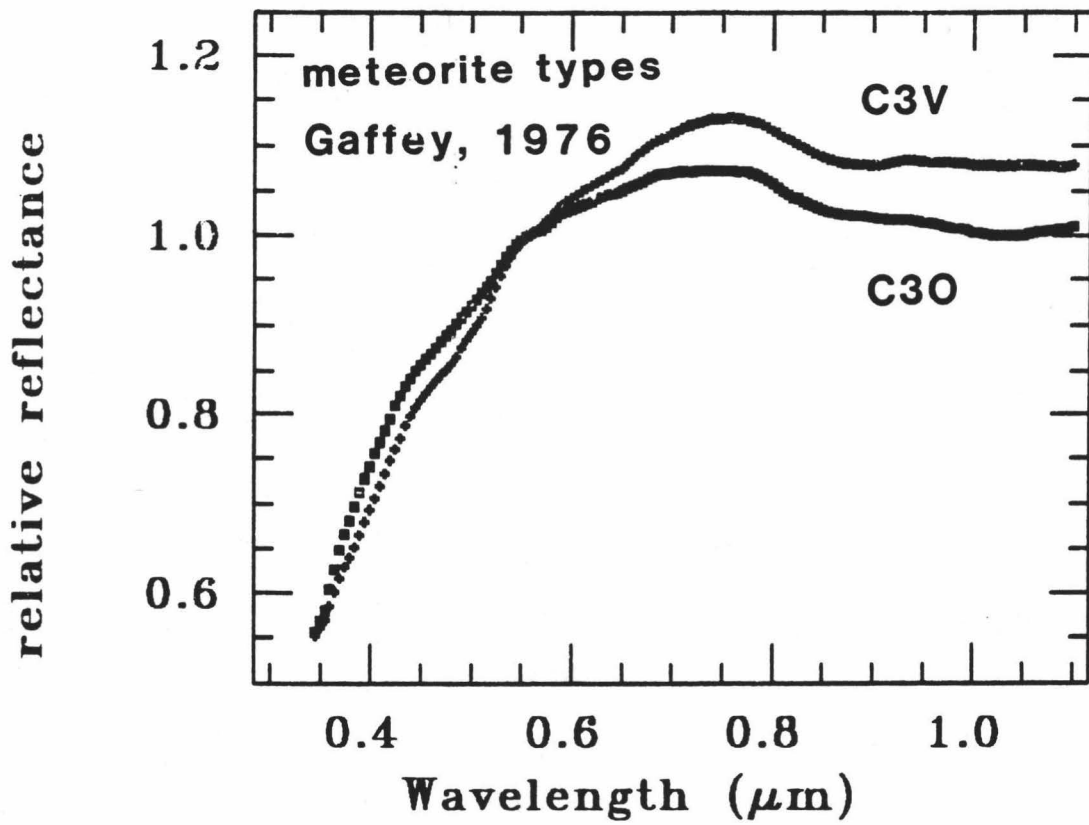


Figure 24

HIGH CALCIUM PYROXENE DIOPSIDE

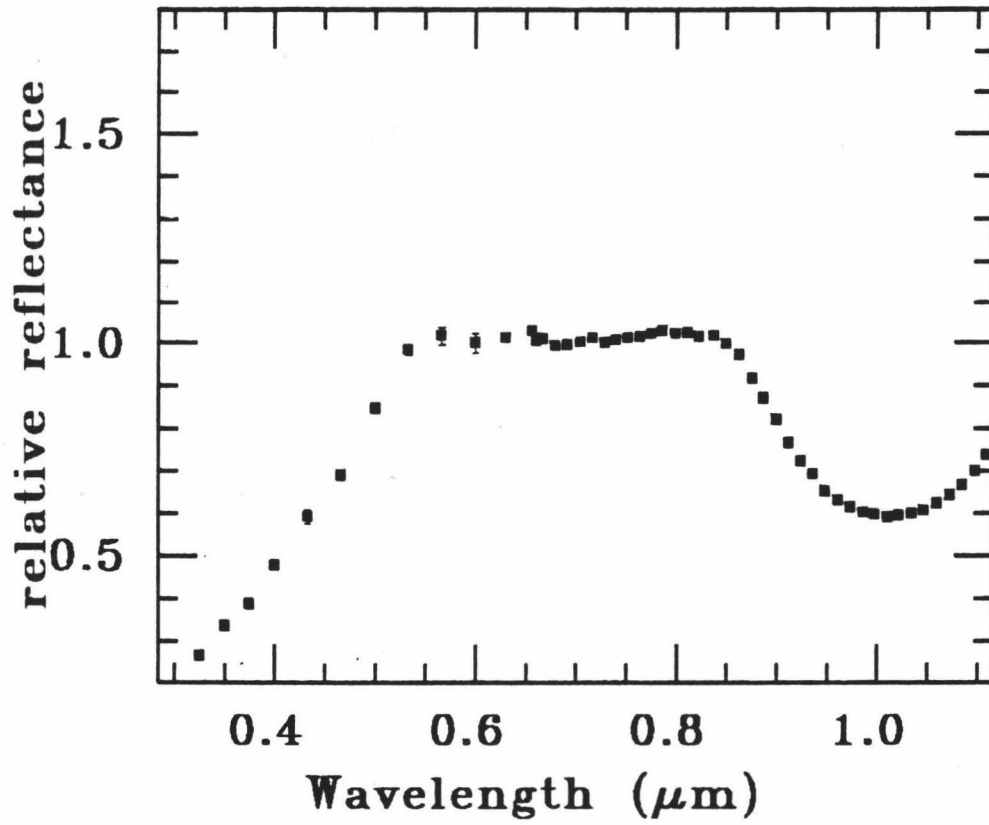


Figure 25

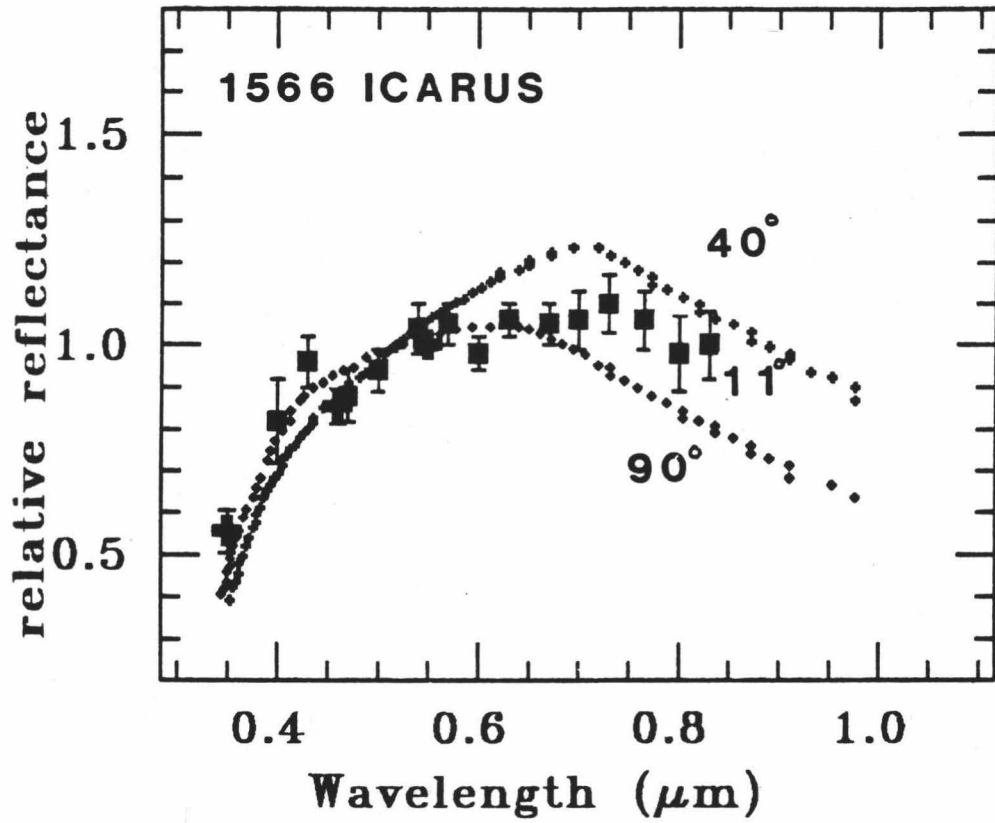


Figure 26

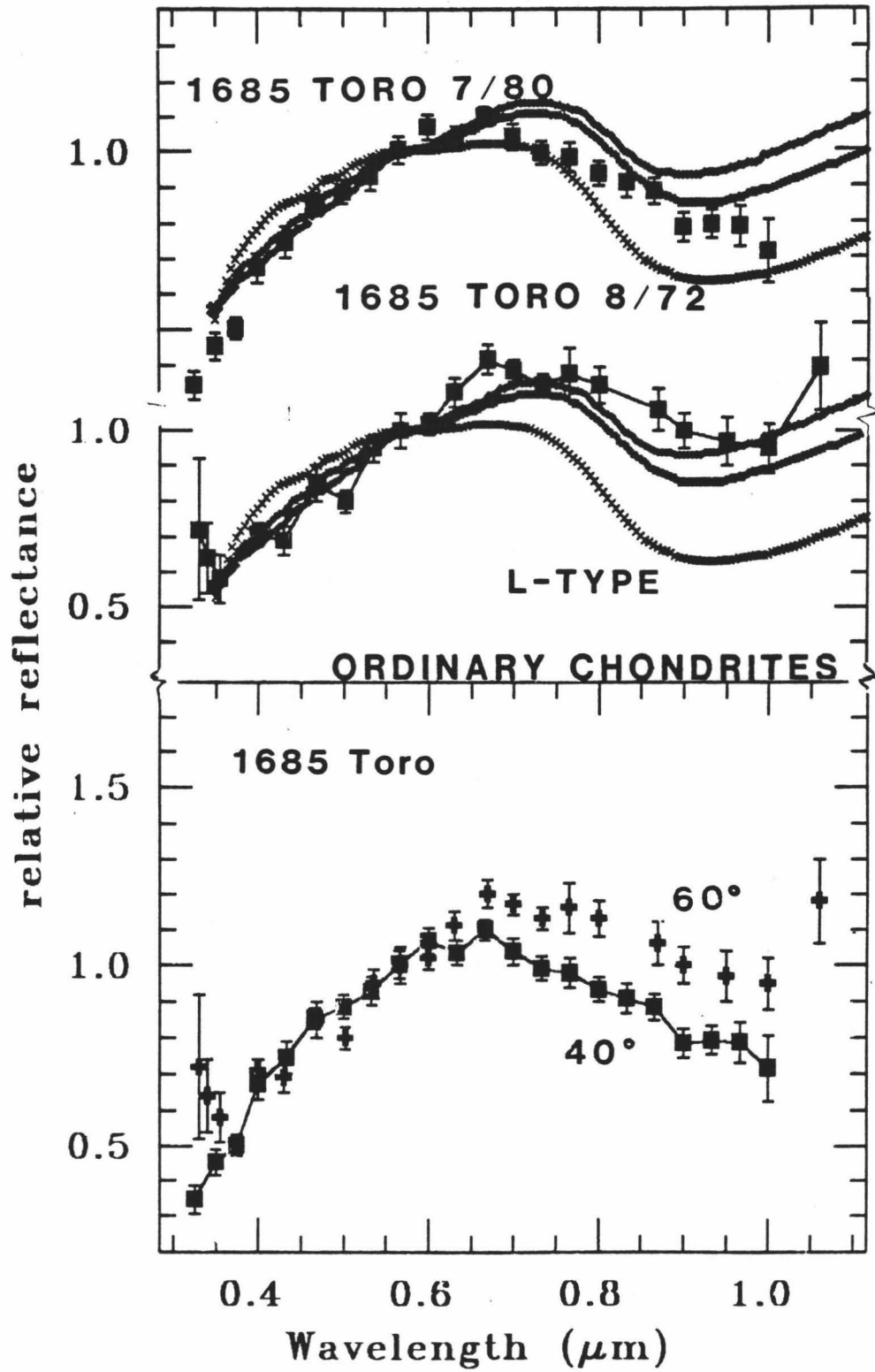


Figure 27

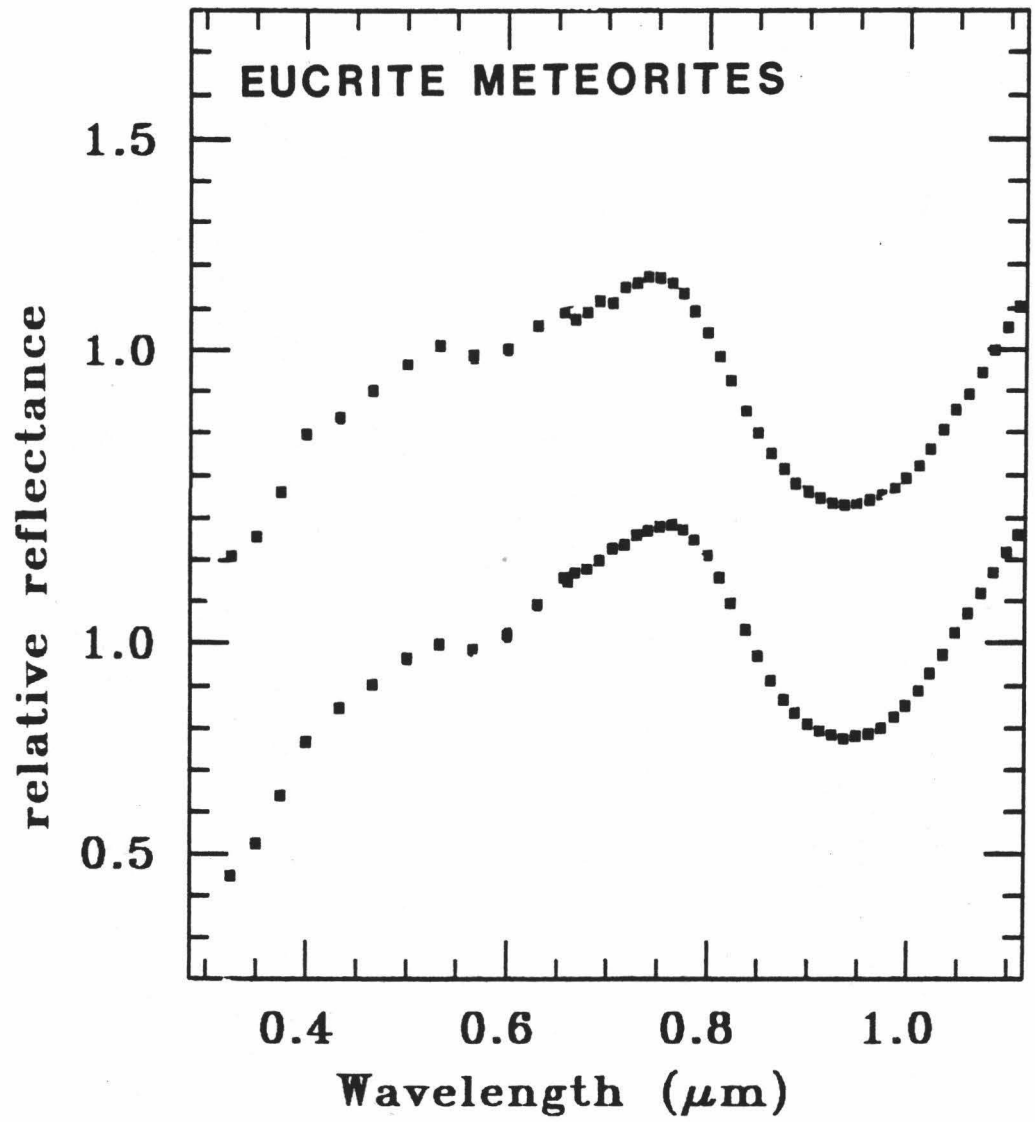


Figure 28

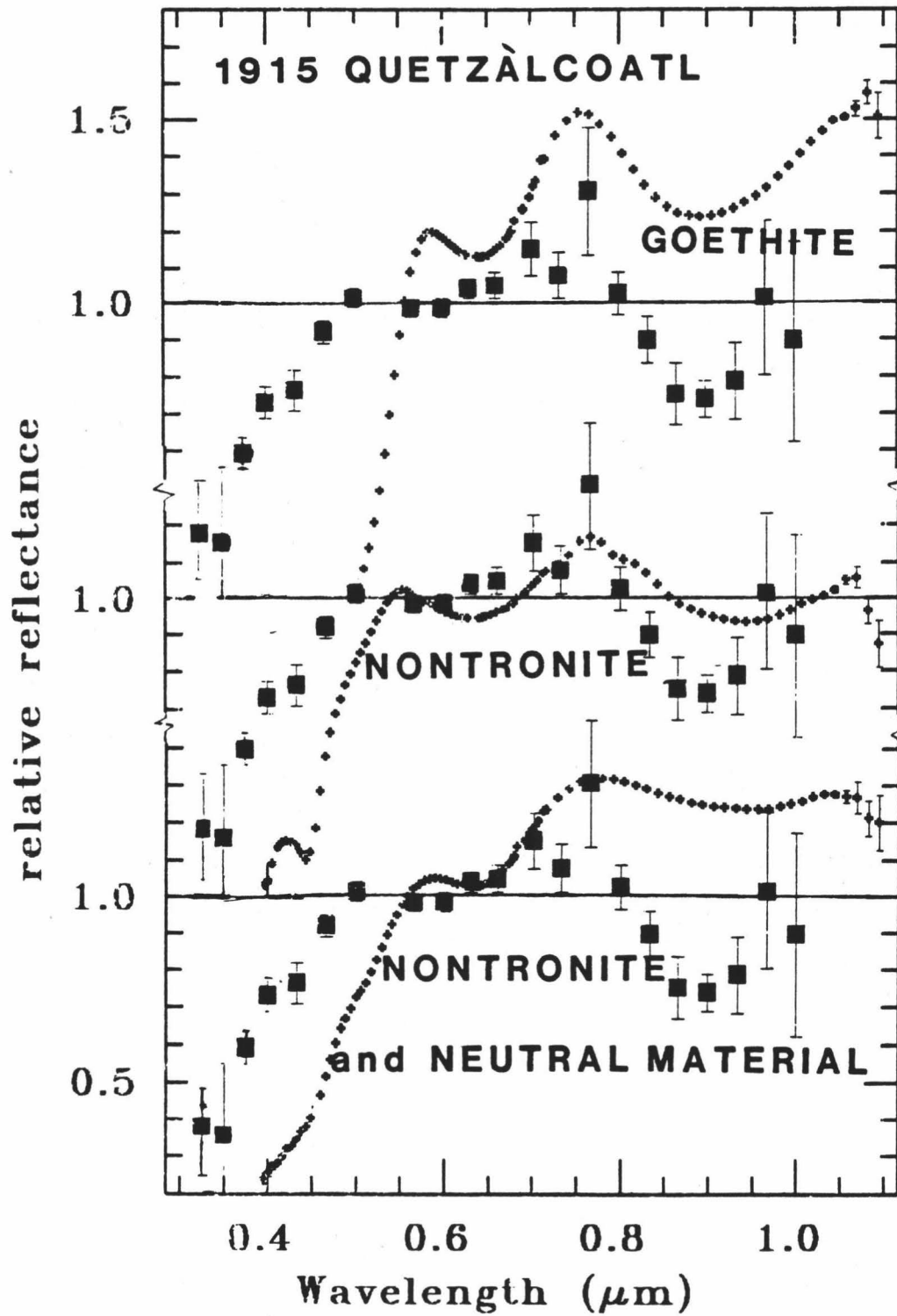


Figure 29

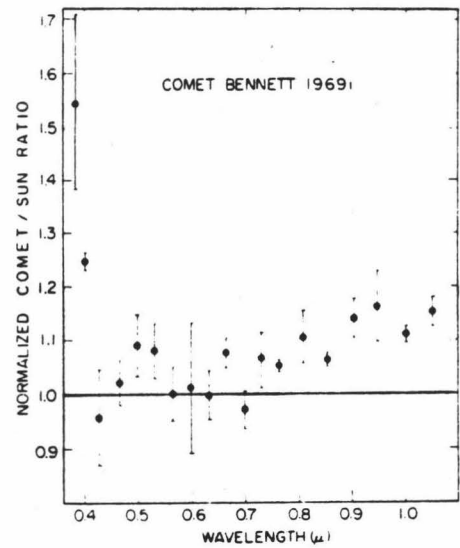
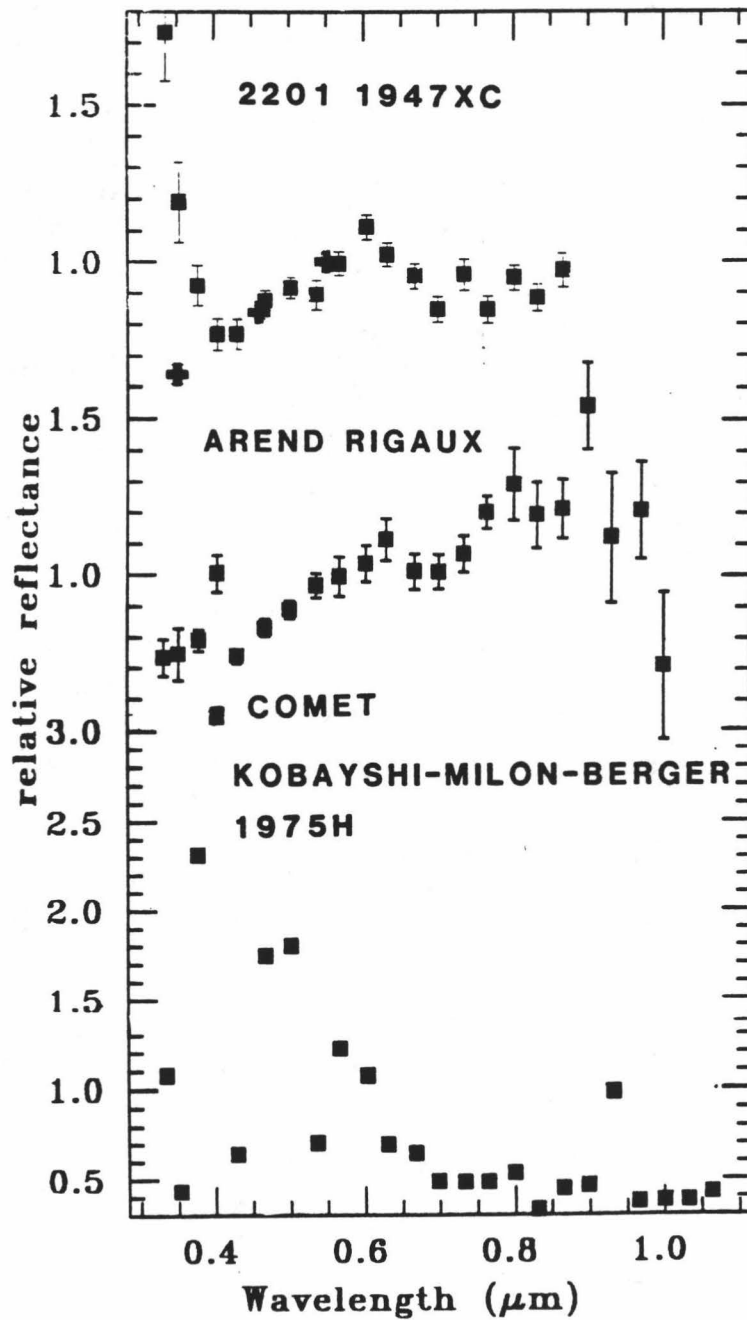


Figure 30

Chapter 2

REVIEW OF PHYSICAL MEASUREMENTS, POPULATION
ESTIMATES, AND SOURCE REGIONS OF NEAR-EARTH
ASTEROIDS AND METEORITES

Introduction

Dynamical studies of the population and origins of near-Earth asteroids have suffered from a paucity of physical measurements to constrain theories. Both observational studies and dynamical theories will be reviewed here. These theories propose different regions of the solar system as sources of near-Earth asteroids. A review of proposed meteorite source regions is included.

Physical Measurements

The physical studies of the near-Earth asteroids studied with reflectance spectroscopy are tabulated in Tables II and III of Chapter 1. Over the years a considerable body of information has accumulated but it is still difficult to determine how representative the results are of the true population.

Prior to the undertaking of this project, reflectance spectra of three near-Earth asteroids had been interpreted and published: 1685 Toro (Chapman et al., 1973, Johnson and Matson, 1973), 433 Eros (McCord and Chapman, 1975, Pieters et al., 1976), and 887 Alinda (Chapman, 1976, Gaffey and McCord, 1978). Four others had been published but not interpreted: 1036 Ganymed, 1566 Icarus, 1580 Betulia, and 1620 Geographos (Chapman and Gaffey, 1979). Gehrels et al. (1970) derived a reflectance for 1566 Icarus based on polarization data and assuming the surface of 1566 Icarus obeys the same inverse relationship between reflectivity and polarization as the Moon. The mineralogical interpretation of 433 Eros and 1685 Toro as H and L type chondrites respectively, has been superseded by interpretations based on new data and a theoretical understanding of reflectance spectroscopy. Chapman (1976) overlaid the

spectrum of 887 Alinda with an H3 ordinary chondrite and showed a match to within the observational errors of the asteroid implying similar surface assemblages. These spectra were reinterpreted in Chapter 1.

Methods and Results of Population Estimates

A systematic survey to discover planet-crossing asteroids began in the 1970's (Helin and Shoemaker, 1979). Until there is evidence that all planet-crossing objects of a certain size and brightness are discovered, it is necessary to estimate the population size to evaluate the significance of its mineralogical character based on observational data. Three techniques are used to estimate population size. The first estimate was based on completeness of search criteria (Opik, 1963) and is still the basis for more recent estimates (Helin and Shoemaker, 1979). Another technique is based on cratering statistics for both the Moon and Earth (e.g., Wetherill, 1976). The third method is based on chance rediscovery statistics and has been subject to controversy in an obscure journal (Kresák, 1978).

Opik (1963) estimated the number of Apollo asteroids at 43 based on the following assumptions: (1) the sky was efficiently covered twice to a limiting magnitude of 18.5 for an object 2.0 AU from the Earth (an exaggeration), (2) a lunar albedo (0.11), (3) 1.0 km diameter, (4) and the relative completeness of existing discoveries is expressed as: $\eta = 1 - \exp(-V/V_0)$ where V is the volume covered by observations and V_0 is the total volume occupied by asteroids. The number of known Apollo asteroids with diameter >1.0 km was 7 at the time. With the number of presently discovered Apollos of this size between 20 and 30 (there are more with diameters <1.0 km) the same statistical assumptions today would yield an estimate over 100. The increased sky coverage would not

affect the estimate since Opik claims to have over-estimated that to begin with. This technique results in a lower limit estimate.

A variation of this estimating technique has been made by Shoemaker and Helin (1977) and Helin and Shoemaker (1979) who estimate the number of Apollo asteroids to absolute visual magnitude 18 as 800 ± 400 based on discoveries of three Apollo asteroids (five by 1979) discovered in their survey and four others discovered in two other surveys. A statistical model using the volume of space searched in each survey and assuming that over a long period of time the argument of perihelion of Apollo objects is randomly distributed in space, provides the estimate. The error derives from the small number of discoveries with known discovery-conditions and errors in estimated magnitude limits of each survey. Using the same technique for Mars-crossers their estimated population size is 10,000-50,000 of these objects.

Population estimates based on cratering statistics (Wetherill, 1976) are made assuming a constant cratering rate subsequent to 3.3 b.y. that was produced by Apollo objects. The observed number of post-mare lunar craters >10 km is used to estimate the flux of projectiles larger than 1 km which created the craters. This estimate will probably provide an upper limit because active comets may contribute to the crater statistics. The number of projectiles impacting the entire moon in 3.3 b.y. is 251. The steady state number of objects larger than 0.5 km with a mean dynamic life time of 2×10^7 yr by Wetherill's calculation is 524. The same calculation using terrestrial craters gives a value of 589 for the population.

A third method of estimating the size of this population was derived by Whipple (1967) and updated (Whipple, 1973). It is based on the then true fact that none of the known Apollos had been accidentally rediscovered. If close to the total population were known, then random

searches would result in rediscoveries of known objects. At the time the estimate of 18th magnitude objects using this relation was 50. The revision in 1973 resulted in an increase to approximately 100. Wetherill (1976) thought that Whipple's treatment of the problem was incorrect. Instead Wetherill (1976) calculated the probability inverse, "the probability that there are S objects given that σ have been discovered and that there have been no chance rediscoveries." The problem stated this way requires an independent estimate of the population size to set an upper limit. Using this form of the problem there is a 50% probability that the population size is 700. If the next discovery of an Apollo were a rediscovery, then the 50% probability size would be reduced to 400. Further chance rediscoveries would alter the upper limits determined from independent techniques. To date there have been three or four chance rediscoveries so the population size estimate should be coming down. However the sky coverage is increasing which must be taken into account. Using the same technique for Amor type objects and the two chance rediscoveries of members of this group, there are an estimated 300-700 Amors. This is the same order of magnitude as the number of Apollos.

In 1978 Kresák analysed the problem of chance rediscoveries and their relation to the size of the Apollo population. His discussion results in the conclusion that the absence of chance rediscoveries is meaningless to the total population of Apollos. His main and relevant point is that the opportunities for rediscovery are not random. Many objects have predictable orbits after their discovery apparition, others have predictable orbits but favorable apparitions have not recurred. These objects are not subject to chance rediscovery. Only four objects are subjects of possible chance rediscoveries. One of them has been rediscovered since Kresák's work was published (2201 1947XC). In spite

of this a lower limit of 10 is placed on the population, a value that has already been exceeded.

Estimates using the three different but sometimes dependent techniques result in Apollo asteroid population size estimates between 300 and 800 with magnitudes brighter than 18 and diameters on the order of one kilometer. With the amount of work put into the planet-crossing asteroid search this seems like a large number. There are less than 50 presently known Apollos and 90% of them have been discovered in the past 20 years with a rapid increase in discovery rate in the past five years. A number of these asteroids appear to have diameters less than 1 km as well.

Mechanisms Resulting in Earth-Crossing Orbit

The mineralogical-petrological characterization of the near-Earth asteroid population provides observational constraints to mechanisms predicting Earth-crossing orbits. If there are objects remaining in the predicted source region that can be compared with near-Earth asteroids on a mineralogical-petrological basis, then a prediction can be tested. This does not necessarily prove or disprove the prediction but it provides an observational constraint to theory.

Opik (1951) first discussed the dynamical instability of planet-crossing orbits and calculated their life time to be 10^8 years against collision with a terrestrial planet or ejection from the solar system. By reason of this mean life time an initial population subject to exponential decay for 4.5 b.y. would have an initial size of 2.5×10^{19} times the then-known population (which numbered 7). An estimated mass would be 100 times that of the Sun. These estimates are obviously impossible and these asteroids therefore have not been decaying from an in

situ population throughout the age of the solar system. A replenishing source or sources must be postulated. Possible sources of near-Earth asteroids include planets, the Moon, asteroids and comets.

Planets and the Moon - Kilometer-sized fragments from planets and the Moon are commonly eliminated from consideration on dynamical grounds as they must be accelerated to the escape velocity of the planets. Large objects cannot achieve such velocities through collision or any other reasonably assumed mechanism.

Asteroids and Cometary Nuclei - Opik (1951,1963) discussed the survival of asteroids and cometary nuclei in Earth-crossing orbits based on first order approximations of the gravitational perturbations of Mars and Jupiter and the number of known Apollos and comets. Some thoughts on these parent bodies are reviewed in the following paragraphs.

Mars-Crossers - The Mars-crossers have orbits stable over the age of the solar system according to calculations of Opik (1963). The rate of injection of perturbed Mars-crossers into the Apollo group is $3.5 \times 10^{-11} N_M$, where N_M is the population of the Mars-crossers. Based on estimates of the size of the Mars-crossers, about 0.36% of the total Apollo population is derived from this source. If the Apollo population is wholly derived from Mars-crossers, then there must be 100-1000 times more Mars-crossers than Apollos, which by some estimates is the case.

Main Belt Asteroid - Perturbations of main belt asteroids by Jupiter into Earth-crossing orbit is eliminated as a possible source mechanism based on the absence of Jupiter crossing asteroids to act as a source. The life time of Jupiter-crossers is shorter than Earth-crossers

by two orders of magnitude. Perturbations of main belt asteroid collisional fragments directly into Earth-crossing orbits are not expected based on the argument that collision fragments must acquire a relative velocity higher than that expected for asteroid collisions (Opik, 1963).

Zimmerman and Wetherill (1973) proposed a mechanism whereby fragments (up to 500m diameter) of collisions of asteroids near the 2:1 Kirkwood gap in the main asteroid belt are injected into the Kirkwood gap at velocities of 50-200 m/sec. In their model, resonant perturbations with Jupiter result in increased eccentricities while the semimajor axis remains constant. Collision probabilities are high for fragments of this size and subsequent collisions remove the libration conditions and permit close approaches to Jupiter. Encounters with Jupiter will result in decreased perihelia on a random basis, increased eccentricities and aphelia near 4.0 AU. Earth-crossing orbits are achieved from statistical calculations within 10^4 years. Scholl and Froeschlé (1977) calculated the frequency distribution of fragments in the Kirkwood gaps that approach the orbit of Jupiter. 30% of 100 calculations of orbits within the 2:1 and 5:2 Kirkwood gap developed aphelia >4 AU indicating that it is statistically possible for objects to approach Jupiter and presumably be subsequently perturbed into Earth-crossing orbit. Objects in the 3:1 Kirkwood gap have perihelia approaching the orbit of Mars which is likely to subsequently perturb asteroids into Earth-crossing orbit.

Comets - If the Apollo asteroids are supplied wholly by comets and a steady state population is assumed, between 10^3 and 4×10^5 comet apparitions a year are required (Opik, 1963). This eliminates comets as the sole source of Apollo objects because there are not 1,000 to 100,000 comets a year. Capture of comets from Jupiter-crossing orbits is

unlikely based on the small number of such objects, their short dynamical life time and the total efficiency required to capture these objects into Earth-crossing orbit (Opik, 1963 and Shoemaker et al., 1979). Comets with aphelia inside the orbit of Jupiter (of which Encke is one) can evolve into Earth-crossing asteroids based on calculations of the rate of devolatilization of Encke (Sekanina, 1972), the existence of a few other comets which are almost extinct (P/Arend-Rigaux and P/Neujmin 1, Kresák, 1979) and Monte Carlo calculations of initial orbits like that of Encke (Wetherill, 1979). Only one Encke-like object is required every $1-10 \times 10^5$ years to maintain the near-Earth population. It is difficult to observationally verify this calculation with statistical significance.

The most likely source of Apollo objects according to the considerations made by Opik, (1963) is comets brought into the terrestrial environment by way of decelerating jet effects of retrograde rotation comets. The time scale of deceleration into an Earth-crossing orbit is approximately the same as the time scale of disintegration of a comet (10^4 yrs). The Apollo population would therefore not be expected to have any active comets in it. The sense of rotation initially being retrograde is capable of evolving as the pole orientations can be changed from the jet effects as well which would explain the observed prograde rotation of the near-Earth asteroids.

Numerical Orbit Calculations - Opik's calculations were made without the benefit digital computers. Marsden (1970) performed long-term direct numerical integrations of several asteroid orbits confirming that the stability of their orbits is maintained even if perturbations of planets other than Jupiter is taken into account. Asteroids thus avoid encounters with Jupiter supporting the results of Opik that the

life time of Jupiter-crossers is 10^3 - 10^4 yrs. Integrations of some cometary orbits are also performed and suggest that low volatile comets may also avoid encounters with Jupiter. In conclusion, if comets do appear to be asteroid-like upon deactivation, their life time as such objects is several orders of magnitude lower than Earth-crossing or main belt asteroids.

Wetherill (1979) calculated the steady-state distribution of orbits of Apollo and Amor objects for asteroids at the inner edge of the main belt, cometary orbits similar to Encke and hypothetical extinct cometary orbits with perihelia larger than that of Encke. Long range perturbations by Jupiter increase the probability of transferring asteroidal material into Earth-crossing orbit. The effects of secular resonances (Williams and Faulkner, 1981) and the increase in eccentricity resulting from objects entering Kirkwood gaps (Zimmerman and Wetherill, 1973, Scholl and Froeschlé, 1977) are taken into account in this work. Approximation methods to include resonance effects into Monte Carlo iterations of Opik's (1951) collision formula as developed by Arnold, (1964b) form the basis of the analysis. It is concluded that both comets and asteroids supply the near-Earth asteroid population. The assumptions include mean collision life times of $<10^9$ yrs of inner belt asteroids (Gault and Wedekind, 1969 as referenced in Wetherill, 1979), and result in a steady-state production rate of 5×10^{-6} objects/yr and a supply from the asteroid belt of only 1.5×10^{-6} objects/yr. These results are lower than the observed Apollo-Amor population by a factor of 10, hence, it is concluded that there must be a significant cometary component. The effects of including the (ν_6) resonance in the calculations reduces the size of the near-Earth population. It does not effect the ratio of cometary versus asteroidal sources.

Shoemaker et al. (1979) suggest that the interaction between a 3:1 commensurability with Jupiter and orbital changes due to Mars encounter may be an important mechanism contributing to the near-Earth asteroid population. The existence of three Earth-crossing Amor asteroids in 3:1 commensurability with Jupiter is the basis for the suggestion although calculations of the strength and rate of this mechanism have not been made. Objects with semimajor axes within the inner part of the main belt (1580 Betulia and 1974MA) may have originally resided close to $(/5$. There are no Earth-crossing asteroids presently located in the $(/6$ resonance even though the Flora family lies near that region and is a potential source of parent bodies as suggested by Levin et al. (1976).

Dynamical Conditions in Near-Earth Orbits

The fate of individual near-Earth asteroids is studied through numerical integration of their orbits taking into account perturbations by the major planets. Orbital resonances of near-Earth asteroids with the terrestrial planets may be stable or unstable resulting in a reservoir or sink for objects in the near-Earth environment. Janiczek et al. (1972) discovered nine minor planets that have close approaches and resonances with Venus or the Earth. The list of objects and their resonances are listed in Table V.

Danielsson and Ip (1972) integrated the orbit of 1685 Toro over a 200 yr interval and showed that it is in an 8:5 resonance with the Earth and a 13:5 resonance with Venus. The resonance with Venus and the particular geometry relative to the Earth makes the resonance vulnerable to instabilities. Janiczek et al. (1972) integrated the orbit over 600 yrs. The stability of the resonances could not be ascertained. Ip and Mehra (1973) discuss the mutual effects of the Earth and Venus

resonances on the orbit of 1685 Toro and concluded that both resonances are unstable due to the off setting forces of each resonance. Williams and Wetherill (1973) integrated the orbit of Toro for 5000 yrs and concluded that if close approaches to Venus and the Earth don't destroy the double resonance, then a close approach to Mars will on a time scale of 3 million years.

Sinclair (1969) and Schweizer (1969) discovered the 3:1 resonance of 887 Alinda with Jupiter. Marsden (1970) integrated the orbit over 1400 years confirming the existence of the libration. He also integrated the orbit of 1915 Quetzàlcoat1 (1953 EA) and suggested that because the characteristics of the orbit are so similar they may have a common origin. He further calculated that they separated from each other 10,000 years ago when they had a common ω (argument of perihelion). Janiczek et al. (1972) concluded that the resonances of 887 Alinda with the Earth, Venus and Jupiter is stable.

433 Eros's orbital period varies regularly with a period of 40 years due to the 4:7 resonance between Eros and the Earth (Ip and Mehra, 1973). The effect of the 7:1 resonance with Jupiter is seen in the variations of the maxima and minima of the orbital period.

1627 Ivar is in a 11:28 resonance with the Earth. According to Ip and Mehra, (1973) this resonance is stable in spite of its high-order nature. According to Janiczek et al. (1972, Table VI) Ivar is in a 2:5 resonance with the Earth.

Weissman and Wetherill (1974) consider the stability of asteroids in the triangular equilibrium points of the Earth-Sun system and found that near-periodic orbits in terrestrial space are stable for at least 10^4 years. No such objects have been found in limited searches for them.

Another dynamical condition of objects in near-Earth orbits are non-random distributions of the component of the angular momentum

perpendicular to the plane of the ecliptic (Wetherill, 1976). There are six clusterings of the perpendicular component of angular momentum which suggest common origins. There has been no explanation of how to preserve this quantity yet change the semi-major axis of the orbits which are not similar within each group.

The Relation Between Near-Earth Asteroids and Meteorites

Possible sources of meteorites include asteroids, comets, extra-solar bodies, the Moon, planets and their satellites. With limited compositional knowledge of solar system bodies there has been more speculation and theoretical consideration given to possible parent bodies. An asteroidal origin is generally assumed. The question however, is by no means answered.

Asteroids - Asteroids are potential sources of meteorites because they are the size (<1000 km diameter) expected of meteorite parent bodies and are located in a stable to metastable region of the solar system (Wasson and Wetherill, 1979) which is necessary in order to currently supply meteorites to the Earth. They are also subject to collisions which can produce fragments of meteorite size. The problem is to determine a mechanism which places the debris in an Earth-crossing orbit on the time scale of 10^6 - 10^7 years as constrained by cosmic ray exposure ages (e.g., Bogard, 1979).

Comets - Based on the orbital elements of 45 meteorites (Simonenko, 1975) they are not compatible with extra-solar or long period comet origins. An association between material entering the Earth's atmosphere and comets has been established from photographic studies of orbits of

meteors (Cepplecha and McCrosky, 1976) and the orbits of known comets. However, it is not clear that the material that survives to land on the Earth is the same as the cometary meteors since only three photographed meteor fireballs (which permit orbital determinations) have been recovered as meteorites (Wasson and Wetherill, 1979). Theoretical arguments of comets being sources of meteorites are the same as those for near-Earth asteroids discussed previously.

The Moon - The Moon is eliminated as a possible meteorite source on the basis of different mineralogy and petrology for all types except basaltic achondrites. The basaltic achondrites differ from lunar basalts in three respects. These include a different oxygen isotope composition (Clayton and Mayeda, 1978, Clayton et al., 1976), absence of a negative europium anomaly characteristic of lunar mare basalts (Consolmagno and Drake, 1977), and older radiometric ages of basaltic achondrites (Wetherill et al., 1981). A meteorite found in Antarctica recently does appear to be of lunar origin, a fact which if proven, will demonstrate an error in dynamical assumptions and calculations.

Planets and their satellites - A planetary origin is usually ruled out by the argument that meteorites from planets would show severe shock effects or be entirely melted or vaporized due to the energy of an impact and the high escape velocity required to eject fragments into meteoritic orbits (Urey and Craig, 1953, Wetherill, 1974). A planetary source cannot presently be ruled out with direct evidence. There is presently indirect evidence that shergottites, nakhlites and chassignites are martian ejecta (reviewed by Wasson and Wetherill, 1979).

Planetary satellites less than 1000 km in diameter having suffered collisions remain potential sources of meteorites however this mechanism

has not been investigated in any detail. Larger satellites have escape velocities which are expected to shock the ejecta to degrees not seen in meteorites.

Observational Evidence

From Asteroids - Laboratory measurements of the reflectance of meteorite powders were reported and compared to available asteroid reflectance measurements between 0.33-1.1 μm (Chapman and Salisbury, 1973, Gaffey and McCord, 1978, 1979). Chapman and Salisbury's (1973) comparisons showed that few asteroid spectra closely match common meteorite spectra in spite of the same range in spectral characteristics being present for both class of objects. From these results they concluded that (1) the meteorites are not members of a uniformly sampled asteroid belt (2) if the meteorites do come from the asteroid belt, then they come from a rare and previously unsampled region. Chapman (1976) discusses the relationship between asteroid and meteorite spectral types and the distribution of asteroidal material in the main belt. He considered the size distribution of the asteroids and the relationship to asteroidal parent bodies. The formation time of gas-rich brecciated meteorites is reasoned to be soon after accretion as the regoliths formed on present-day asteroids cannot be modelled to be similar to the brecciated meteorites. In spite of the fact that few asteroid spectra are a good match to meteorite spectra, the composition of main belt asteroids are similar to meteoritic material. These conclusions ignore the physical significance of the lack of a good spectral match.

From Meteorites - Fish et al. (1960) discuss the origin of meteorites from asteroidal sized bodies (<250 km). They show that diamonds in

meteorites form as a result of impact, not as a function of pressure in large planet-sized bodies and that differentiation of silicates and metal can occur on small bodies in 10^2 - 10^4 years.

Wetherill (1969) uses cosmic-ray exposure ages, local time of fall and apparent radiant (apparent point of origin in the sky) of meteorites to look for distributions of orbital elements of ordinary chondrites. Monte Carlo methods are used to calculate evolving orbits terminating in Earth impact. The effect of secular perturbations of Jupiter and close encounters with planets are included. Only initial orbits with low inclination, aphelia near Jupiter and perihelia inside the Earth's orbit impact the Earth.

Levin and Simonenko (1969) discuss constraints on the orbits of meteorites based on radiants and upper limits of the velocity required for an object to survive passage through Earth's atmosphere. Calculated orbits are consistent with origins in the asteroid belt.

Anders (1975) determines the place of origin of stony meteorites based on trapped solar-wind gas abundances. His results are not conclusive however, as he concludes that implantation took place between 1 and 8 AU from the Sun. Moreover, the cratering rate had to be 10^2 - 10^3 times higher than at 1 AU. He rules out cometary parent bodies as many of the gas-rich meteorites are the result of anhydrous differentiation which contradicts the observations of volatile rich comets. In addition the relatively short life time of comets in the asteroid belt, approximately 10^7 , is too short for the development of a significant regolith which enables gases to be trapped. Thirdly, there were no exotic xenoliths found in meteorites at the time. This observation may no longer be valid (e.g., Neal and Lipschutz, 1981).

Dynamical Model Calculations - Arnold (1964a) used theory developed by Opik (1951) and Monte Carlo methods to calculate the history of objects with a statistically significant number of starting orbits. Orbital evolution was followed until capture by a planet or ejection from the solar system taking into account perturbations by the major planets. These calculations were made on the assumptions that (1) the time scale for planetary collisions is long such that the distribution of orbital elements is random and (2) secular perturbations are small compared to perturbations of major planets. The starting orbits were those of asteroids crossing both the Earth and Mars, Mars-crossers only and lunar ejecta. He then used cosmic ray exposure ages to constrain the results of his dynamical models. The results showed that (1) the mean life time of planet-crossing orbits are shortened and homogenized by major planet perturbations, (2) Octahedrites (with older cosmic ray exposure ages) probably formed in Mars-crossing orbits and were perturbed into Earth-crossing orbit, and (3) approximately 10% of all meteorites have passed as close to the sun as the orbit of Mercury, a prediction affecting rare gas contents in meteorites.

Arnold (1964b) modified his calculations to include (1) destruction by further collision with asteroids, (2) the effects of elliptical orbits, and (3) starting orbits from physical assumptions including a cometary orbit. The implications of the calculations are discussed in Arnold, (1964c). An asteroidal origin for chondrites is possible only if they formed from multiple collisions of a body 5-20 times larger than Jupiter in cross-section. Because this is unlikely, a source of ordinary chondrites must be sought elsewhere and/or the model reworked. Bombardment ages of iron meteorites are consistent with an asteroidal origin.

Wetherill and Williams (1968) propose that collisions within the near-Earth asteroid population will produce meteorite-sized fragments

with the short (10^7) cosmic ray exposure ages observed in ordinary chondrites. However, if Apollos are derived from main belt asteroids, there should be more meteorites with older cosmic ray exposure ages than short ones. Since this does not occur, it seems that the Apollos were not derived from the main belt. However, this does not effect the hypothesis that meteorites are fragments of Apollos because the Apollos are not necessarily derived from the asteroid belt. The expected mass yield from fragments of Apollo asteroids is not large enough to account for the meteorites. In addition, the known orbits of Apollo asteroids are not consistent with the observed distribution of chondrite radiants and the time of the day at which chondrites fall. Wetherill (1976) reconsiders the earlier work of Wetherill and Williams (1968) and revises the size of the Apollo population. A higher mass yield of meteorites from Apollo asteroids is calculated using observational data indicating larger diameters than previously believed (albedo measurements became available for more objects). This higher mass yield can account for the entire flux of chondritic material (10^8 - 10^9 g/yr). However, he concludes that the source of Apollo objects is still most likely comets.

Levin et al. (1976) reconstructed the orbit of the Farmington meteorite based on a radiant determined from newspaper reports of the fall and assuming different velocities. They conclude that this meteorite is a fragment of an Apollo asteroid because its calculated orbit is Earth-crossing with aphelion in the inner edge of the asteroid belt and cosmic ray exposure age is short (25,000 yrs) implying that the collision exposing it to radiation took place in near-Earth orbit. None of the known Apollo asteroids of the time of publication have orbits similar to that of Farmington. 1862 Apollo, Hermes and 1865 Cerberus were passable matches.

Considerations of the abundance and delivery rate of material from the inner asteroid belt by way of secular perturbations and encounters with Mars and Earth as sources of differentiated meteorites is addressed by Wetherill and Williams (1978). The older cosmic ray exposure ages of iron meteorites (10^8 - 10^9) has to be consistent with dynamical theory bringing material to the Earth. It is clear that the collisions fragmenting these objects did not take place in Earth-crossing orbit as the exposure ages are longer than the mean life times of near-Earth asteroids. The young exposure ages of achondrites (<20 m.y.) are accounted for by collisional destruction of the older fragments. The estimates of the abundance of meteorites supplied by this mechanism is enough to produce the observed distribution of differentiated meteorites.

Composition of Large, Earth Impacting Projectiles - Wolf et al. (1980) analyzed the composition of eleven impact melts by neutron activation analysis to characterize the nature of the enrichments over basement rock composition. The enrichments are compared with meteoritic material. The results are summarized in Table VI. It is interesting that all classes of meteorites are represented, chondrites, irons and achondrites. Ordinary chondrites seem to be under represented relative to their abundance in the meteorite collection. This might be a function of the strength of ordinary chondrites compared to other classes although there is evidence of carbonaceous projectiles which are even weaker than ordinary chondrites.

Meteors and Near-Earth Asteroids - Drummond (1982) associated some meteor showers with near-Earth asteroids as did Sekanina (1976). This indicates that some meteors might be collisional debris associated with

asteroids. If any of these meteors survive to become meteorites and are recovered, we will know we have an asteroid fragment in hand. Studies of the chemical composition and physical strength of meteors (Wetherill and Revelle, 1982) are possible and provide information of meteor parent bodies. The asteroid-meteor associations are newly discovered and no physical studies of these meteors have been made yet.

Summary

The background for discussing the implications of the mineralogical-petrological interpretation presented in Chapter 1 has been reviewed. In the final chapter the results from Chapter 1 will be applied to the theories and information reviewed above in an effort to determine the origin of near-Earth asteroids and their relation to meteorites.

References

- Anders, E. (1975) Do stony meteorites come from comets?. *Icarus*, **24**, 363-371.
- Arnold, J.R. (1964a) The origin of meteorites as small bodies. In Iso-
topic and Cosmic Chemistry, ed., H. Craig, S.L. Miller, and G.J. Wasser-
burg, North-Holland Publ. Co., Amsterdam, 347-364.
- Arnold, J.R. (1964b) The origin of meteorites as small bodies II. The
model. *Astrophys. J.*, **141**, 1536-1547.
- Arnold, J.R. (1964c) The origin of meteorites as small bodies III. Gen-
eral considerations. *Astrophys. J.*, **141**, 1548-1556.
- Bogard, D.D. (1979) Chronology of asteroid collisions as recorded in
meteorites. In Asteroids, T. Gehrels, ed., The University of Arizona
Press, Tucson, 558-578.
- Cepilecha, Z. and McCrosky, R.E. (1976). Fireball and heights: A diagnos-
tic for the structure of meteoric material. *J. Geophys. Res.*, **81**,
6257-6275.
- Chapman, C.R. (1976) Asteroids as meteorite parent-bodies: The astron-
omical perspective. *Geochim. Cosmochim. Acta*, **40**, 701-719.
- Chapman, C.R. and Salisbury, J.W. (1973) Comparisons of meteorite and
asteroid spectral reflectivities. *Icarus*, **19**, 507-522.

Chapman, C.R. and Gaffey, M.J. (1979) Reflectance spectra for 277 asteroids. In Asteroids, T. Gehrels, ed., The University of Arizona Press, Tucson, 655-687.

Chapman, C.R., McCord, T.B., and Pieters, C. (1973) Minor planets and related objects. X. Spectrophotometric study of the composition of (1685) Toro. **Astron. J.** 78, 502-505.

Clayton, R.N. and Mayeda, T.K. (1978) Genetic relations between iron and stony meteorites. **Earth Planet. Sci. Lett.**, 30, 10-18.

Clayton, R.N., Onuma, N., and Mayeda, T.K. (1976) A classification of meteorites based on oxygen isotopes. **Earth and Planet. Sci. Lett.**, 30, 10-18.

Consolmagno, G.J. and Drake, M.J. (1977) Composition and evolution of the eucrite parent body: Evidence from rare earth elements. **Geochim. Cosmochim. Acta**, 41, 1271-1282.

Danielsson, L. and Ip, W.-H. (1972) Capture resonance of the asteroid 1685 Toro by the Earth. **Science**, 176, 906-907.

Drummond, J.D. (1982) Theoretical meteor radiants of Apollo, Amor, and Aten asteroids. **Icarus**, 49, 143-153.

Fish, R.A., Goles, G.G., and Anders, E. (1960) The record in the meteorites. III. On the development of meteorites in asteroidal bodies. **Astrophys. J.**, 132, 243-258.

Gaffey, M.J. and McCord, T.B. (1978) Asteroid surface materials: Mineralogical characterization from reflectance spectra. **Space Science Reviews**, 21, 555-628.

Gaffey, M.J. and McCord, T.B. (1979) Mineralogical and petrological characterizations of asteroid surface materials. In Asteroids, T. Gehrels, ed., The University of Arizona Press, Tucson, 688-723.

Gault, D.E. and Wedekind, J.A. (1969) The destruction of tektites by micrometeorite impacts. **J. Geophys. Res.**, 74, 6780-6794.

Gehrels T., Roemer, E., Taylor, R.C., and Zellner, B.H. (1970) Minor Planets and related objects. IV. Asteroid (1566) Icarus. **Astron. J.**, 75, 186-195.

Helin, E.F. and Shoemaker, E.M. (1979) The Palomar planet-crossing asteroid survey, 1973-1978. **Icarus**, 40, 321-328.

Ip, W.-H. and Mehra, R. (1973) Resonances and librations of some Apollo and Amor asteroids with the Earth. **Astron. J.**, 78, 142-147.

Janiczek, P.M., Seidelmann, P.K., and Duncombe, R.L. (1972) Resonances and encounters in the inner solar system. **Astron. J.**, 77, 764-773.

Janssens, M.-J., Hertogen, J., Takahashi, H., Anders, E., and Lambert, P. (1977) Rochechouart meteorite crater: Identification of projectile. **J. Geophys. Res.**, 82, 750-758.

Johnson, T.V. and Matson, D.L. (1973) Minor planets and related objects.

XI. 0.4-0.8 μm spectrophotometry of (1685) Toro. **Astron. J.**, **78**, 505-507.

Kresák, L'. (1978) The total number of the apollo asteroids and their chance rediscoveries. **Bull. Astron. Inst. Czechosl.**, **29**, 149-154.

Kresák, L'. (1979) Dynamical interrelations among comets and asteroids. In Asteroids, T. Gehrels, ed., The University of Arizona Press, Tucson, 289-309.

Levin, B.J. and Simonenko, A.N. (1969) Meteorite radiants and orbits. in Meteorite Research, ed., P.M. Millman, D. Reidel, Dordrecht, 552-558.

Levin, B.J., Simonenko, A.N., Anders, E. (1976) Farmington meteorite: A fragment of an Apollo asteroid? **Icarus**, **28**, 307-324.

Marsden, B.G. (1970) On the relationship between comets and minor planets. **Astron. J.**, **75**, 206-217.

McCord, T.B. and Chapman, C.R. (1975) Asteroids: Spectral reflectance and color characteristics. II. **Astrophys. J.**, **197**, 781-790.

Morgan, J.W., Higuchi, H., Ganapathy, R. and Anders, E. (1975) Meteoritic material in four terrestrial meteorite craters. **Proc. Lunar Sci. Conf. 6th**, 1609-1623.

Morgan, J.W., Janssens, M.-J., Hertogen, J., Gros, J., and Takahashi, H. (1979) Ries impact crater: Search for meteoritic material. **Geochim. Cosmochim. Acta**, **43**, 803-815.

Neal C.W. and Lipschutz, M.E. (1981) Cumberland falls chondritic inclusions: Mineralogy/petrology of a forsterite chondrite suite. **Geochim. Cosmochim. Acta**, 45, 2091-2107.

Opik, E.J. (1951) Collision probabilities with the planets and the distribution of interplanetary matter. **Proc. Roy. Irish Acad.**, 54A, 165-199.

Opik, E.J. (1963) The stray bodies in the solar system. Part I. Survival of cometary nuclei and the asteroids. **Adv. Astron. Astrophys.**, 2, 219-262.

Palme, H., Janssens, M.-J., Takahashi, H., Anders, E., and Hertogen, J. (1978a) Meteoritic material at five large impact craters. **Geochim. Cosmochim. Acta**, 42, 313-323.

Palme, H., Wolf, R., and Grieve, R.A.F. (1978b) New data on meteoritic material at terrestrial impact craters. **Lunar Planet. Sci. IX**, 856-858.

Palme, H., Gobel, E., and Grieve, R.A.F. (1979) The distribution of volatile and siderophile elements in the impact melt of East Clearwater (Quebec). **Proc. Lunar Planet. Sci. Conf. 10th**, 2465-2492.

Pieters, C., Gaffey, M.J., Chapman, C.R., and McCord, T.B. (1976) Spectrophotometry (0.33-1.07 μ m) of 433 Eros and compositional implications. **Icarus**, 28, 105-115.

Scholl, H. and Froeschlé, C. (1977) The Kirkwood gaps as an asteroidal source of meteorites. In Comets, Asteroids, Meteorites-Interrelations,

Evolution and Origins. ed., A.H. Delsemme, The University of Toledo, Toledo, 293-296.

Sekanina, Z. (1972) A model for the nucleus of Encke's comet. In The Motion Evolution of Orbits, and Origin of Comets. eds., G.S. Chebotarev and Kazimirchak-Polonskaya, D. Reidel, Dordrecht, 301-307.

Schweizer, F. (1969) Resonant asteroids in the Kirkwood gaps and statistical explanations of the gaps. Astron. J., 74, 779-788.

Shoemaker, E.M. and Helin E.F. (1977) Populations of planet-crossing asteroids and the relation of apollo objects to main-belt asteroids and comets. In Comets, Asteroids, Meteorites-Interrelations, Evolution and Origins. ed., A.H. Delsemme, The University of Toledo, Toledo, 297-300.

Shoemaker, E.M., Williams, J.G., Helin, E.F., and Wolfe, R.F. (1979) Earth-crossing asteroids: Orbital classes, collision rates with earth, and origin. In Asteroids, T. Gehrels, ed., The University of Arizona Press, Tucson, 253-282.

Simonenko, A.N. (1975) Orbital elements of 45 meteorites Atlas (Moscow: Nauka).

Sinclair, A.T. (1969) The motions of minor planets close to commensurabilities with Jupiter. Mon. Not. Roy. Astron. Soc. 142, 289-294.

Urey, H.C. and Craig, H. (1953) The composition of the stone meteorites and the origin of the meteorites. Geochim. Cosmochim. Acta, 4, 36-82.

Wasson, J.T. and Wetherill, G.W. (1979) Dynamical, chemical and isotopic evidence regarding the formation locations of asteroids and meteorites. In Asteroids, T. Gehrels, ed., The University of Arizona Press, Tucson, 926-974.

Weissman, P.R. and Wetherill, G.W. (1974) Periodic Trojan-type orbits in the Earth-Sun system. **Astron. J.**, 79, 404-412.

Wetherill, G.W. (1969) Relationships between orbits and sources of chondritic meteorites. In Meteorite Research, ed., P. M. Millman, D. Reidel, Dordrecht, 573-589.

Wetherill, G.W. (1974) Solar system sources of meteorites and large meteoroids. **Ann. Rev. Earth and Planet. Sci.**, 2, 303-331.

Wetherill, G.W. (1976) Where do the meteorites come from? A re-evaluation of the Earth-crossing Apollo objects as sources of chondritic meteorites. **Geochim. Cosmochim. Acta**, 40, 1297-1317.

Wetherill, G.W. (1979) Steady state populations of Apollo-Amor objects. **Icarus**, 37, 96-112.

Wetherill, G.W. and Williams, J.G. (1968) Evaluation of the Apollo asteroids as sources of stone meteorites. **J. Geophys. Res.**, 73, 635-648.

Wetherill, G.W. and Williams, J.G. (1978) Origin of differentiated meteorites. In Origin and Distribution of the Elements, ed. L.H. Ahrens, Pergamon Press, Oxford, 19-31.

Wetherill, G.W. and D.O. Revelle (1982) Relationships between comets, large meteors, and meteorites. in Comets, ed. L. Wilkening, The University of Arizona Press, Tucson, 297-319.

Wetherill, G.W., Allègre, C.J., Brooks, C., Eberhardt, P., Hart, S.R., Murthy, V.R., Tera, F., and Van Schmus, W.R. (1981) Review of chronologic data for basaltic achondrites. In Basaltic Volcanism on the Terrestrial Planets, ed., W. Kaula, Lunar and Planetary Institute, Houston, 935-947.

Whipple, F.L. (1967) The meteoritic environment of the Moon. *Proc. Roy. Soc.* **296A**, 304-315.

Whipple, F.L. (1973) Note on the number and origin of Apollo asteroids. *The Moon*, **8**, 340-345.

Williams, J.G. and Faulkner, J. (1981) The positions of secular resonance surfaces. *Icarus*, **46**, 390-399.

Williams, J.G. and Wetherill, G.W. (1973) Minor planets and related objects. XIII. Long-term orbital evolution of (1685) Toro. *Astron. J.*, **78**, 510-515.

Wolf, R., Woodrow, A.B., and Grieve, R.A.F. (1980) Meteoritic material at four canadian impact craters. *Geochim. Cosmochim. Acta*, **44**, 1015-1022.

Zimmerman, P.D. and Wetherill, G.W. (1973) Asteroidal source of meteorites. *Science*, **182**, 51-53.

Table V

Possible Resonances and Encounters in the Inner Solar System

Minor planet	Period Yr	Semi- major axis A.U.	Eccentricity	Major planet	Multiple major planet mean motion <i>i</i>	Multiple minor planet mean motion <i>j</i>	Possible encounters
Eros (433)	1.76	1.4581	0.2229	Venus	1	3	Yes
				Earth	4	7	
Alinda (887)	3.99	2.5158	0.5436	Venus	2	13	Yes
				Earth	1	4	
				Mars	8	17	
				Jupiter	3	1	
Ganymed (1036)	4.33	2.6584	0.5424	Venus	1	7	Yes
				Earth	3	13	
				Mars	10	23	
Amor (1221)	2.67	1.9223	0.4358	Venus	3	13	Yes
				Earth	3	8	
				Mars	12	17	
				Jupiter	9	2	
Icarus (1566)	1.12	1.0777	0.8267	Venus	5	9	Yes
				Venus	6	11	Yes
				Venus	11	20	Yes
				Earth	8	9	Yes
				Earth	17	19	Yes
Mars			Yes				
Betulia (1580)	3.25	2.1949	0.4928	Venus	3	16	Yes
				Earth	4	13	
				Mars	11	19	
Geographos (1620)	1.39	1.2440	0.3353	Venus	4	9	Yes
				Earth	5	7	Yes
				Earth	13	18	Yes
				Mars			Yes
Ivar (1627)	2.55	1.8642	0.3967	Venus	1	4	Yes
				Earth	2	5	
				Mars	17	23	
Toro (1685)	1.60	1.3679	0.4360	Venus	5	13	Yes
				Earth	5	8	Yes
				Mars	20	17	Yes

Table VI

Meteorites Associated with Large Impact Craters

Crater	Diam. km	Meteorite	Reference
Rochechouart	~20	IIA Iron	<i>b</i>
Bosumtwi	10.5	Iron?	<i>cd</i>
Mistastin	28	Iron??	<i>ag</i>
Gow Lake	5	Iron??	<i>g</i>
Clearwater East	22	C1 or C2	<i>cde</i>
Lake Wanapitei	8.5	C or LL	<i>g</i>
Brent	4	L?	<i>d</i>
Nicholson Lake	12.5	Nakhlite, Ureilite	<i>g</i>
Ries	24	Aubrite?	<i>f</i>
Manicouagan	70	Achondrite??	<i>cd</i>

- a.* Morgan et al. (1975). *e.* Palme et al. (1979).
b. Janssens et al. (1977). *f.* Morgan et al. (1979).
c. Palme et al. (1978a). *g.* This work.
d. Palme et al. (1978b).

Chapter 3

**RELATION OF NEAR-EARTH ASTEROIDS TO POTENTIAL SOURCE REGIONS
BASED ON MINERALOGY AND PETROLOGY**

Introduction

In the previous chapter, literature covering near-Earth asteroid population estimates, dynamical models predicting source regions, and the relation of near-Earth asteroids to meteorites was reviewed. In this chapter, the results of mineralogical and petrological characterization of near-Earth asteroids is compared to the known mineralogy and petrology of predicted source regions. This is the largest observational data base available to provide constraints to dynamical theories. The relation of meteorites to the observed near-Earth asteroids is discussed in the second part of this chapter.

Procedure

Each potential source region of near-Earth asteroids will be considered. These include the surface of planets and satellites, main belt asteroids, asteroids near Kirkwood gaps (Scholl and Froeschlé, 1977) and secular resonances (Williams and Faulkner, 1981), Mars-crossers, the Flora, Phocaea and Hungaria families, and comets (e.g., Opik, 1963). A comparison based on mineralogy and petrology will be made first if possible. Such an analysis can only be made with the Moon. When data are not adequate for a mineralogical analysis, a comparison based on similar spectral properties and albedo is made. Physical measurements of asteroids are not complete enough to answer the question of mineralogical similarity. A number of asteroids are targetted for further measurement of either spectral reflectance and/or albedo as their surface compositional similarity is only suggestive. Table VII summarizes the results. The first order assumption that fragments of parent bodies have the same spectral signatures and albedo as the source from which

they are derived is made. The validity of this assumption will be discussed at the end of the chapter.

In the process of comparing near-Earth asteroid spectra with existing asteroid spectra, a number of potential matches were eliminated because of a lack of agreement between the data in the mid-visible region where the flux and detector sensitivity are high. These matches are only suggestive until additional coverage can verify the match through all wavelengths observed. If the data do not agree to within the experimental error of both spectra, the comparison was carried no further and the asteroid was eliminated as a potential compositional analogue because of the different mineralogy implied by the absence of a match. In some cases a spectrum matched very well in the visible but there was no coverage across the 1.0 μm region for the main belt asteroid. If the near-Earth asteroid was observed in the 1.0- μm region, it was only compared with asteroids with similar wavelength coverage. A number of mineralogical similarities are suggested between near-Earth asteroids without 1.0- μm region coverage and main belt asteroids with 1.0- μm region coverage. These potential analogues are discussed in the following section. Many asteroids with similar spectral characteristics have different albedos. This criterion alone eliminated many potential analogues. In a few cases IR data is available. These data often eliminate matches that were based on the visible spectra alone.

Results

Planets and Satellites

The surface composition of the terrestrial planets and the Moon are known to varying degrees of thoroughness and certainty as a result

of manned exploration and ground-based reflectance measurements. The surface composition as determined from reflectance spectroscopy of Mercury (Figure 31a Vilas and McCord, 1976), and Mars (Figure 31b Singer et al., 1979) show surface compositions different than any of the near-Earth asteroids in both the visible and near-infrared (NIR). This is not a surprising result as the gravity field and weathering environments control the regolith properties of planets and large satellites. The regolith is not expected to be retained on a large ejecta fragment from a planet. The important question is whether or not their bedrock compositions are similar to near-Earth asteroids, as some of them could be large fragments from grazing impacts. This question cannot be answered without knowledge of sub-regolith mineralogy and petrology which is not known for Mercury and Mars. If martian bedrock is ultramafic, its spectral properties might be similar to those of 1685 Toro (Figure 3). 1915 Quetzàlcoat1 (Figure 3) has a basaltic composition which could be similar to that of Mercury or Mars. These associations are purely speculative due to the presently limited knowledge of both the planets and near-Earth asteroids.

near-Earth asteroids. The spectrum of 1915 Quetzàlcoat1 (Figure 3) has the spectral features of a basaltic achondrite, which in the absence of additional constraints (e.g., oxygen isotope and trace element analyses), may be similar to lunar basalts (Figures 31c-a). Some lunar basalts such as high-titanium mare basalts would have a low albedo and pyroxene bands masked by ilmenite. It is possible that such basalts would have similar spectral features to 1980AA or 1580 Betulia (Figure 3). The anorthositic composition of the lunar highlands (Figures 31c-a) is not seen in any near-Earth asteroids.

Most of the satellites of the outer solar system are icy bodies but their visible reflectance spectra contain signatures of the non-ice

component. If the near-Earth asteroids originated from these objects or their environment, the asteroids might have the same non-ice component on their surface. A comparison of the reflectance spectra of near-Earth asteroids with the satellites of the outer solar system reveals no spectral similarities. The satellites of Saturn (Figure 32a McCord et al., 1970) show no UV silicate absorptions indicating a paucity of silicates which is not characteristic of near-Earth asteroids. The visible reflectance spectra of the Galilean satellites of Jupiter (Figure 32b McFadden et al. 1980) have UV absorption band slopes and weak to absent 1.0- μm bands which are different than any of the near-Earth asteroid spectra. J8, and J9 (Figure 32c Smith et al., 1981) have spectra characteristic of RD-type asteroids. They are not spectrally similar to near-Earth asteroids. The Uranian satellites Titania and Oberon (Figure 32d Bell et al., 1979, Cruikshank, 1982) are not similar to any of the near-Earth asteroids measured to date. They have slopes and inflections not seen in near-Earth asteroid spectra. Triton, a neptunian satellite (Figure 32e Bell et al., 1979) also has no analogue in the near-Earth population. These conclusions are not unexpected but are considered for the sake of completeness.

Main Belt Asteroids

The results of the mineralogical-petrological interpretation of the near-Earth asteroids reported in Chapter 1 indicate that the surface of these objects are composed of common minerals found on asteroids and throughout the inner solar system with a few tentative exceptions. Interpretation of 277 visible reflectance spectra (Chapman and Gaffey, 1979) is not complete. Feierberg et al. (1982) have interpreted a selected sample of these asteroids. Gradie and Tedesco, (1982) used

lower resolution spectra and albedo determinations to study the distribution of compositional types between 1.8 and 5.2 AU. They concluded that the compositional variation observed through the main belt is primordial, meaning that it has not changed since the formation of the solar system. Compositional types in the near-Earth population may have originated in regions where these types predominate.

Among the nine compositional types used by Gradie and Tedesco (1982, Table VIII) there are no representatives of the D or E types found in the near-Earth population to date. There is one U-type (2201 1947XC). The predominant groups are S and R types to which 12 out of 17 near-Earth asteroids belong. There are four asteroids that are either members of the C, F, P or M group. The absence of albedo measurements for some of these asteroids prevents definite classification into these groups at this time.

The surface composition of 1915 Quetzälcoat1 consists of orthopyroxene and a neutral, unspecified component or shocked minerals consistent with the spectral features of diogenite meteorites, a subset of the basaltic achondrites. The mineralogical characteristics of parts of the surface of the main belt asteroid 4 Vesta (Figure 33) are the same as 1915 Quetzälcoat1.

Asteroids Near Resonances

2:1 Kirkwood Gap - Table IX (Wasson and Wetherill, 1979) lists the 14 large asteroids with semimajor axes within 0.1 AU of the 2:1 Kirkwood Gap (Figure 34). Half of the asteroids on the list have measured reflectance spectra. A comparison was made between these spectra and near-Earth asteroid spectra. None of the near-Earth asteroids measured to date have similar spectral characteristics to measured asteroids near

the 2:1 Kirkwood gap.

5:2 Kirkwood Gap - There are 45 asteroids larger than 50 km diameter within 0.1 AU (Table X, Wasson and Wetherill, 1979) of the 5:2 Kirkwood gap (Figure 34). Thirty-two of these asteroids have been measured by reflectance spectroscopy and were examined for spectral features and albedo similar to near-Earth asteroids.

The spectrum of 1580 Betulia and 2 Pallas are similar (Figure 35a). Both these asteroids have unusually high inclinations, low albedo (0.03-0.06 Lebofsky et al., 1978 and 0.06 Morrison and Zellner, 1979 respectively) and a similar reflectance spectrum. 2 Pallas is the largest member of a family of asteroids lying between the $(\sqrt{5})$ and $(\sqrt{16})$ secular resonances (Williams and Faulkner, 1981). The similar surface composition and high inclination orbits are suggestive of a genetic relation between these two objects.

The spectrum and albedo of 68 Leto and 1620 Geographos are similar to the extent of spectral overlap (Figure 35b). Measurements of 1620 Geographos covering the 1.0 μm region are needed to confirm the similarity.

The spectrum of 1862 Apollo has similar spectral features to 471 Papagena, 39 Laetitia and 349 Dembowska (Chapman and Gaffey, 1979, Figure 36). The albedo of 1862 Apollo is higher (0.21 \pm 0.02, Lebofsky et al., 1981) than 471 Papagena (0.163, Morrison and Zellner, 1979) and 39 Laetitia (0.167, Morrison and Zellner, 1979). Based on a comparison of the JHK spectrum of 39 Laetitia (Larson and Veeder, 1979) and the VJHK spectrum of 1862 Apollo (Hartmann et al., 1982), the width and depth of the 1.0- μm band indicate different mineralogies for these two asteroids (Figure 37a). The albedo of 349 Dembowska is higher (0.278, Morrison and Zellner, 1979) than 1862 Apollo indicating the presence of brighter or a smaller amount of opaque material on the surface of Dembowska. The

IR spectrum of 1862 Apollo has a broader 1.0- μm band and a lower IR reflectance relative to 0.56 μm than 349 Dembowska (Figure 37b, Feierberg et al., 1980). These comparisons show that similarities of the visible spectra alone do not necessarily imply mineralogical similarities. Additional data can prove otherwise. There are therefore no asteroid analogues to 1862 Apollo found in the vicinity of the 5:2 Kirkwood gap.

The spectrum of 349 Dembowska and 1685 Toro (Figure 38a) have similar spectral features. Recent results of radar observations of 1685 Toro (Ostro et al., 1982) indicate an albedo (p_v) close to 0.30, more than twice as high as that reported by Dunlap et al. (1973). This brings the albedo of 1685 Toro and 349 Dembowska to within measurement error of each other. The reflectance relative to H at JHK wavelengths of these two asteroids is the same to within measurement error (Figures 4 and 37b). Because the JHK reflectance of 1685 Toro is not tied in with the visible data there remains a possibility that there is a vertical offset between the infrared spectra of the two asteroids which will indicate different mineralogies. The existing case for mineralogical similarity is strong and should be verified with further measurements.

Five S-type asteroids near the 5:2 Kirkwood gap have similar spectral features to those of 1036 Ganymed to the extent of spectral overlap (Figure 39). An albedo determination of 1036 Ganymed is necessary to confirm mineralogical similarity. All of these asteroids have albedos between 0.14 and 0.16 (Morrison and Zellner, 1979).

(ν_6 - Asteroids near the (ν_6 resonance (Figure 40) number 23 (Williams, 1979). Seven asteroids near this resonance have measured reflectance spectra. Another nine asteroids are identified on the plot of secular resonances (Williams and Faulkner, 1981), six of which have measured reflectance spectra. In spite of 40% coverage of these asteroids,

there is only one spectral analogue to any of the near-Earth asteroids. 1981QA and 18 Melpomene (Figure 41) are regarded as spectral matches except in the NIR where agreement is poorer. Albedo measurements are needed on 1981QA to be consistent with the mineralogical similarity implied by the spectral match.

Flora Family

The flora family lies near the $(\frac{1}{6})$ resonance (Figure 40 Williams and Faulkner, 1981) and has 259 members (Kozai, 1979). Eighteen members of this family have measured reflectance spectra. Similarities of reflectance spectra of near-Earth asteroids and measured Flora family members is quite common.

The visible spectrum of 40 Harmonia and 433 Eros are similar (Figure 41b) although Feierberg et al. (1982) classify these two asteroids into different groups. The albedo of Harmonia (0.148, Morrison and Zellner, 1979) is within the errors of the 0.125 +/- 0.025 albedo of 433 Eros (Lebofsky and Reike, 1979). The IR reflectance indicates a higher olivine content in 433 Eros than on 40 Harmonia.

The spectra of 496 Gryphia, 1055 Tynka, 341 California, and 1830 Pogson (Chapman and Gaffey, 1979) are similar to that of 887 Alinda. The albedo of 341 California (0.216, Gradie and Tedesco, personal communication) is equally higher than that of 887 Alinda (0.18, Morrison and Zellner, 1979) as that of 496 Gryphia (0.154, Gradie and Tedesco, personal communication) is lower. 1830 Pogson and 1055 Tynka (Figure 42) have no measured albedo. It is possible that the surface composition of these two asteroids are all different based on the limited data available. An albedo determination will give more information.

Two Flora family members have similar spectral characteristics to those of 1036 Ganymed: 453 Tea and 1055 Tynka (Figure 43). Albedo measurements are not available for any of these asteroids and spectral coverage is limited.

The spectrum and albedo of 1058 Grubba (Chapman and Gaffey, 1979) and 1620 Geographos (Figure 44a) are similar to the extent of their spectral coverage. Extended wavelength coverage for both asteroids and an albedo determination for 1058 Grubba will address the similarity of their surface compositions.

The general shape of the reflectance spectrum of 770 Bali and 1627 Ivar are similar (Figure 44b). They alone appear to be unique among the measured population of asteroids. Higher signal/noise data may eliminate this uniqueness.

The spectrum of 1830 Pogson, 341 California and 1449 Virtanen (Chapman and Gaffey, 1979) suggest similarities in spectral characteristics with 1981QA (Figure 45). Measurements of albedo and additional reflectance spectra are needed to ascertain mineralogical similarities among these asteroids.

In Figure 46 similar mineralogy between 1862 Apollo and 496 Gryphia and 1088 Mitaka are suggested. Only 496 Gryphia has an albedo measurement (0.154, Morrison and Zellner, 1979) which is lower than 1862 Apollo, eliminating this asteroid as mineralogically similar. An albedo of 1088 Mitaka is needed to address mineralogical similarity.

Phocaea and Hungaria Family

Only three members of the Phocaea family have measured reflectance spectra. Of those three only 25 Phocaea (Chapman and Gaffey, 1979) has a good spectrum with spectral coverage through the 1.0- μ m region. Similar

spectral features exist between 433 Eros and 25 Phocaea but the albedos are different. This eliminates the possibility of mineralogical similarity between these two asteroids. None of the few Hungaria family members with measured reflectance spectra have spectral similarities to any near-Earth asteroids.

Mars-crossers

There are 73 numbered asteroids with orbits which cross that of Mars (Williams, 1979, Bowell et al., 1979). The Amors and some Apollos are subsets of this class. Some inner belt asteroids cross the orbit of Mars but have semi-major axes larger than Amors. Only six members in addition to nine Amors and Mars-crossing Apollos of this group have measured reflectance spectra. None of the measured Mars-crossers have spectra similar to the near-Earth asteroids. There are too few Mars-crossers with measured reflectance spectra to allow conclusions to be drawn from these data. An observational program to measure more Mars-crossers is needed.

The mineralogy and petrology of 887 Alinda and 1915 Quetzàlcoatl do not indicate a genetic relation to each other as the similarity of their orbits suggest (Marsden, 1970). It is possible that these two asteroids are derived from different layers of the same parent body and have different surface compositions. More information on the composition of the silicates on 887 Alinda is needed to determine petrological compatibility with the mineralogy of 1915 Quetzàlcoatl.

Spectral similarity between 1620 Geographos and 1036 Ganymed is implied by logical arguments associating both asteroids with the composition of 68 Leto. Extended spectral coverage and an albedo determination for 1036 Ganymed will test this association. 887 Alinda and 1981QA

also have similar spectral properties but await an albedo determination of 1981QA before mineralogical similarity can be implied.

Comets

An interpretation of the spectrum of 2201 1947XC (Figure 3) in terms of cometary phenomena was made in Chapter 1 to explain the features of the spectrum that are not characteristic of common rock-forming minerals. The common emission features seen in active comets could not explain the observed features.

Our knowledge of the characteristics of comets exhausted of volatiles is presently very poor. At times when comets are inactive, they are dark and at great distances making measurements difficult. There is presently no observational data on extinct (volatily exhausted) comets to compare with the silicate-rich near-Earth asteroids.

Meteorites

In Chapter 1 the question of meteoritic analogues was addressed for each asteroid to aid in the mineralogical-petrological interpretation of this population. Table IV lists the results. Six out of 17 measured near-Earth asteroids are meteorite analogues. It has been shown that three near-Earth asteroids that have previously been determined to be most-like ordinary chondrite meteorites (1685 Toro, 887 Alinda, and 433 Eros) do not have the spectral features characteristic of these classes of meteorites. The mineralogical interpretation of 887 Alinda of Gaffey and McCord, (1978) has been further interpreted as a C3 of the Ormans type. 2100 Ra-Shalom and possibly 1981QA are also C3-analogues. Two ordinary chondrite analogues have been found in 1862 Apollo (LL4) and

1980AA (black L chondrite). 1915 Quetzàlcoatl is the only achondrite analogue presently known. 1981QA cannot be distinguished from an E6 analogue without an albedo determination. None of the other near-Earth asteroids observed to date have meteoritic analogues.

1915 Quetzàlcoatl is a rare meteorite analogue. There were nine diogenites in the world's meteorite collection prior to the discovery of diogenites from three separate falls in Antarctica (e.g., Takeda et al., 1981). The mineralogical and petrological differences among these meteorites is small. In addition there is a clustering of the time of year in which these meteorites have fallen to Earth meaning that most of these meteorites intersected the Earth from the same orbit. One of the diogenites (Peckelsheim) struck the Earth the day 1915 Quetzàlcoatl was discovered on one of its close approaches to the Earth. This fall was not during the time of year of the observed clustering, however. The other diogenite falls cluster in the summer when 1915 Quetzàlcoatl is on its way into the asteroid belt and the Earth has moved 145° in its orbit. This observation may be no more than interesting coincidence. There is a stray fall in November.

Discussion

Planets and satellites - There is not sufficient information on the composition of the terrestrial planets to eliminate the possibility that some of them are planetary projectiles. Possibly some lunar mare fragments are near-Earth asteroids but the dynamics of this situation are not favorable. The spectral signatures of the non-ice components of the outer solar system satellites do not indicate any mineralogical similarity to near-Earth asteroids. Our preconceived ideas on the different origins of near-Earth asteroids and outer solar system satellites

remains unchanged by new observational data.

Asteroids - There are no asteroid analogues to 1566 Icarus, 2201 1947XC, and 1865 Cerberus based on the data available for comparison. The asteroids measured in 8-color photometry were not considered for analogue analysis. All other near-Earth asteroids have at least one analogue somewhere in the asteroid belt.

The case for compositional similarity between 4 Vesta and 1915 Quetzàlcoatl, 2 Pallas and 1580 Betulia, 349 Dembowska and 1685 Toro is very convincing because these main belt asteroid compositions were previously unique. A compositional link between 433 Eros and 40 Harmonia is likely because there are no other asteroids with spectral characteristics similar to 433 Eros. The dynamical evidence for the 5:2 Kirkwood Gap (of which 349 Dembowska is a neighbor) and members of the Pallas and Flora families (of which 40 Harmonia is a member) being source regions for these asteroids coupled with the mineralogical similarity based on existing reflectance spectra is a convincing argument in favor of genetic relations between these objects. A dynamically favorable mechanism to bring fragments from 4 Vesta into Earth-crossing orbit has not been proposed. The genetic relation implied between these asteroids with rare surface mineralogy may indicate that their composition is only rare in large bodies. It is possible that there are many small asteroids presently below detection limits with the composition observed in the small near-Earth asteroids. If this is the case, the large remnant bodies are probably the parent bodies unless dynamical conditions preclude a genetic relation.

The population of near-Earth asteroids is decidedly different from the main-belt population as it is presently known. The fact that some analogues are found at all in dynamically favorable regions, if additional data indicate similar surface compositions, does support

dynamical models. Except in the case of the Mars-crossers which are poorly sampled and the 2:1 Kirkwood gap (which is well sampled) there is evidence of near-Earth asteroid analogues among each predicted source region and the main belt as well.

The ability to determine mineralogical similarity of near-Earth asteroids to other near-Earth asteroids will help determine part of their history. If there is mineralogical similarity among these asteroids and their orbital characteristics do not preclude a genetic relation, then some of these bodies may have formed in their present location from collisions. This is a source that has been ignored probably because the collision frequency is much lower in the inner solar system than in the main asteroid belt.

Comets - If we assume that the dynamical models are correct and that most or some of the near-Earth asteroids are extinct cometary remnants then these observational results imply that cometary cores consist of common asteroidal material, formed inside the orbit of Jupiter and transported to the Oort cloud acquiring volatiles in the process. This is contradictory to the dirty snowball model of Whipple (e.g., Donn and Rahe, 1982) which has assumed a position of prominence in cometary science. The scenario implied by the mineralogy and petrology of near-Earth asteroids is a scenario that has been proposed by Opik (1966) but with no observational evidence to support it.

Meteorites - The observational data indicate that not all near-Earth asteroids are meteoritic analogues. This means that there may be more meteorite types that have not yet been recovered, if meteorites do come from near-Earth asteroids, or not all near-Earth asteroid fragments survive to become meteorites. It is also possible that the meteorite types not presently found among the near-Earth asteroids have not been

observed yet. An equally valid argument is that their parent bodies may be totally fragmented and reside in regions of the asteroid belt that are below detection limits of existing instrumentation. The greater proportion of non-meteorite analogues among presently known near-Earth asteroids (9 out of 17) indicates that not all meteorites come from near-Earth asteroids. The existing data also suggest a disproportionate number of C3 analogues in the near-Earth and main belt asteroid population (there are C3-type main belt asteroids, Gaffey and McCord, 1978) that is not reflected in meteorite statistics. It is likely that but not necessary for the C3 parent body to presently reside in the near-Earth asteroid population.

The date of diogenite falls suggest some mechanism preferentially favoring falls in the summer. The statistics of diogenite falls are insignificant and summer months are supposedly favored for meteorite recoveries, nevertheless it would be interesting if a mechanism were found that would preferentially send debris from 1915 Quetzàlcoatl near the Earth when it is at 120° longitude in its orbit. It is difficult to overlook a trend that stands out among many sets of poor statistics which is the case with the diogenites among meteorite fall statistics. A few other types appear to cluster too.

The abundance of ordinary chondrites is not reflected in the near-Earth or main belt asteroid populations. This indicates that the parent bodies of ordinary chondrites are few in number or totally disrupted and too small to be detected as asteroids. The presence of two known ordinary chondrite analogues supports the theory that a phase of their lifetime is passed in near-Earth orbit. The orbits of 1862 Apollo and 1980AA are not similar to any of the five determined orbits of ordinary chondrites (Ballabh et al., 1978, Halliday et al., 1978, Levin et al., 1976, McCrosky et al., 1971, Ceplecha, 1961) which supports the theory that

most ordinary chondrite parent bodies are too small to be detected as asteroids.

Extra-terrestrial Resources - Our present knowledge of the mineralogy and petrology of near-Earth asteroids indicates that they consist of common rock-forming minerals, namely olivine, pyroxene and opaques of different compositions occurring in varying proportions. The nature of the population in general has not changed since the population was last assessed in terms of useful extraterrestrial resources (Gaffey et al., 1979). There are three or four asteroids with a significant opaque component. The mineralogy of 1580 Betulia has been shown to contain an opaque component. It is not possible to distinguish between fine-grained metal or volatiles such as carbon but both materials are useful. No near-Earth asteroids with a nickel-iron surface has been observed. The population is no longer dominated by ordinary chondrite compositions, however two are found which presumably contain nickel-iron, one with small amounts (LL-type -low metallic iron), the other with more iron (H-type, black chondrite). The carbonaceous chondrite analogues are of the low volatile type consisting mostly of olivine and <4% water and <2% carbon by weight. No volatile-rich C1 or C2 analogues have been found. It is possible that 1979VA or 1580 Betulia which do not have meteoritic analogues have more volatiles than C1 and/or C2 meteorites. This information is not presently available.

Future directions - It has only been in the past few years that physical measurements of the near-Earth asteroids has become possible. Our data base is just becoming useful. Obviously the acquisition of data must continue. We know that the near-Earth asteroids, like the main belt asteroids are diverse mineralogical assemblages but in a manner different from the majority of main belt asteroids. Investigations into

the nature of these differences should continue. Polarization measurements have virtually ceased in the asteroid community. Because near-Earth asteroids move through large phase angle ranges in a short period of time, polarization measurements of them is less time consuming. They also constrain mineralogical and radiometric interpretations. These types of measurements should be encouraged. Radar measurements are particularly feasible for near-Earth asteroids. Considerable work is necessary to relate the information contained in the radar data to physical properties. When a link is found our understanding of the surface of these bodies will be considerably enhanced.

Space craft missions to these objects will increase our capability to learn about their nature and history. Because there are so many of them, it is not economically feasible to visit all of them in the foreseeable future. Therefore, ground-based measurements should continue to be made as they are economically feasible. In the event that a space craft mission does go to any asteroids, it seems desirable that there be experiments which look at all views of the object from the macroscopic, hand lense and microscopic range. In addition, basic physical parameters need to be determined such as density, moment of inertia, and seismic profiles to characterize their internal profile.

References

Ballabh, G.M., Bhatnagar, A. and Bhandari, N. (1978) The orbit of the Dhajala meteorite. *Icarus*, **33**, 361-367.

Bell, J.F., Clark, R.N., and McCord, T.B. (1979) Reflection spectra of Pluto and three distant satellites. *B.A.A.S.*, **11**, 570.

Bowell, E., Gehrels, T., and Zellner, B. (1979) Appendix VII. Magnitudes, colors, types and adopted diameters of the asteroids. In Asteroids, T. Gehrels, ed., The University of Arizona Press, Tucson, 1108-1129.

Cepilecha, Z. (1961) Multiple fall of Pribram meteorites photographed. *Bull. Astron. Inst. Czech.*, **12**, 21-47.

Chapman, C.R. and Gaffey, M.J. (1979) Reflectance spectra for 277 asteroids. In Asteroids, T. Gehrels, ed., The University of Arizona Press, Tucson, 655-687.

Cruikshank, D.P. (1982) The satellites of Uranus. In Uranus and the Outer Planets, ed., G. Hunt, Cambridge University Press, Cambridge, 193-216.

Donn, B. and Rahe, J. (1982) Structure and origin of cometary nuclei. In Comets, ed., L. Wilkening, The University of Arizona Press, Tucson, 203-226.

Dunlap, J.L., Gehrels, T., and Howes, M.L. (1973) Minor planets and

related objects. IX. Photometry and polarimetry of (1685) Toro. **Astron. J.**, 78, 491-501.

Feierberg, M.A., Larson, H.P., Fink, U. and Smith, H.A. (1980) Spectroscopic evidence for two achondrite parent bodies: 349 Dembowska and 4 Vesta. **Geochim. Cosmochim. Acta**, 44, 513-524.

Feierberg, M.A., Larson, H.P., and Chapman, C.R. (1982) Spectroscopic evidence for undifferentiated S-type asteroids. **Astrophys. J.**, 257, 361-372.

Gaffey, M.J. and McCord, T.B. (1978) Asteroid surface materials: Mineralogical characterizations from reflectance spectra. **Space Sci. Rev.**, 21, 555-628.

Gaffey, M.J., Helin, E.F., and O'Leary, B.T. (1979) An assessment of near-Earth asteroid resources. In Space Resources and Space Settlements, eds., J. Billingham, W. Gilbreath, and B. O'Leary, NASA SP-428, Washington, D.C., 191-204.

Gradie, J. and Tedesco, E. (1982) Compositional structure of the asteroid belt. **Science**, 216, 1405-1407.

Halliday, I., Blackwell, A.T. and Griffin, A.A. (1978) The Innisfree meteorite and the Canadian camera network. **J. Roy Astron. Soc. Canada**, 72, 15-39.

Hartmann, W.K., Cruikshank, D.P. and Degewij, J. (1982) Remote comets and related bodies: VJHK colorimetry and surface materials. **Icarus**, 52,

in press.

Kozai, Y. (1979) The dynamical evolution of the Hirayama family. In Asteroids, T. Gehrels, ed., The University of Arizona Press, Tucson, 334-358.

Lebofsky, L.A. and Rieke, G.H. (1979) Thermal properties of 433 Eros. *Icarus*, **40**, 297-308.

Lebofsky, L.A., Veeder, G.J., Lebofsky, M.J., and Matson, D.L. (1978) Visual and radiometric photometry of 1580 Betulia. *Icarus*, **35**, 336-343.

Lebofsky, L.A., Veeder, G.J., Rieke, G.H., Lebofsky, M.J., Matson, D.L., Kowal, C., Wynn-Williams, C.G., and Becklin, E.E. (1981) The albedo and diameter of 1862 Apollo. *Icarus*, **48**, 335-338.

Levin, B.J., Simonenko, A.N. and Anders, E. (1976) Farmington meteorite: A fragment of an Apollo asteroid. *Icarus*, **28**, 307-324.

McCord, T.B., Johnson, T.V. and Elias, J.H. (1970) Saturn and its satellites: Narrow-band spectrophotometry (0.3-1.1 μm). *Astrophys. J.*, **165**, 413-424.

McCord, T.B., Clark, R.N., Hawke, B.R., McFadden, L.A., Owensby, P.D., Pieters, C.M., and Adams, J.B. (1981) Moon: Near-infrared spectral reflectance, a first good look. *J. Geophys. Res.* **86**, B11, 10883-10892.

McCrosky, R.E., Posen, A., Schwartz, G., Shao, G.-Y. (1971) Lost City meteorite - Its recovery and a comparison with other fireballs. *J.*

Geophys. Res., **76**, 4090-4108.

McFadden, L.A., Bell, J.F., and McCord, T.B. (1980) Visible spectral reflectance measurements (0.33-1.1 μm) of the Galilean satellites at many orbital phase angles. **Icarus**, **44**, 410-430.

Morrison, D. and Zellner, B. (1979) Appendix V. Polarimetry and radiometry of the asteroids. In Asteroids, T. Gehrels, ed., The University of Arizona Press, Tucson, 1090-1097.

Opik, E.J. (1963) The stray bodies in the solar system. Part I. Survival of cometary nuclei and the asteroids. **Adv. Astron. Astrophys.**, **2**, 219-262.

Opik, E.J. (1966) The stray bodies in the solar system II: The cometary origin of meteorites. **Adv. Astron. Astrophys.** **4**, 302-336.

Ostro, S.J., Campbell, D.B., and Shapiro, I.I. (1982) Radar observations of asteroid 1685 Toro. **Astron. J.**, submitted for publication.

Scholl, H. and Froeschlé, C. (1977) The Kirkwood Gaps as an asteroidal source of meteorites. In Comets, Asteroids, and Meteorites - Interrelations, Evolution and Origins, ed., A.H. Delsemme, The University of Toledo, Toledo, 293-298.

Singer, R.B., McCord, T.B., Clark, R.N., Adams, J.B., and Huguenin, R.L. (1979) Mars' surface composition from reflectance spectroscopy: A summary. **J. Geophys. Res.**, **84**, 8415-8426.

Singer, R.B. (1982) The composition of the martian dark regions: I. Visible and near-infrared spectral reflectance of analog materials and interpretation of telescopically observed spectral shape. *J. Geophys. Res.*, Submitted for publication.

Smith, D.W., Johnson, P.E., and Shorthill, R.W. (1981) Spectrophotometry of J8, J9, and four Trojan asteroids from 0.32 to 1.05 μm . *Icarus*, **46**, 108-113.

Takeda, H., Mori, H., Yanai, K. (1981) Mineralogy of the Yamato diogenites as possible pieces of a single fall. *Proc. 6th Symp. Antarctic Meteorites*, ed., T. Nagata, National Institute of Polar Research, Tokyo, 81-99.

Vilas, F., and McCord, T.B. (1976) Mercury: Spectral reflectance measurements (0.33-1.06 μm) 1974/75. *Icarus*, **28**, 593-599.

Wasson, J.T. and Wetherill, G.W. (1979) Dynamical, chemical and isotopic evidence regarding the formation locations of asteroids and meteorites. In *Asteroids*, T. Gehrels, ed., The University of Arizona Press, Tucson, 926-974.

Williams, J.G. (1979) Appendix III. Proper elements and family memberships of the asteroids. In *Asteroids*, T. Gehrels, ed., The University of Arizona Press, Tucson, 1040-1063.

Williams, J.G. and Faulkner, J. (1981) The positions of secular resonance surfaces. *Icarus*, **46**, 390-399.

Table VII

SOURCE REGIONS AND NEAR-EARTH ASTEROID ANALOGUES

Source	Albedo	Diameter	Taxonomy	Analogue
Planets and Satellites				
Mercury				?1915 Quetzàlcoatl?
Lunar Mare				?1915 Quetzàlcoatl? ?1980AA? ?1580 Betulia?
Mars				?1685 Toro?
satellites				none
Asteroids				
4 Vesta	0.255	530	U	1915 Quetzàlcoatl
<u>2:1 Kirkwood Gap</u>				
None				
<u>5:2 Kirkwood Gap</u>				
2 Pallas	0.066	692	U	1580 Betulia
68 Leto	0.147	127	S	1620 Geographos 1036 Ganymed
349 Dembowska	0.27		R	1685 Toro
471 Papagena	0.163	144	S	1036 Ganymed
354 Eleonora	0.165	154	S	1036 Ganymed
39 Laetitia	0.167	157	S	1036 Ganymed
532 Herculina	0.16	220	S	1036 Ganymed

Source	Albedo	Diameter	Taxonomy	Analogue
<u>U</u> ₆				
18 Melpomene	0.149	162	S	1981QA
<u>Flora Family</u>				
1055 Tynka			S	887 Alinda
1830 Pogson			S	1036 Ganymed 887 Alinda 1981QA
453 Tea			S	1036 Ganymed
1058 Grubba	0.16	13.4	S	1620 Geographos
770 Bali			U	1627 Ivar
1449 Virtanen			S	1981QA
341 California	0.216	16	S	1981QA
1088 Mitaka			R	1862 Apollo
<u>Phocaea Family</u>				none
<u>Mars-Crossers</u>				none

Table VIII**ASTEROID COMPOSITIONAL TYPES**

Type	Visual geometric albedo	Spectral reflectivity (0.3 to 1.1 μm)
C	Low (< 0.065)	Neutral, slight absorption blueward of 0.4 μm
S	Moderate (0.07-0.23)	Reddened, typically an absorption band 0.9 to 1.0 μm
M	Moderate (0.07-0.23)	Featureless, sloping up into red
F	Low (< 0.065)	Flat
P	Low (< 0.065)	Similar to M, hence pseudo-M or P
D	Low (< 0.065)	Very red longward of 0.7 μm
R	Very high (> 0.23)	Very red, bands deeper than S
E	Very high (> 0.23)	Featureless, flat or sloping up into red
U		Unclassifiable in this system*

*Includes Vesta, Pallas, and other unique objects which may be sole representatives of an undefined type

Table IX

Large Asteroids with Semimajor Axis within 0.1 AU of 2:1 Kirkwood

Gap

Asteroid	a	e	i	B(1,0)	Class	Diameter (km)
106 Dione	3.17	.18	5	8.8	C	139
511 Davida	3.18	.18	16	7.4	C	323
154 Bertha	3.18	.10	21	8.5	C	191
92 Undina	3.19	.07	10	7.9	C	244
702 Alauda	3.19	.03	21	8.3	C	205
750 Mancunia	3.20	.13	6	9.6	C	119
175 Andromache	3.21	.20	3	9.6	C	113
530 Turandot	3.21	.20	8	10.3	C	81
381 Myrrha	3.21	.12	13	9.7	C	126
108 Hecuba	3.22	.09	4	9.7	S	61
122 Gerda	3.22	.06	2	9.2	C	139
895 Helio	3.22	.14	26	9.5	?	
745 Mauritius	3.24	.07	14	11.0	?	
903 Nealley	3.24	.05	12	10.9	?	

Classifications and diameters from Morrison (1977) and Zellner and Bowell (1977), Bowell *et al.*, (1978), and Bowell (private communication, 1978). Absolute magnitudes from Gehrels and Gehrels (1978).

Table X

Large Asteroids with Semimajor Axis within 0.1 AU of 5:2 Kirkwood

Gap

Asteroid	a	e	i	B(1,0)	Class	Diameter (km)
146 Lucina	2.72	.07	13	9.2	C	141
45 Eugenia	2.72	.08	7	8.3	C	226
410 Chloris	2.72	.24	11	9.5	C	134
156 Xanthippe	2.73	.23	10	9.8	C	104
140 Siwa	2.73	.21	3	9.6	C	103
110 Lydia	2.73	.08	6	8.7	C	170
200 Dynamene	2.74	.13	7	9.5	C	123
185 Eunike	2.74	.13	23	8.7	C	169
247 Eukrate	2.74	.24	25	9.3	C	142
387 Acquitania	2.74	.24	18	8.4	S	112
173 Ino	2.74	.21	14	9.1	C	142
308 Polyxo	2.75	.04	4	9.3	U	138
128 Nemesis	2.75	.12	6	8.8	C	164
71 Niobe	2.76	.17	23	8.3	S	115
93 Minerva	2.76	.14	9	8.7	C	168
356 Liguria	2.76	.24	8	9.3	C	150
41 Daphne	2.76	.27	16	8.1	C	204
1 Ceres	2.77	.07	11	4.5	C	1003
88 Thisbe	2.77	.17	5	8.1	C	210
39 Laetitia	2.77	.11	10	7.4	S	163
2 Pallas	2.77	.23	35	5.2	U	608
148 Gallia	2.77	.19	25	8.5	S	106
532 Herculina	2.77	.17	16	8.0	S	150
393 Lampetia	2.77	.33	15	9.2	C	129
28 Bellona	2.78	.15	9	8.2	S	126
68 Leto	2.78	.18	8	8.2	S	126
139 Juewa	2.78	.17	11	9.2	C	163
446 Aeternitas	2.79	.07	11	10.2	O	40
216 Kleopatra	2.79	.25	13	8.1	M	128
354 Eleonora	2.80	.12	18	7.5	S	153
346 Hermentaria	2.80	.10	9	8.9	S	84
236 Honoria	2.80	.19	8	9.5	S	65
441 Bathilde	2.81	.08	8	9.5	M	66
804 Hispania	2.84	.14	15	8.9	C	141
385 Ilmatar	2.85	.13	14	8.8	?	?
81 Terpsichore	2.85	.21	8	9.6	C	112
129 Antigone	2.87	.21	12	7.9	M	115
47 Aglaja	2.88	.14	5	9.2	C	158
471 Papagena	2.89	.24	15	7.9	S	143
386 Siegena	2.90	.17	20	8.4	C	191
238 Hypatia	2.91	.09	12	9.2	C	154
22 Kalliope	2.91	.10	14	7.3	M	177
16 Psyche	2.92	.13	3	6.9	M	250
674 Rachele	2.92	.20	14	8.5	S	102
349 Dembowska	2.92	.09	8	7.2	O	144

Data from same source as Table IX.

Figure Captions

Figure 31: Reflectance spectra of terrestrial planets and the Moon: (a) Mercury; (b) Bright and Dark region of Mars, (c) The Moon- a. Mare Serenitatis 2; b. J. Herschel highland crater; c. Apollo 11 site; d. Apollo 16; e. Aristarchus crater from McCord et al., 1980.

Figure 32: Visible reflectance spectra of outer solar system satellites:

(a) satellites of Saturn; (b) Galilean satellites of Jupiter; (c) J8 and J9 satellites of Jupiter; (d) two satellites of Uranus: Oberon and Titania; (e) satellite of Neptune: Triton.

Figure 33: Reflectance spectrum of 1915 Quetzàlcoatl (squares connected by solid line) and 4 Vesta (crosses-Gaffey personal communication).

Figure 34: The frequency of asteroids as a function of distance from the Sun in AU showing the existence of the Kirkwood Gaps at commensurabilities with the period of Jupiter.

Figure 35: (a) Spectrum of 1580 Betulia (squares connected by solid line) and 2 Pallas (crosses). (b) Spectrum of 1620 Geographos (squares connected by solid line) and 68 Leto (crosses).

Figure 36: Spectrum of 1862 Apollo (squares connected by solid lines) and 471 Papagena, 39 Laetitia and 349 Dembowska (crosses). Additional physical properties eliminate the possibility of mineralogical similarity between these asteroids and 1862 Apollo.

Figure 37: Visible and infrared spectra of (a) 1862 Apollo (squares and crosses connected by solid line) and 39 Laetitia (diamonds and x's). (b) three different data sets of 349 Dembowska.

Figure 38: Spectra of 1685 Toro measured at two different apparitions (8/72 and 7/80 Chapman personal communication) compared to 349 Dembowska. The different spectra may imply varying olivine abundance or composition. The difference between the two spectra are too large to be due to body shape or aspect or phase angle.

Figure 39: Spectrum of 1036 Ganymed (squares connected by solid line) compared to 532 Herculina, 68 Leto, 39 Laetitia, 354 Eleonora, and 471 Papagena (crosses).

Figure 40: Surfaces of secular resonances in proper inclination and semimajor axis space (Williams and Faulkner, 1981) and locations of some asteroids and families.

Figure 41: Spectrum of 1981QA (squares connected by solid line) and 18 Melpomene (crosses).

Figure 42: Visible and IR spectrum of 433 Eros (squares and crosses connected by solid line) and 40 Harmonia (diamonds and x's).

Figure 43: Spectrum of 887 Alinda (squares connected by solid line) and 1830 Pogson and 1055 Tynka (crosses).

Figure 44: Spectrum of 1036 Ganymed (squares connected by solid line) and 453 Tea and 1055 Tynka (crosses).

Figure 45: (a) Spectrum of 1620 Geographos (squares connected by solid line) and 1058 Grubba (crosses). (b) Spectrum of 1627 Ivar (squares connected by solid line) and 770 Bali (crosses).

Figure 46: Spectrum of 1981QA (squares connected by solid lines) and 1830 Pogson, 341 California, and 1449 Virtanen (crosses).

Figure 47: Visible and IR spectrum of 1862 Apollo (squares and crosses connected by solid line) and 496 Gryphia and 1088 Mitaka (diamonds and x's).

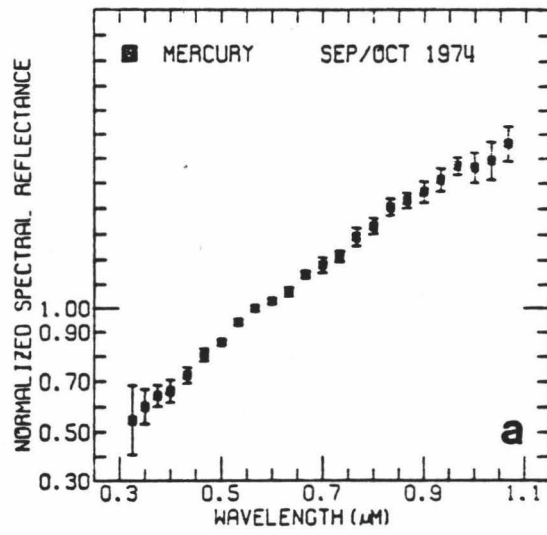


Figure 31a

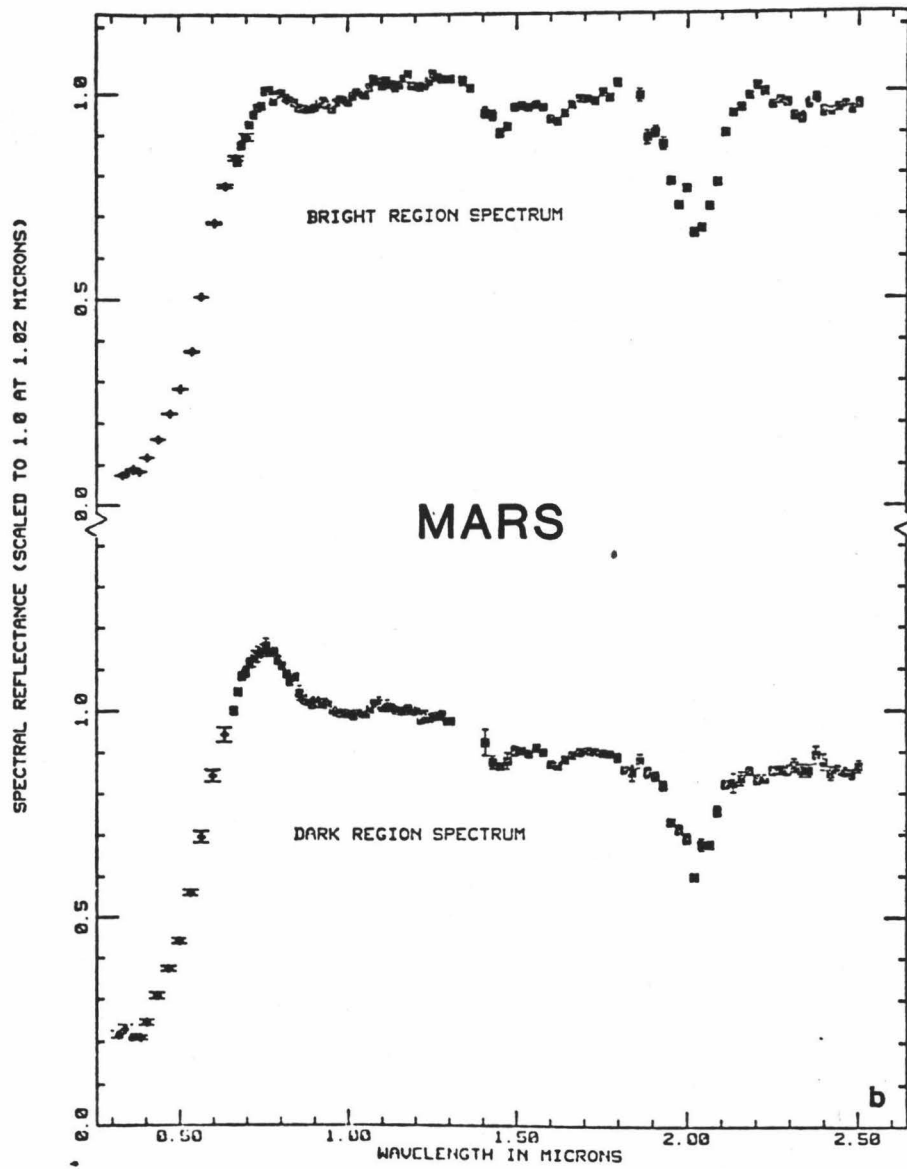


Figure 31b

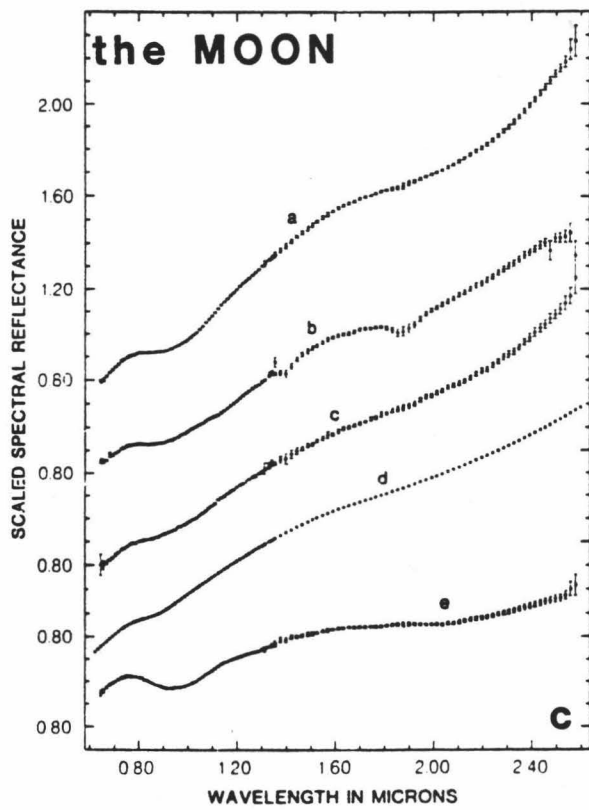


Figure 31c

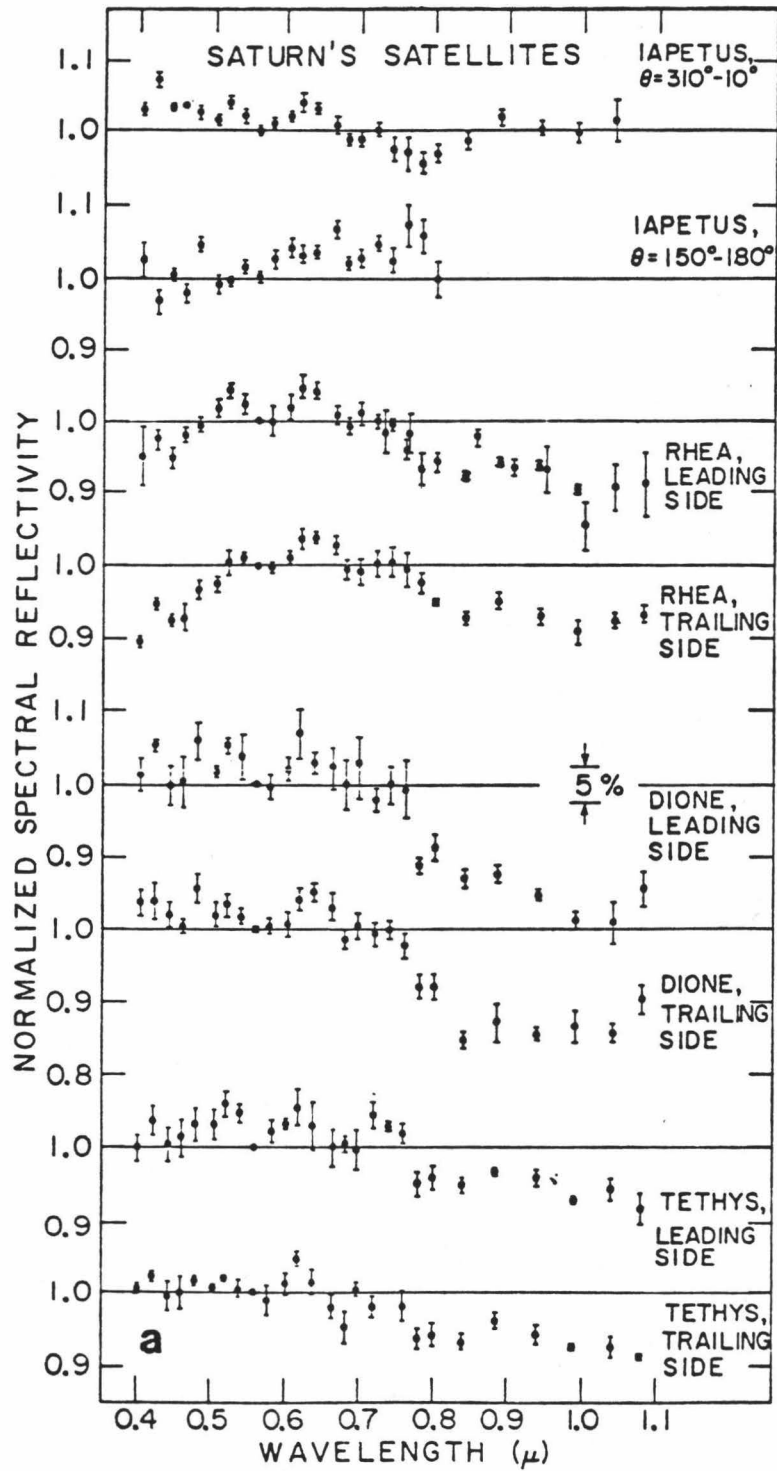


Figure 32a

GALILEAN SATELLITES

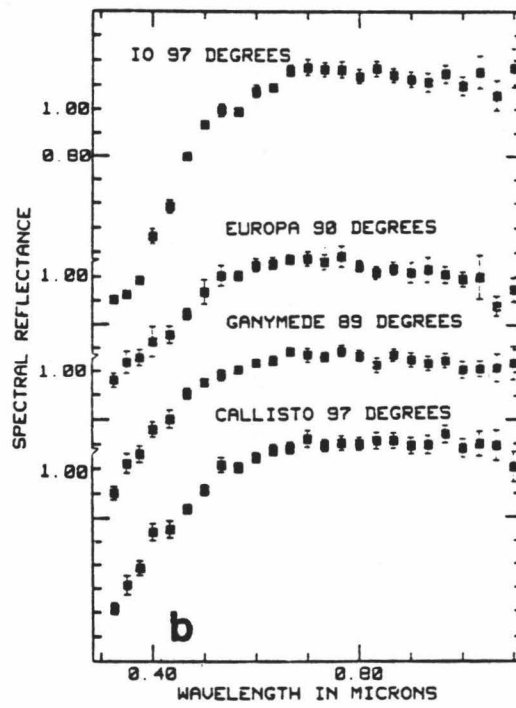


Figure 32b

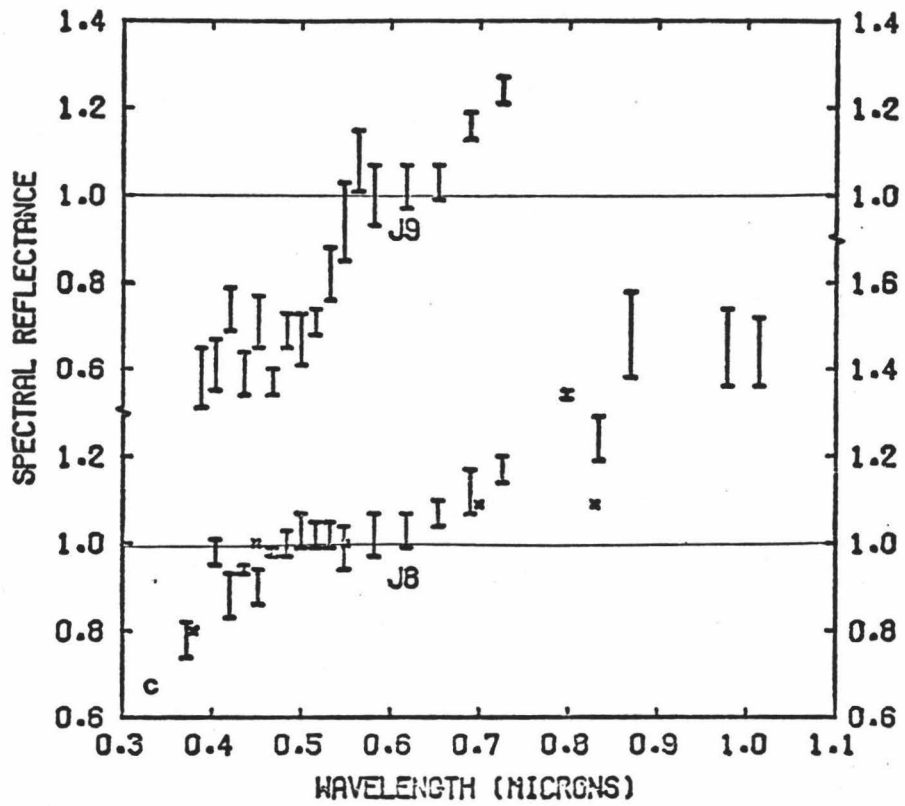


Figure 32c

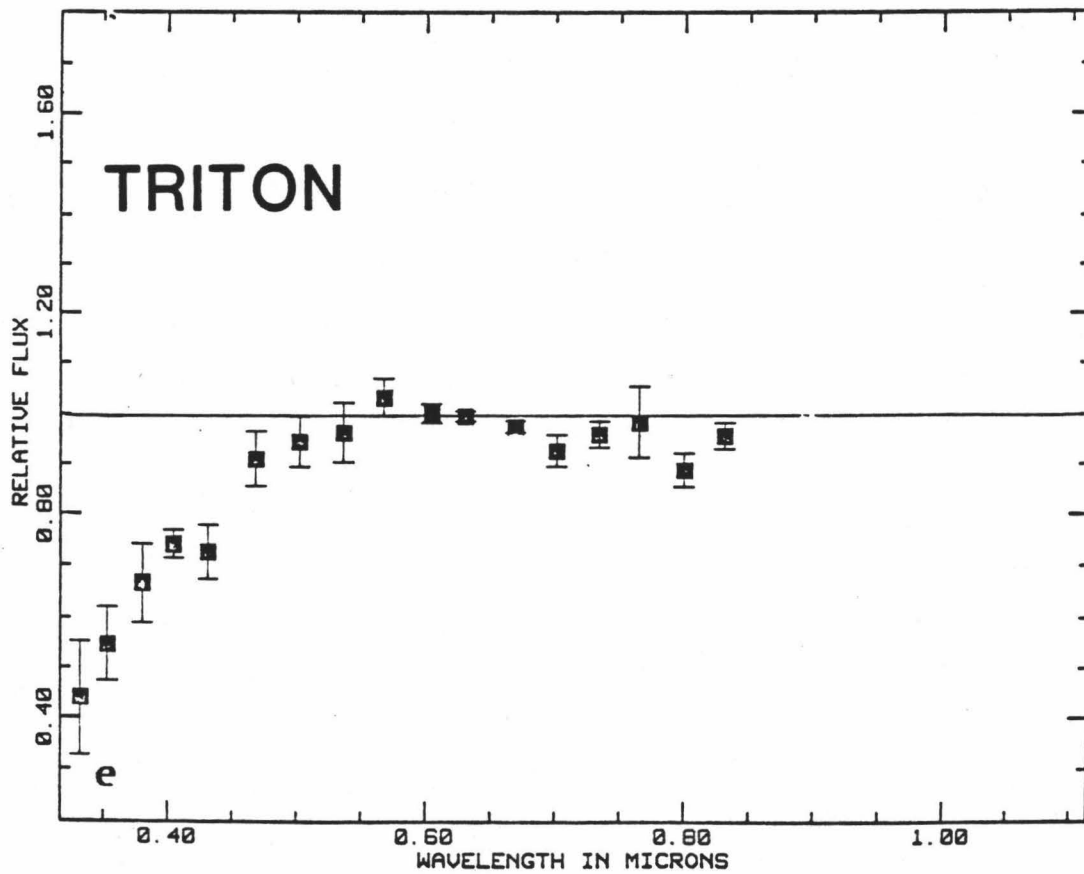
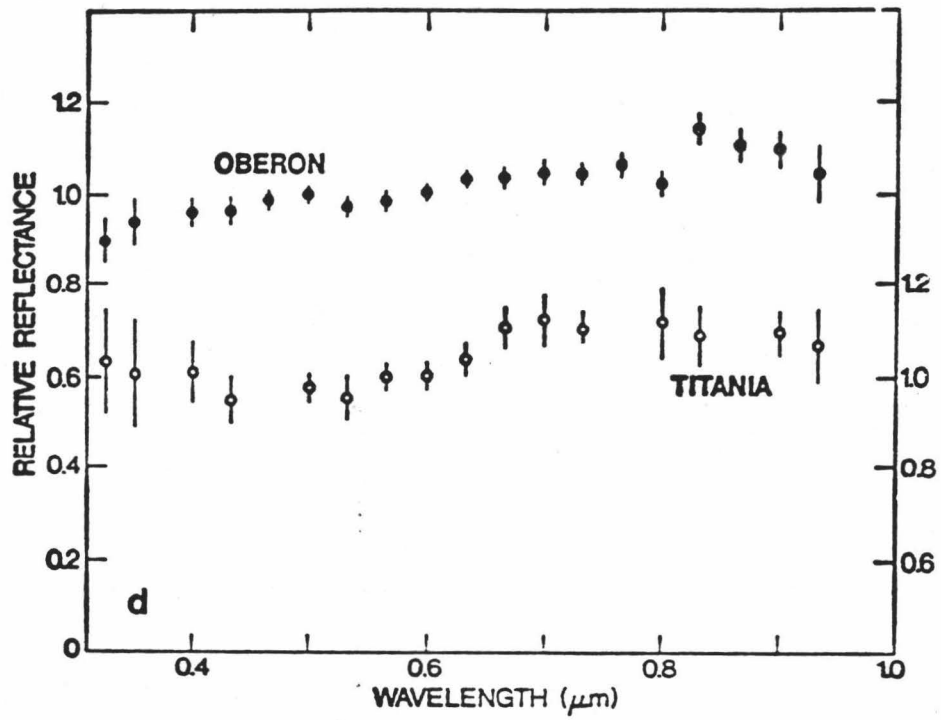


Figure 32d-e

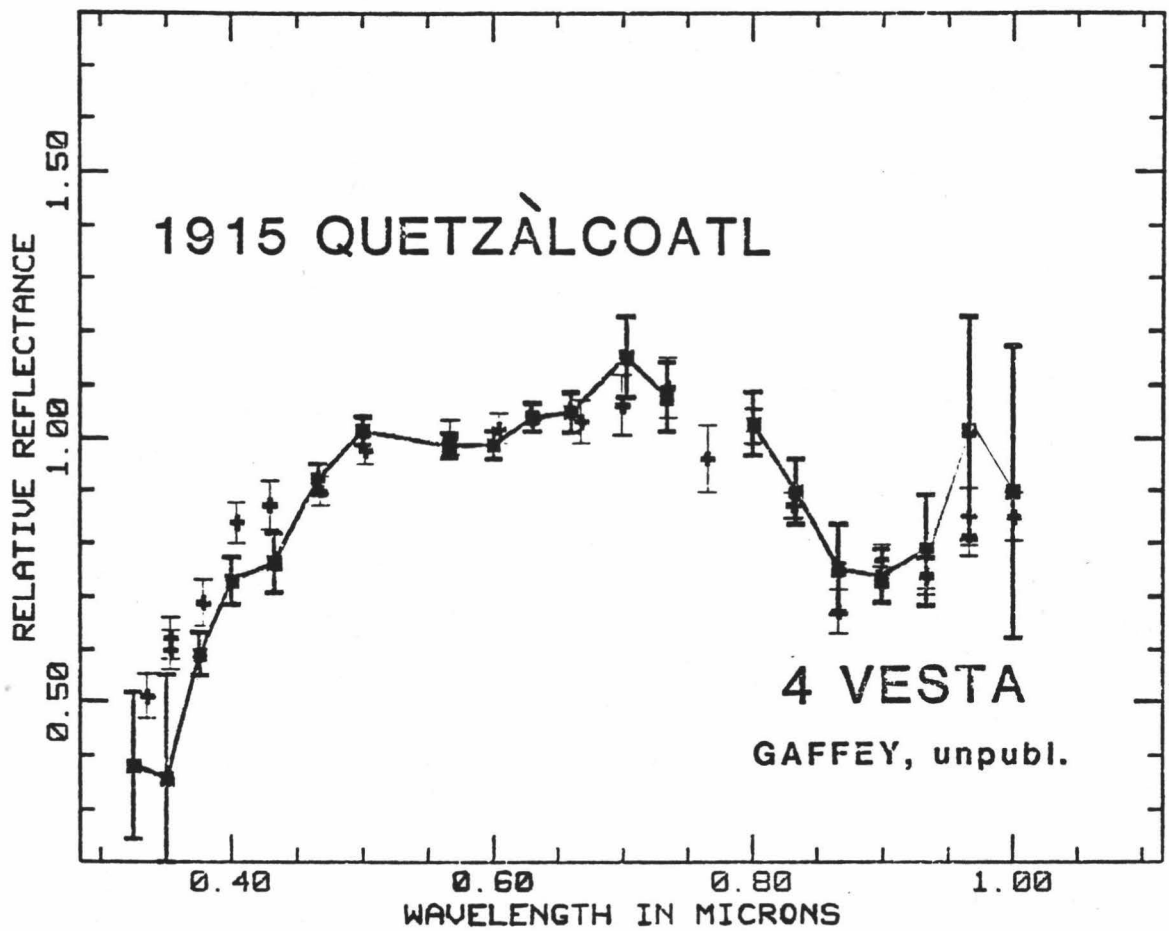


Figure 33

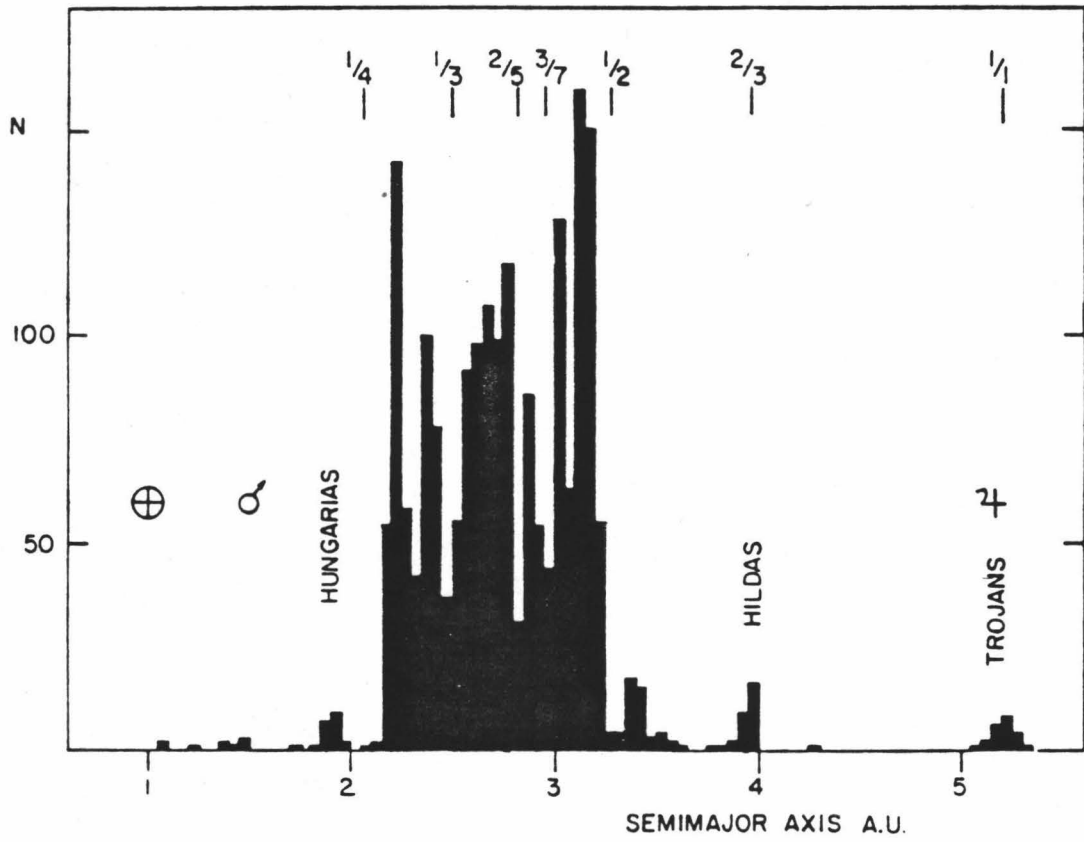


Figure 34

relative reflectance

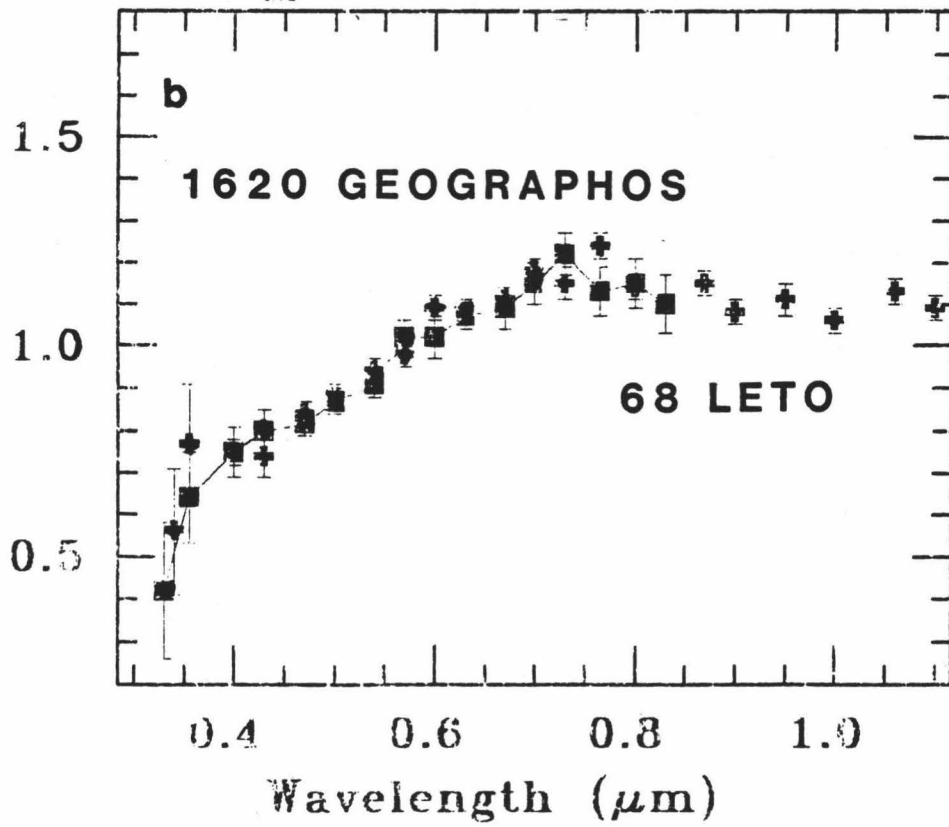
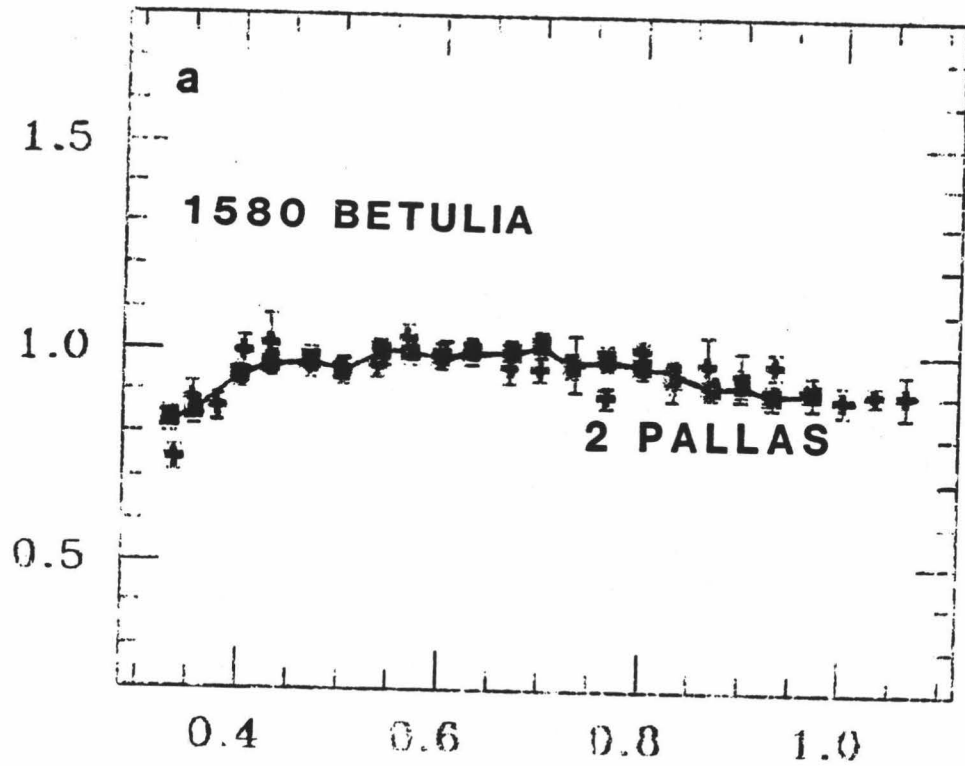
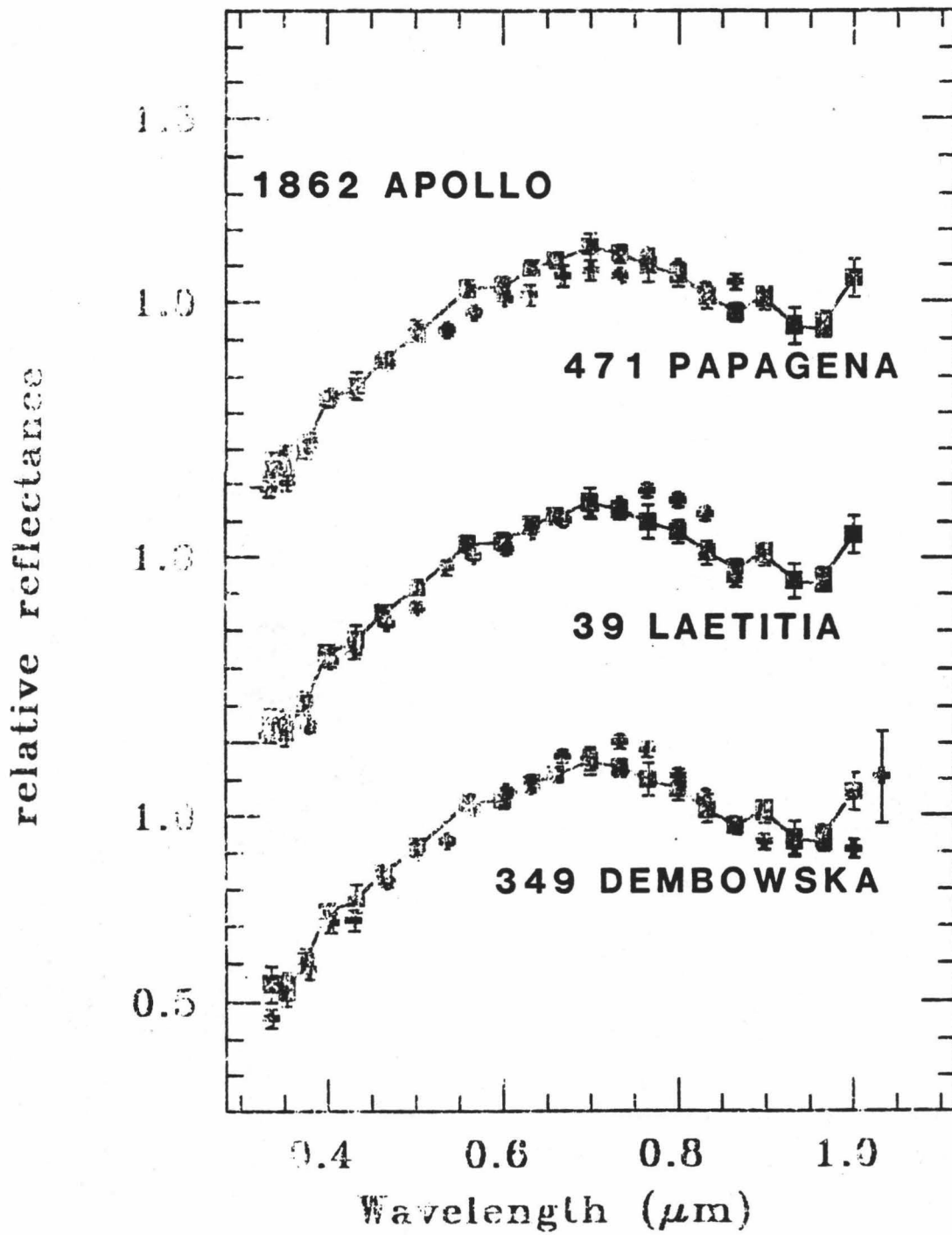


Figure 35



* Figure 36

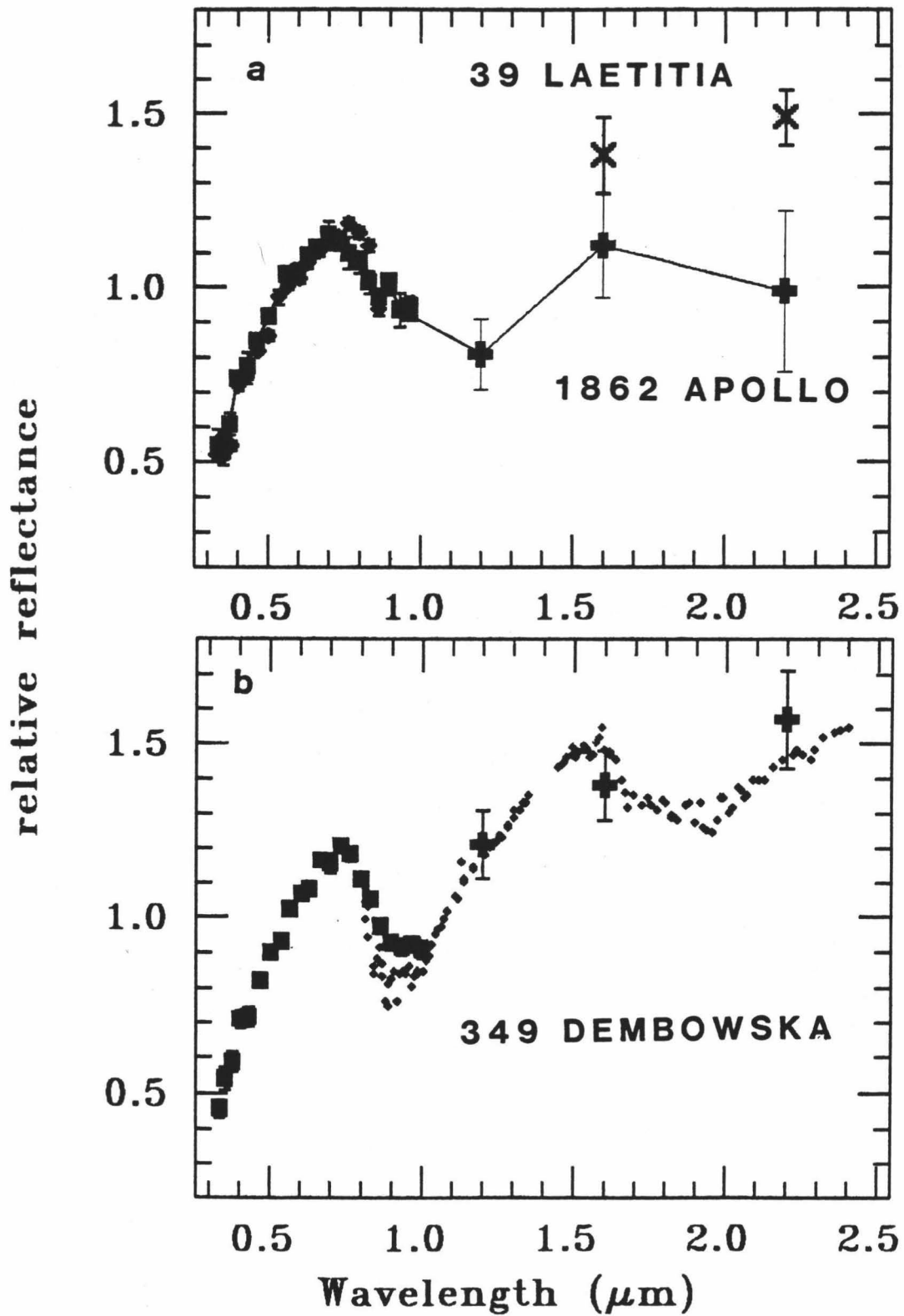


Figure 37

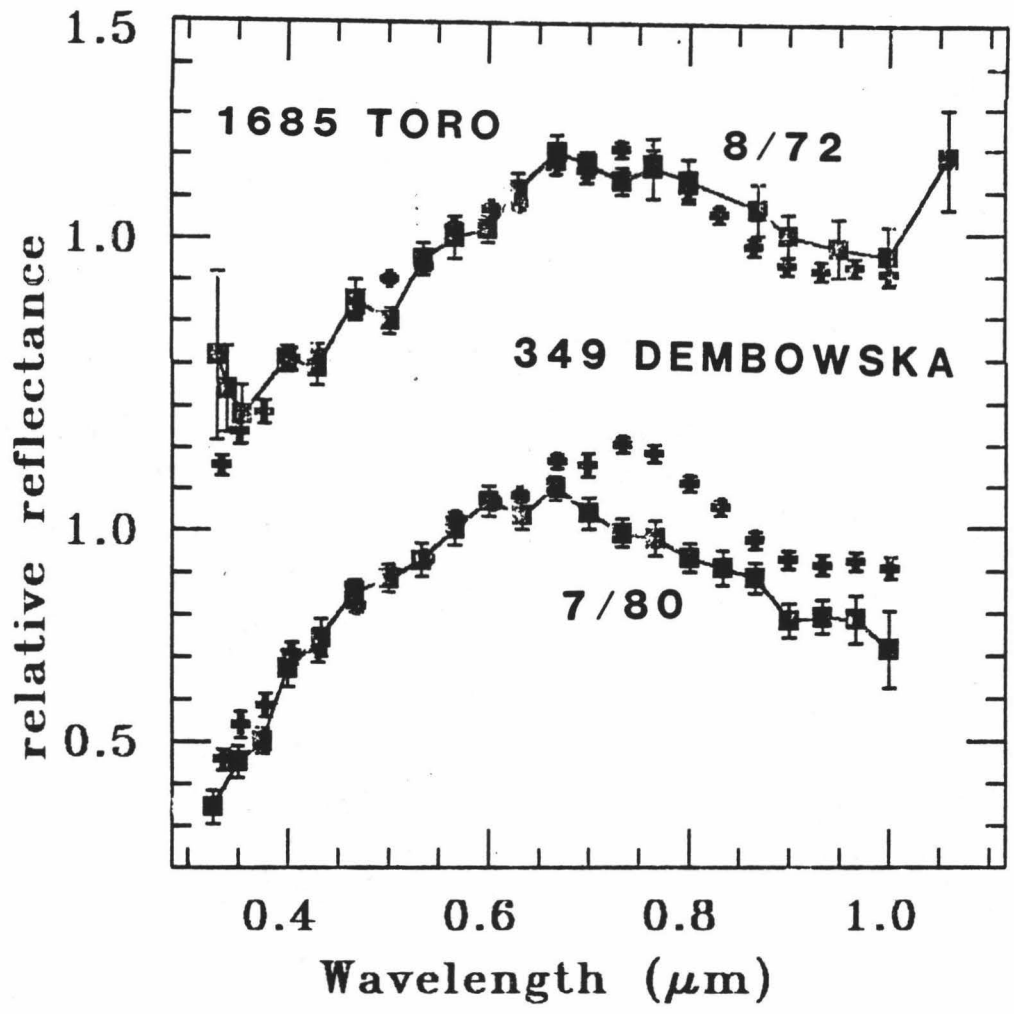


Figure 38

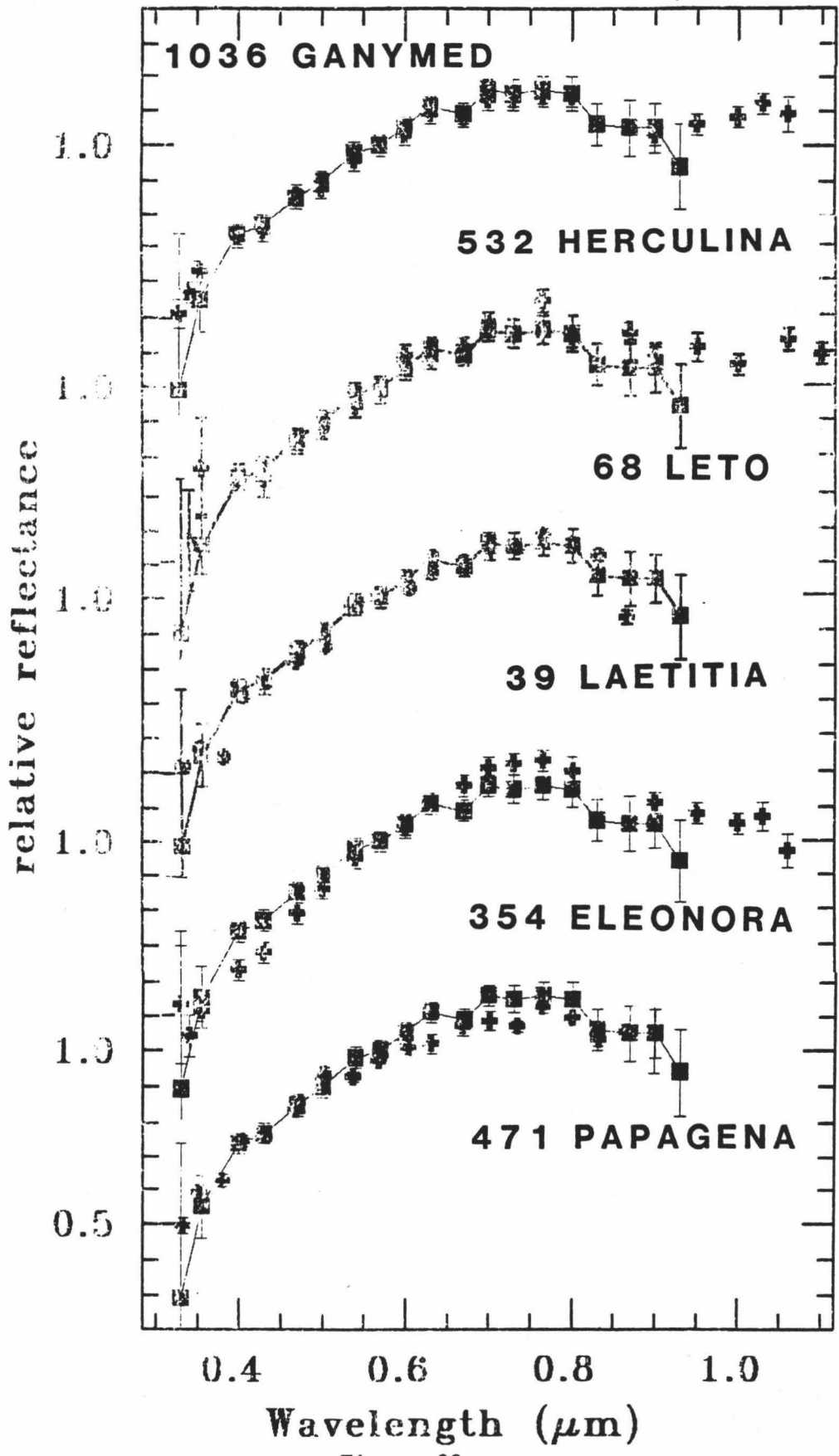


Figure 39

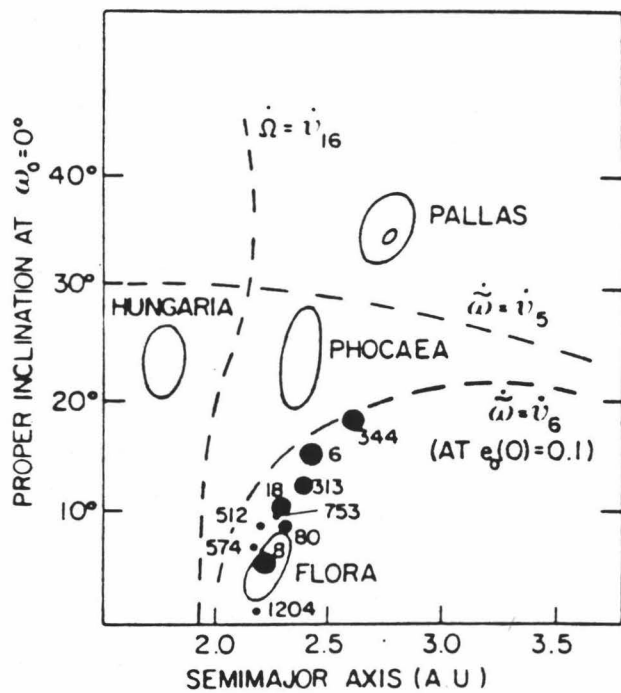


Figure 40

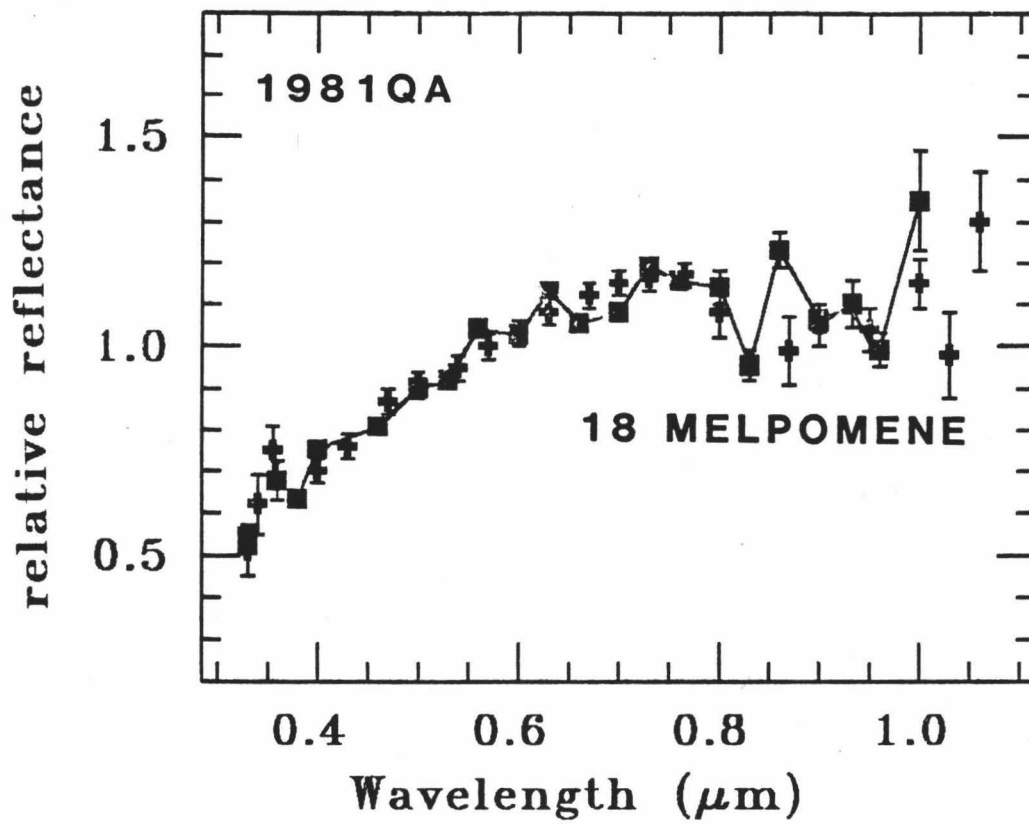


Figure 41

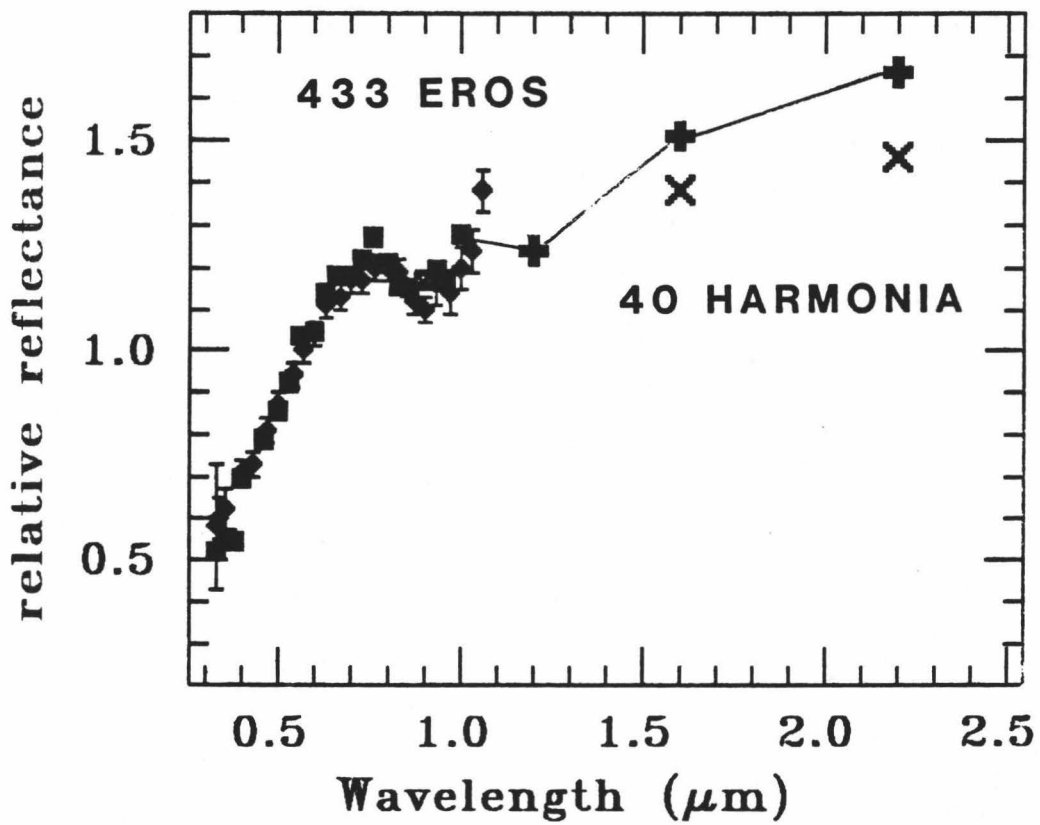


Figure 42

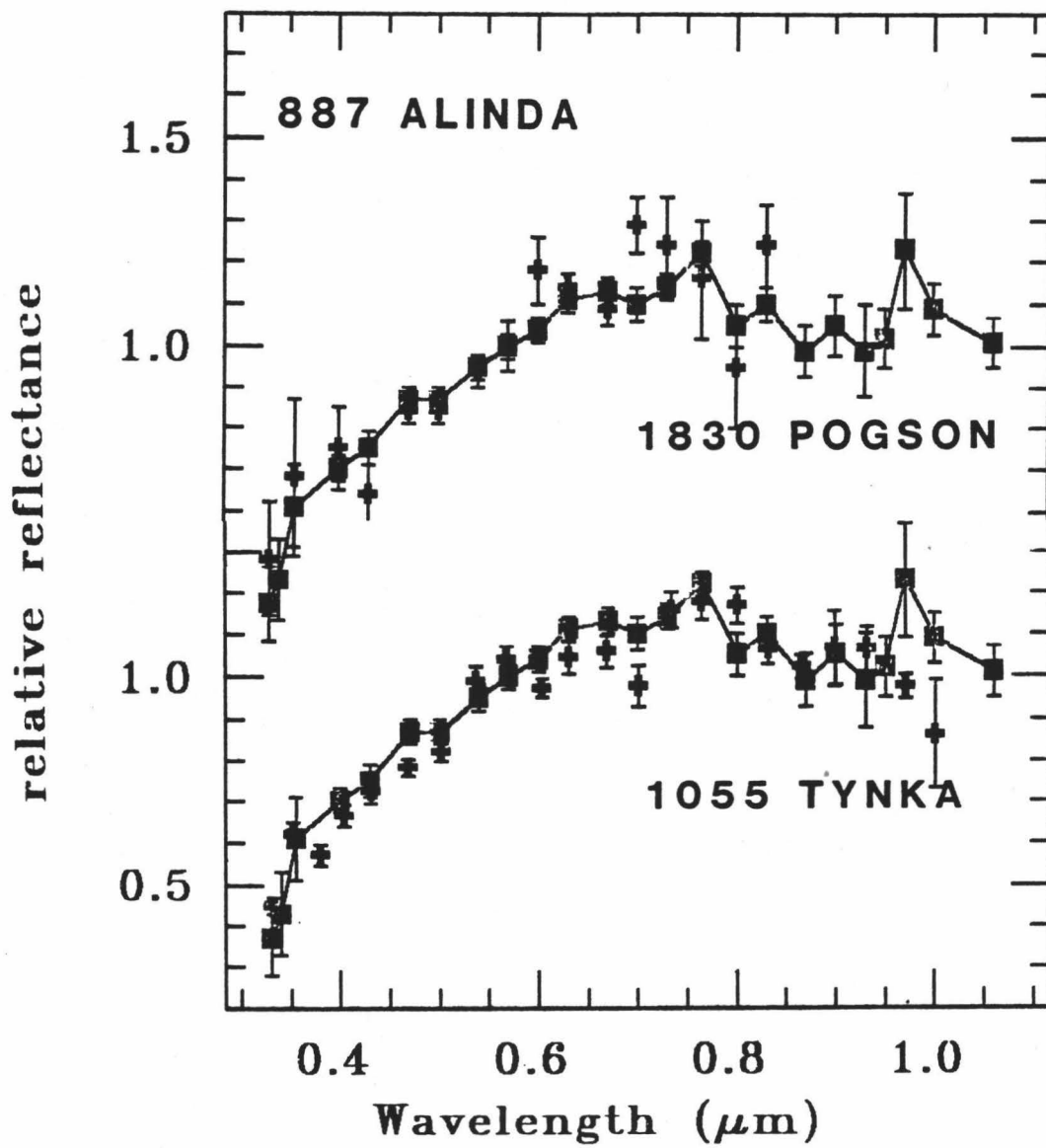


Figure 43

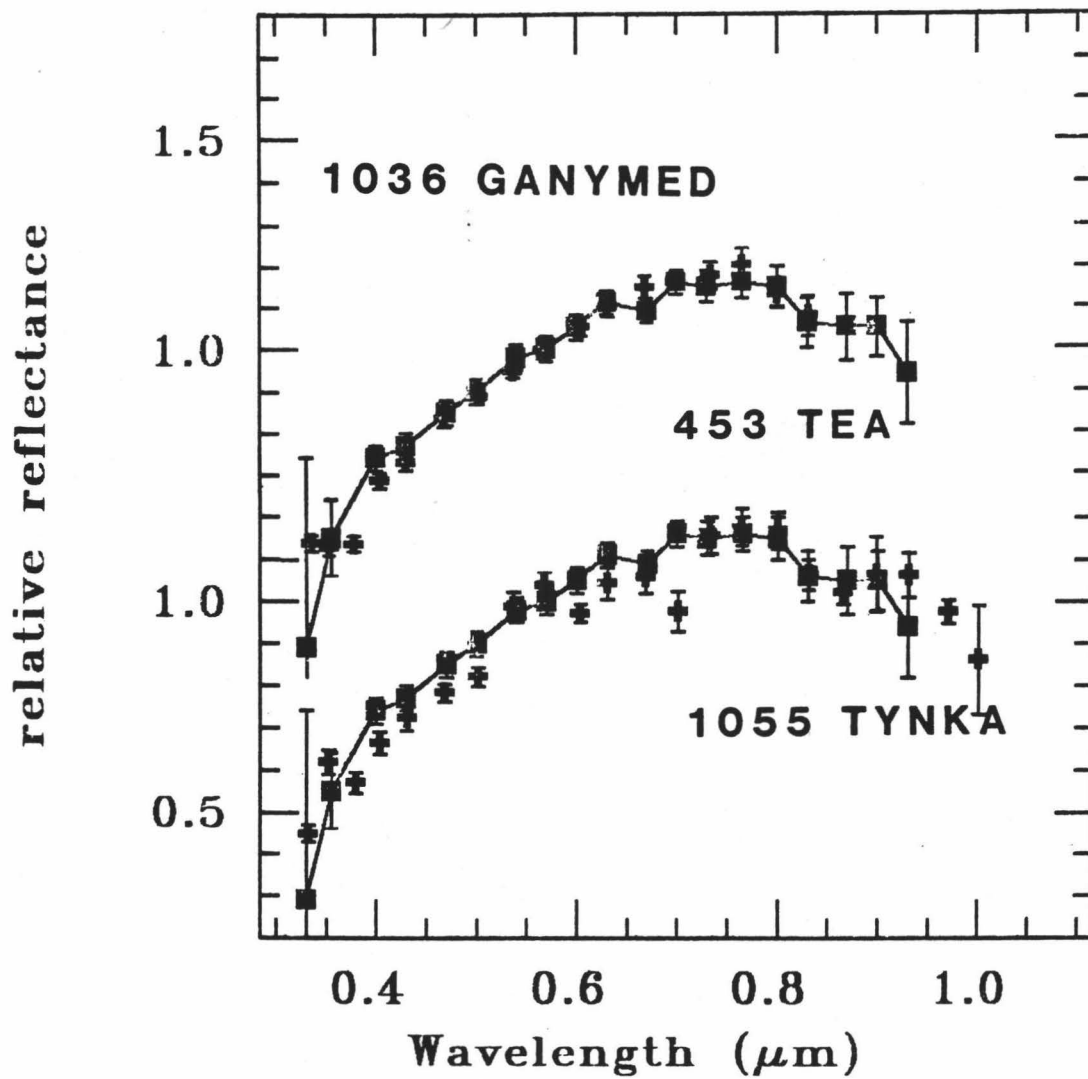


Figure 44

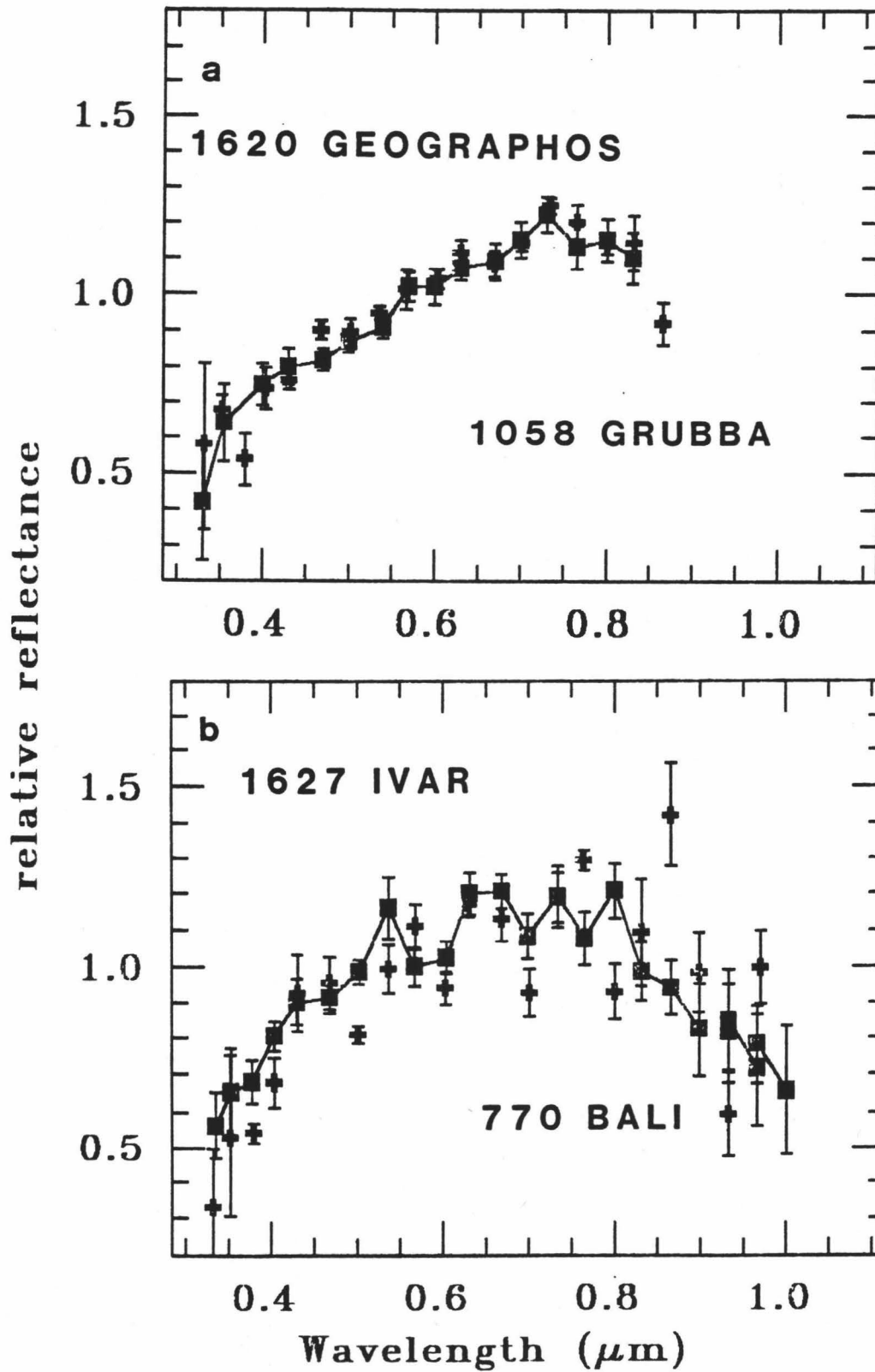


Figure 45

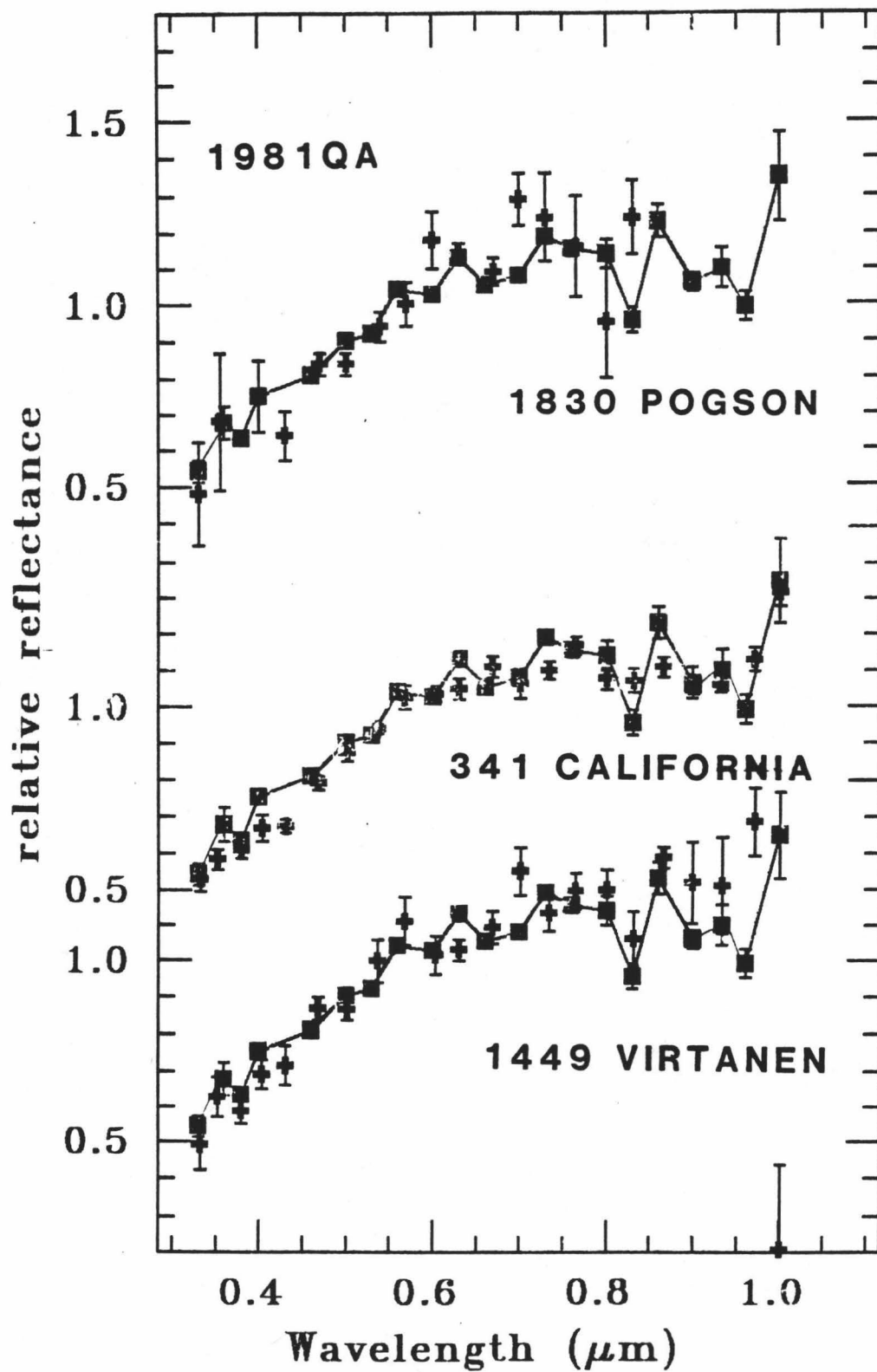


Figure 46

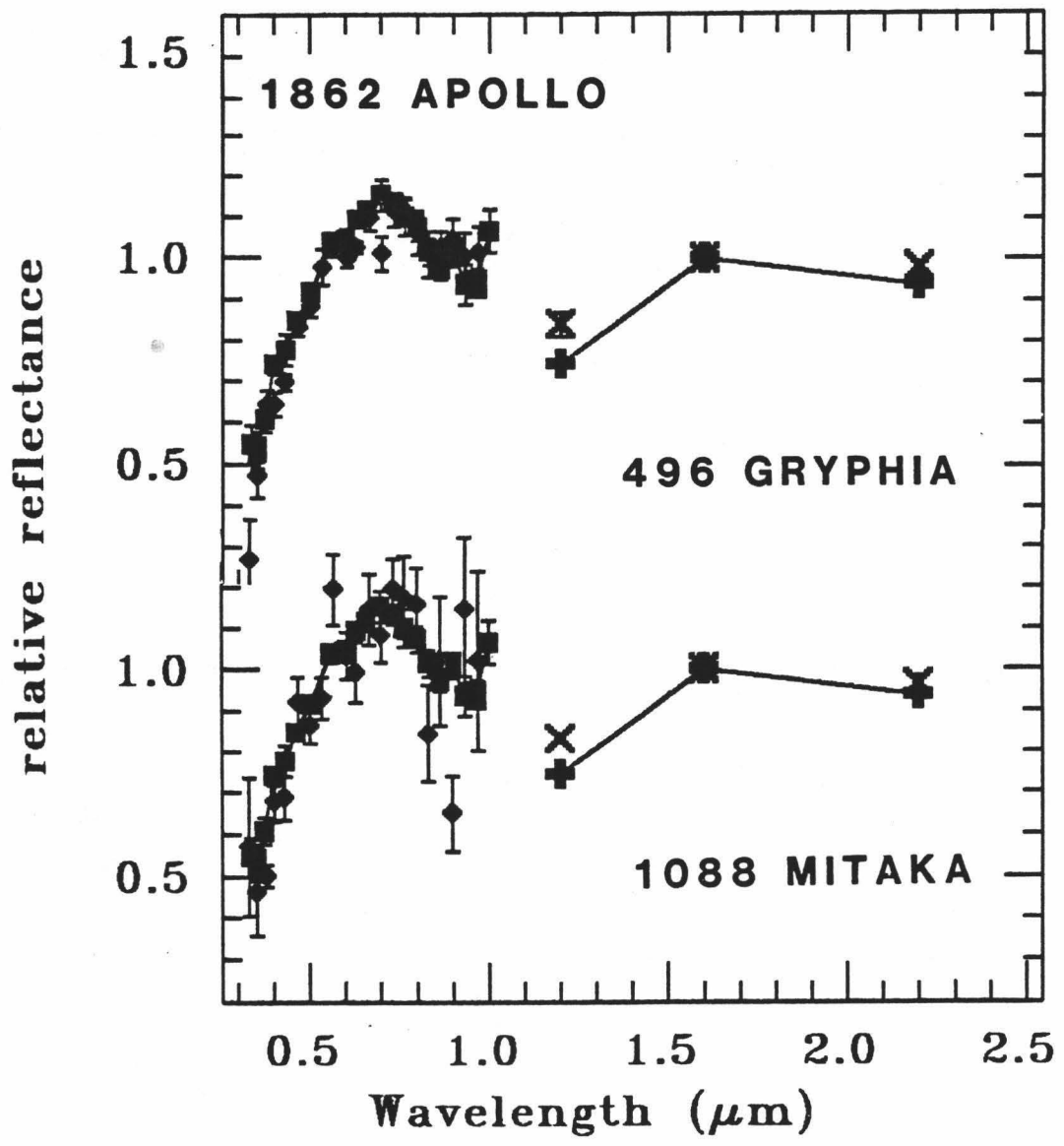


Figure 47

Summary

The near-Earth asteroid population as presently known consists of common rock-forming minerals with one possible exception (2201 1947XC). In spite of their common components there are few main belt asteroids with similar surface compositions. A number of potential analogues are noted but some of them will be shown to have different compositions when additional data are available. With the presently available data there are near-Earth asteroid analogues in all hypothesized asteroid source regions based on dynamical theory, except in the 2:1 Kirkwood gap and among Mars-crossers. The Mars-crossers are presently poorly sampled in terms of measured reflectance spectra. There is no satisfactory test of the relation between near-Earth asteroids and extinct cometary nuclei.

Meteoritic analogues are surprisingly scarce among near-Earth asteroids. Yet some analogues are found in the population. It seems that irons, stony-irons and carbonaceous chondrites types 1 and 2 are either not present or have not yet been observed. Only one achondrite analogue has been found. The majority of the achondrite parent bodies remain elusive to existing detection techniques. C3 analogues are abundant relative to their frequency in the meteorite collection. Two but not a lot of ordinary chondrites are found. Three asteroids that had previously been interpreted as possible ordinary chondrite analogues have spectral characteristics which differ from those of ordinary chondrites. The near-Earth population is apparently more diverse than the meteorite collection.

This observed diversity will be useful in extra-terrestrial space activities. Silicates are abundant and phyllosilicates and volatiles are present in some bodies but not as frequently as in the main belt. Water may be expensive in space and not available on all asteroids. There are

no nickel-iron-dominated objects found although the presence of some metallic iron is implied by the existence of two ordinary chondrite analogues.

Future Directions

The most interesting project to pursue related to mineralogy and petrology is an interpretation of 2201 1947XC. Some effort will be put into what a low activity comet might look like and trying to interpret the spectrum of 2201 1947XC. This asteroid will be observable in June, 1983 and should be reobserved. It will be a useful exercise to try to interpret the existing spectrum to develop tests for the relation of near-Earth asteroids and cometary nuclei.

Additional data to test for near-Earth asteroid analogues is needed. Some asteroids should have their spectra remeasured with extended coverage to 1.0- μ m including some of the near-Earth asteroids. The albedo of a number of asteroids is needed too. Ed Tedesco of JPL has the numbers of the asteroid albedos needed and has agreed to measure them if they are observable.

The Palomar planet-crossing asteroid survey continues to discover near-Earth asteroids. Many of them are below the detection limits of the two-beam photometer used in this study. A project using a faint object spectrometer should continue to collect mineralogical-petrological information to reassess the results of this work. Such a project is underway at the University of Arizona. Efforts should continue to evaluate the observational bias in these observations.

Of course nothing is better than sending one or more spacecraft to these asteroids to obtain in situ measurements of their chemical and physical nature. These results will hopefully aid in planning such a

mission. It would be very useful to have some microscopic imaging capability on a space craft mission. This has never been done before and the absence of seeing at this scale has made interpretation of other experiments more difficult. Other types of experiments determining surface composition, elemental abundances and internal structure should also be part of such a mission. Ground-based efforts have to continue, of course, for economical reasons.

APPENDIX A

Criteria for verifying measured reflectance spectra: (1) Observe an object and obtain the same results on two different nights. (2) Measure a previously observed object on an observing run with newly observed objects. Check for repeatable results taking into consideration differences in geometry. (3) Calculate star/star ratios of previously observed standard stars. Check for agreement with previous results.

The ephemerides for the objects were provided by Ted Bowell of Lowell Observatory, Jim Williams of the Jet Propulsion Laboratory and the Russian Ephemeris of Minor Planets. The object was located with a Quantex image intensified camera mounted to the photometer. The telescope was set up on the predicted coordinates a few minutes ahead of the time it was predicted to be at a given position. We then waited for the object to enter the field of view and then began tracking it. This technique met with the most success in finding a fast-moving object. Systematically scanning an area of the sky in the vicinity of the predicted position was never successful. The scan took longer than the time for the object to cross the area of the scan. Once set up on the object we stepped through the filters.

DATA REDUCTION NOTES

December 28-29, 1979 1979XA 1h 06m 8d 25m
1979XA=2201 1947XC 1h 00m 7d 55m

The 12/29/79 ratio is fairly constant, but not exactly. It is a smooth curve however. I tried calculating a starpack from the asteroid data, but the results are very inconsistent with our expectations of what a spectrum should look like. Remaining left to try is reducing the data

relative to a secondary standard measured for another object.

The spectrum of 511 Davida was measured on 12/28/79. There was some question at the time of observation as to the identification of the object. The spectrum matches fairly well with measurements made on January 26, 1980 and with previous measurements (Chapman and Gaffey, 1979) although I haven't a plot yet of the old data.

1980AA - Notes on run of January 26, 1980 1980AA The data of this run were collected by Mike Gaffey, Jeff Bell on the 2.2m telescope at Mauna Kea Observatory January 26, 1980UT. Only one night of data were collected on this object. The Ga-As-c photomultiplier tube was used at an operating voltage of 2000v. Characteristics of this run worthy of note are that the beam ratio was close to 1.0, and the winds were about 35-40mph at sunset. Some shaking of the telescope due to the wind was reported at the end of data collection for this object. 1980AA was located in a rich star field during the time of observation. Contamination from field stars was insignificant. The only potential danger is if the asteroid passes by a faint star which happens to be in the sky beam. This would result in an incorrect sky measurement and improper sky subtraction. Such reports appear in the data logbook, however the data reduction yields no spurious results.

Data Reduction-The data of this run were reduced twice almost two years apart. The standard reduction procedure was used. At the second reduction, the standard star was corrected for the ND filter used (ND2) before the extinction corrections were made. This enabled the scaling factors to be used to determine the light curve.

Channels 4-12 were used to scale the data and determine the light curve. Two maxima and one minimum was observed. A period of 2.75 hours is measured between the two maxima. This measurement is consistent with

that measured by Harris of 2.70 hours (reference from a list he sent dated 2/81 unpublished). The magnitude of the period is 0.2 magnitudes, twice the value determined by Harris.

The main belt asteroid 511 Davida was also observed during this run. These data were reduced and compared with previous measurements (Chapman and Gaffey, 1979) in order to verify the results of the 1980AA data. The UV absorption below 0.5 microns agrees with previous measurements. The 0.9 micron band is superimposed on a continuum with a higher reflectance relative to 0.56 microns than previous measurements.

Ratios of $10 \tau/\alpha \text{ lyr}$ and $\text{bet vir}/\alpha \text{ lyr}$ were calculated from measurements of $10 \tau/\eta \text{ hyd}$ and $\text{bet vir}/\eta \text{ hyd}$. The previously calculated $\eta \text{ hyd}/\alpha \text{ lyr}$ ratio (Owensby personal communication) was multiplied by the measured ratios to derive the two $\text{standard}/\alpha \text{ lyr}$ ratios. Previous calculations of these ratios are compared with those presently calculated. The agreement is not totally satisfactory, nor can I presently provide explanations of the discrepancies.

July 15,1980 KPNO 1685 TORO 22:09:00 +10d 57m

phase angle=39

These data were collected by Clark Chapman and Mark Rognstad at Kitt Peak National Observatory using the Ga-In-AsC photomultiplier tube, operating at 2000 volts with a 40 millisecond integration time. Internal chop mode was used and sky measurements were made at 15-minute intervals. The standard star 58 Aquila was observed at the beginning and end of the twenty minutes in which Toro was observed (22:18-22:40 UT). The logbook records patches or banks of high clouds throughout the night but the data for 1685 Toro were prejudged to be O.K. A $\text{nd}1.0/\text{nd}0$ correction was applied to the reduced data (58 aq1 was measured through

the nd1 filter). The nd1.0 correction used was that measured between 4/29/79 and 5/3/79 at KPNO. Atmospheric extinction corrections were calculated from 58 Aquila and applied to measurements of Toro upon dividing by the standard star flux. The 58 Aquila/Sun ratio was multiplied by the measured Toro/standard ratio to convert to reflectance relative to Sun. Comparison of the new spectrum with previously existing spectra is made in Figure 27.

Data were obtained for only one night from this object. No other previously measured asteroids were measured on this run. A theta vir/58 Aquila ratio may be calculated but has not been done. No light curve was extracted from the data because the period of observation was short relative to the period of rotation of the asteroid.

November 4-7, 1980 1627 Ivar 3:07:27 -2d 43m 46s phase=11.0

1865 Cerberus 2:48:23 3d 47m 23s phase=9.8

The data reduction process for this run has been painful to say the least. To begin with (Figure 3) there is an extreme offset in the spectrum between 0.50 and 0.53 microns in both the spectrum of Ivar and Cerberus on all three days of observation. Even if the 0.53 micron filter is considered to be bad, the 0.56 micron data still introduces a large offset in the spectrum not characteristic of reflectance spectra. The measured nd2/nd0 ratio also shows this offset at 0.53 and 0.56 microns and it does not show up in laboratory calibrations of the nd filters. The spectrum of 7 Iris measured during this run has an offset in the opposite direction than seen in the Ivar, Cerberus and Psyche spectrum at 0.53 microns. In addition, the wing of the IR absorption band of both the Ivar and the Cerberus spectrum extends far into the visible (0.60 microns), has a steep slope, a convex shape and a large band depth. The spectrum of 1627 Ivar has point to point scatter similar to that seen in

the spectrum of 2201 1947XC. In this case the relative reflectance at 0.66, 0.73, and 0.80 microns is high relative to the reflectance at 0.70, 0.76 and possibly 0.83 microns. This characteristic is not identical to the phenomenon in the 2201 1947XC data. However the identical phenomenon is observed in the spectrum of Psyche and the inverse is seen in the spectrum of Iris measured on the same date.

It is difficult to associate these spectral characteristics with a mineral or mixture of minerals with our present understanding of the interaction of light with surface materials. The facts that the same unusual spectral characteristics appear in all asteroid spectra observed during this run, and even the neutral density calibration confirm the suspicion that a systematic error is dominating the spectra. The size of the standard deviation of the mean is remarkably small, especially in the spectrum of Ivar, indicating that the observed phenomenon was operational continually throughout this observing run. The standard deviation of data of 1865 Cerberus spectrum are larger, however the object was fainter than Ivar by a magnitude and a larger standard deviation of the mean is expected. The spectrum of Iris measured 11/5/80 as an object of magnitude 8.9 does not match measurements by Chapman and Gaffey, 1979 particularly at wavelengths of 0.53, 0.60, 0.63, 0.66, 0.73, 0.76, 0.80 and 1.0 microns. The spectrum of 16 Psyche does not agree with previous measurements at 0.50-0.60 and 0.66-0.86 microns. In addition the 8 filter photometry of Tedesco and Tholen (unpublished) of both Ivar and Cerberus do not agree with our measurements.

The criteria for determining a valid correction for these spectra are elimination of unusual spectral characteristics and agreement of the Iris and Psyche data with previous measurements. The corrected Ivar and Cerberus spectrum should also agree with the measurements of Tedesco and Tholen.

While searching for the cause of the spectral characteristics various hypotheses were tested including:

(1) The filters were put in in the reverse order. The spectra of Ivar and Cerberus almost look believable when the data are plotted in reverse order, but Iris plotted this way is obviously wrong therefore the filters were not in reverse order.

(2) I was observing non-asteroidal objects. Since the objects were moving like a bat out of hell, they were either near-Earth objects or man-made satellites. They could not have been satellites since they were both located on three different nights with the ephemerides for each object. Therefore, I was observing the correct objects.

(3) The standard stars were misobserved. If the telescope were set on the wrong object we could not have found the asteroids, unless we told the telescope operator to go to the wrong star. It might be possible to misdirect the operator to one star but not to two or three. Since the spectra reduced through different standards yield the same spectrum, the problem is not due to misidentifying the standards.

(4) We could have given the right coordinates for a star we called by the wrong name, i.e. we could have given the coordinates for omi tau and called it 10 tau. However, multiplying the object/standard ratio by the omi tau/sun ratio does not eliminate the unusual spectral features. A similar type of confusion for other stars is not likely.

(5) The wind screen might have been obscuring the field of view. This could not be the case because Ivar and Cerberus were located in different regions of the sky (5 degrees apart). As the objects rose and set the obscuration by the wind screen would change. The small value of the standard deviation of the measurements preclude any variation in the phenomenon such as varying obscuration as the cause of the unusual spectral features.

(6) There was a light leak of some sort in the instrument. If this were the case the excess flux would be most excessive in the mid visible spectral region and the object would receive a proportionately higher amount of contamination than the standard. Would the spectrum then mimic that of the black body curve of the light bulb that may have been left on? This would not explain the low relative reflectance at 0.53 and 0.56 microns. But it would explain the maximum reflectance at 0.6 microns.

(7) The dark slide was partially closed. It is extremely unlikely that the dark slide would have remained in one position throughout the run except completely opened.

(8) A linearity test was performed in which the log of two ratios were plotted relative to one another to see if the photometer response was linear through the range of the neutral density filter. The photometer response was linear over the range of magnitudes observed.

(9) It was suggested that a chopping phase error might create the observed phenomenon. If the electronic chopping device was not synchronous with the mirror chopping, then part of the object signal could be counted as the sky signal and vice versa. Under certain conditions this can be calibrated and corrected. The algorithm for this correction was derived and applied to the data. Unfortunately, the results were not entirely satisfactory.

(10) I tested to see if any of the standard corrections could be wrong by eliminating them all together and then reapplying them one by one. I used Cerberus since this spectrum needed the most correcting (its weird features were most extreme). First I calculated Cerberus/sun with no sky subtraction. This did not correct the problem. Sky subtractions need to be made and the offset at 0.53 microns is present already. But if the 0.53 micron filter is bad, the effect may not be showing.

Since the shape of the raw sky flux mimicks the shape of the relative reflectance spectrum, if I divide out the raw sky flux I should theoretically be able to correct for the problem. The raw sky does not embody the signature of only the weird spectral features. The slopes of the extinction corrections also mimic the shape of the spectra, I should be able to use that as a correcting factor too. I wish I knew what this is telling me.

There seems to be a magnitude dependence on the unusual spectral phenomenon. The faintest objects show the most extreme spectral characteristics. Starting from the sky, the order of the magnitude of the effect continues through Cerberus, Ivar, and Psyche from magnitudes of 15.1, 14.5, and 10.5. What seems to be important is the difference in the magnitudes of the objects being ratioed.

Another thing to try is to correct the observed nd_2/nd_0 calculation measured at the telescope during the 11/4-7/80 run, to that measured 11/15-18/80 and then apply the lab/tel correction that worked for 1862 Apollo.

In my last attempt to salvage the data of the November 4-7, 1980 observing run I will reduce the data of Pallas and see if the correction factor is intermediate between that of 7 Iris and the measurements of Ivar and Cerberus. If the correction factor varies as a function of magnitude I should then be able to extrapolate the correction to the fainter objects.

What I actually did was use the standard star SA0094488, which was observed to make extinction corrections for the Pallas data, to make extinction corrections for 1627 Ivar. I then divided the extinction-corrected spectrum of 1627 Ivar by the extinction-corrected spectrum of 2 Pallas and multiplied by a previously measured solar-calibrated spectrum of 2 Pallas to get the spectrum of 1627 Ivar relative to the sun.

The results are in agreement with the 8-color photometry of Tedesco and Tholen except for the last two filters at 0.95 and 1.06 μm .

November 15-17, 1980

1862 Apollo was first observed November 15 and 17, 1980UT with the photoelectric photometer used in this study and the Ga-As-c photomultiplier operating at 1800v. The standard data reduction resulted in a spectrum with a strong convex-shaped absorption in the UV which reached a maximum at 0.60 μm . The reflectance decreases with an increase in wavelength. The high frequency noise pattern is present superimposed on the convex-shaped absorption. The reflectance at 0.70, 0.76, 0.83, 0.86 and 1.0 μm is low, creating the noise pattern.

16 Psyche was observed on the night of November 15, 1980UT. The newly measured spectrum of 16 Psyche does not match previous measurements (Chapman and Gaffey, 1979).

Star/star ratios were calculated of chi ori/alph aqr and omi tau/alph aqr. The omi tau/alph aqr ratio does not agree well with previous measurements. Therefore omi tau was not used as a standard star. The general agreement of the chi ori/alph aqr ratio with previous measurements indicates that the alph aqr data are good. This star was used as the standard for the reduction of these data.

The light curve of 1862 Apollo was calculated from data obtained on November 17, 1980UT. Two maxima and two minima were observed. There is some possibility that four maxima and three minima were observed. The period between the two highest magnitude maxima is 3.2 hours. The maximum light curve variation observed is 0.59 magnitudes. This is in fair agreement with measurements by Harris (personal communication) of a period of 3 hours and amplitude of 0.6 magnitudes. The measurements obtained on 11/15/80 UT did not extend over a significant portion of the

light curve to warrant inclusion in this presentation.

March 3-5, 1981

Notes on reduction of data for 1915 Quetzàlcoat1, March, 1981. These data were reduced twice, about nine months apart. The first time, the star pack was calculated as beta virgo nd2. The second time, the nd2/nd0 correction was made before the calculation of extinction corrections in order to determine the magnitude of the light curve from the normalization values. The first reduction normalized from channels 6-23, the second used channels 9-14. These channels used during the second reduction all have positive values.

The data of this run are observed to have abnormally high and varying dark counts as determined from the signal in the first and last channels. These were blocked off with aluminum disks and covered with black tape after we noticed the sky channel to fluctuate with time and magnitude of the object under observation. In the initial reduction when dark and sky signal were subtracted, I calculated the dark for each file by averaging the four data points consisting of beam 1 and 2 of channels 1 and 25 and subtracted individual darks from each file. This worked well for some files, but not for others. After the subtraction was performed some channels contain negative signal. This seems to indicate that the dark noise was fluctuating more rapidly than the duration of one run, about two minutes. There seems to be no choice but to throw these data away. Fortunately, there is enough good data, from the beginnings of both nights, to get a good, high signal-to-noise spectrum of Quetzàlcoat1 from an average of about 23 runs. I will continue to reduce the bad data only to obtain a light curve from the channels in which all of the signal is positive, channels 9-14. These channels had filters with transmissions varying between 47-76%.

Extinction corrections were made with coefficients calculated from data bracketing the corrected data. This usually required the calculation of two or three sets of corrections for each standard. A set of corrections (called a starpack) were calculated from fitting a straight line to two data points, or clusters of data points from the same time interval.

Standard stars - The standard stars observed during this run included beta virginis which was used to calculate extinction corrections, 109 virgo, chi 1 orionis, and eta hydra. To check for proper response of the system, the ratios chi 1 orionis/beta virginis and epsilon hydra/beta virginis were compared to those ratios measured previously.

August 25-28, 1981

These spectra appear to have some systematic point to point scatter. I suspect that if the voltage on the photomultiplier was higher we wouldn't have had this problem.